Journal of Medicinal Chemistry

pubs.acs.org/jmc

Article

Novel Dual-Target μ-Opioid Receptor and Dopamine D_3 Receptor Ligands as Potential Nonaddictive Pharmacotherapeutics for Pain Management

Alessandro Bonifazi,* Francisco O. Battiti, Julie Sanchez, Saheem A. Zaidi, Eric Bow, Mariia Makarova, Jianjing Cao, Anver Basha Shaik, Agnieszka Sulima, Kenner C. Rice, Vsevolod Katritch, Meritxell Canals, J. Robert Lane, and Amy Hauck Newman*

Cite This: *J. Med. Chem.* 2021, 64, 7778−7808

Read Online

ACCESS | Metrics & More | Article Recommendations | Supporting Information

ABSTRACT: The need for safer pain-management therapies with decreased abuse liability inspired a novel drug design that retains μ-opioid receptor (MOR)-mediated analgesia, while minimizing addictive liability. We recently demonstrated that targeting the dopamine D_3 receptor (D_3R) with highly selective antagonists/partial agonists can reduce opioid self-administration and reinstatement to drug seeking in rodent models without diminishing antinociceptive effects. The identification of the D_3R as a target for the treatment of opioid use disorders prompted the idea of generating a class of ligands presenting bitopic or bivalent structures, allowing the dual-target binding of the MOR and D_3R. Structure−activity relationship studies using computationally aided drug design and *in vitro* binding assays led to the identification of potent dual-target leads (**23**, **28**, and **40**), based on different structural templates and scaffolds, with moderate (sub-micromolar) to high (low nanomolar/sub-nanomolar) binding affinities. Bioluminescence resonance energy transfer-based functional studies revealed MOR agonist−D_3R antagonist/partial agonist efficacies that suggest potential for maintaining analgesia with reduced opioid-abuse liability.

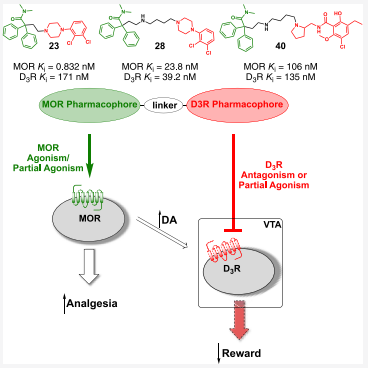

INTRODUCTION

Over the last decade, the United States has faced a devastating opioid epidemic with an estimate of over 130 people dying from opioid overdose every day.[1] The misuse and often consequent addiction to opioids (*e.g.*, prescription pain relievers and synthetic opioids, in general) are a serious national health, social, and economic emergency. Coupled with the SARS-CoV-2 pandemic, the mortality rate involving opioid overdose is increasing, and the need for new therapeutic strategies is more urgent than ever.[2,3] According to recent reports,[4] >20% of patients being treated for chronic pain will misuse their opioid prescriptions[5] and 8−12% develop opioid use disorders (OUD).[5] Ultimately, an estimated 5% of patients are reported to transition from misuse of prescription opioids to heroin[6−8] or other synthetic opioids.

The National Institutes of Health (NIH) launched the Helping to End Addiction Long-Term (HEAL) initiative to promote and support innovative research addressing this national health emergency. Moreover, the National Institute on Drug Abuse (NIDA) recently proposed a list of the "ten most wanted" medication development strategies to tackle the opioid epidemic/crisis.[9] Among them, the dopamine D_3 receptor (D_3R) antagonists and partial agonists are a "new" proposed class of ligands as therapeutics to attenuate opioid self-administration.

In the past, D_3R-selective antagonists, such as **GSK598809**, have been investigated as potential treatments for psychostimulant use disorder (*e.g.*, cocaine);[10] however, the potentiation of hypertensive effects observed in dogs produced by cocaine in the presence of this selective D_3R antagonist prevented further development[11] and suggested that this may be a class effect. We recently demonstrated that our novel D_3R antagonists and partial agonists look promising for the treatment of OUD.[12−14] Highly selective antagonists, such as **VK4-116** (**1**) and **VK4-40** (**2**) (Figure 1), attenuate oxycodone self-administration and reinstatement to drug seeking, without compromising oxycodone's antinociceptive effects, in rodents. Importantly, these D_3R antagonists/partial agonists do not potentiate the cardiovascular effects induced by cocaine or oxycodone in rats.[15] In combination, these studies support the development of D_3R antagonists/partial agonists to reduce the risk of opioid misuse and the consequent development of OUD.

Received: April 2, 2021
Published: May 20, 2021

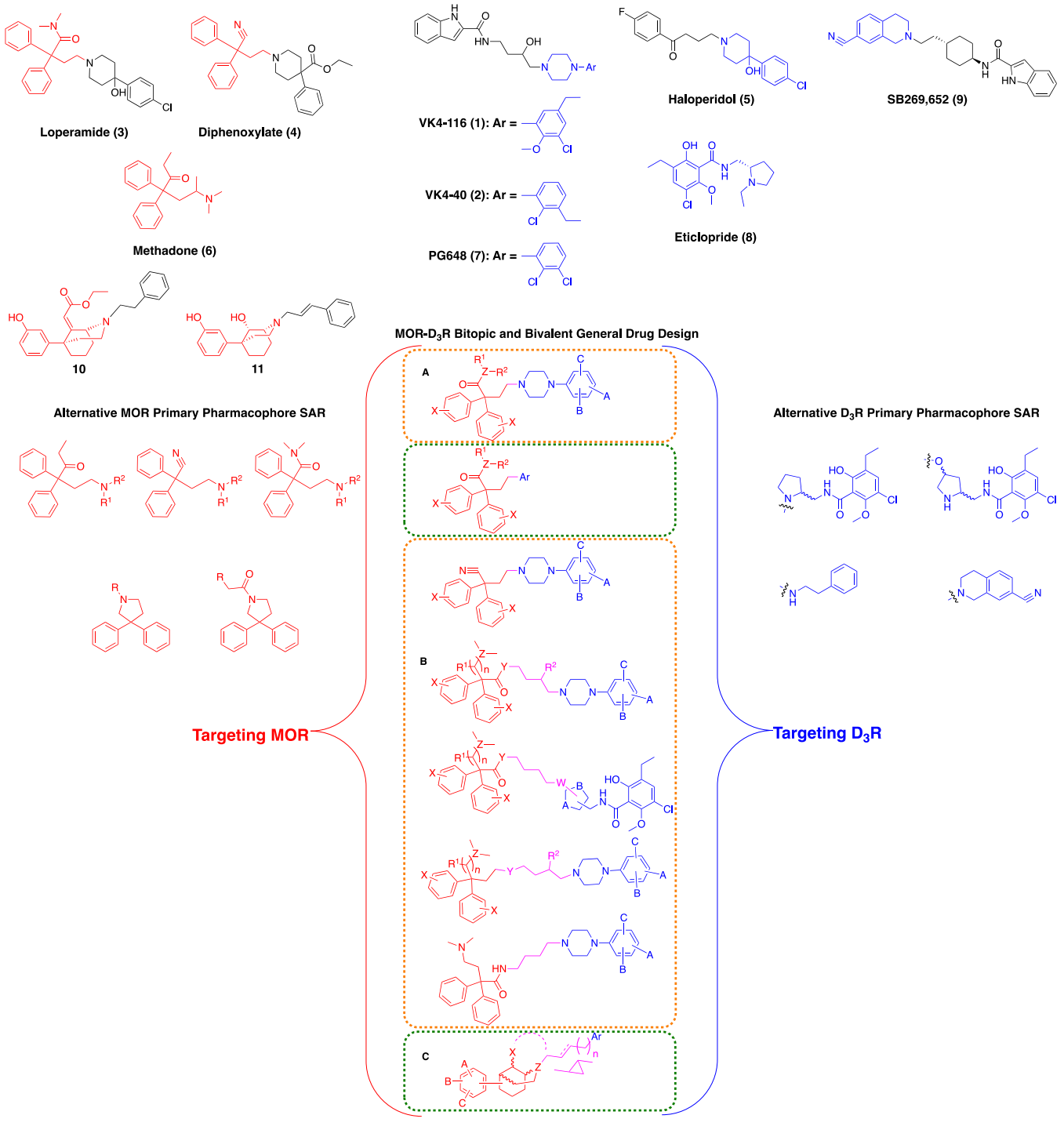

Figure 1. Drug design based on structural modification of canonical synthons inspired by agonists, antagonists, and partial agonists selectively targeting the MOR and D_3R. Orange boxes denote bivalent templates, and green boxes denote bitopic templates. Variables **A**, **B**, and **C** correspond to the aromatic substitutions seen in compounds **1**, **2**, **7**, **10**, or **11**. The general **Ar** group corresponds to the aromatic substituents in compounds **7**, **9**, **10**, and **11**. General $\mathbf{R^1}$ and $\mathbf{R^2}$ groups represent H, Me, or OH or (O). Variables **Y** and **Z** represent C or N, and variable **X** is H, OMe, or OH or (O).

Until now, the main target for pain-management therapies and drug development has been the opioid system, in particular, the μ-opioid receptors (MORs), belonging to the G-protein coupled receptors (GPCR) family. However, due to the abuse liability and development of tolerance associated with the most common MOR agonists used in pain therapy, including chronic pain, for which opioid agonists are largely ineffective in the long term,[16−18] research efforts have been directed toward identifying specific physiological responses associated with MOR agonists' cellular activation pathways. Functionally biased agonists have been posited to reduce the side effect profile of classic opioid analgesics and augment their utility not only as analgesics but also in the treatment of OUD.[19−22]

Design, synthesis, and pharmacological characterization of signaling-pathway-biased agonists targeting the MORs allowed

https://doi.org/10.1021/acs.jmedchem.1c00611
J. Med. Chem. 2021, 64, 7778−7808

the identification of highly selective G-protein-biased agonists, with limited activation of β-arrestin pathways, highlighting different physiological effects mediated by each independent pathway.[19,23] It has been suggested that the MOR G-protein pathway seems to be the predominant mediator of the analgesic effects of MOR agonists; meanwhile, it has been posited that the simultaneous hindering of β-arrestin recruitment might reduce the respiratory depression and other side effects, such as constipation, associated with opioid-like drugs.[24−28] However, this has been a topic of intensive investigation, and recently, it has been reported that classical MOR agonists, such as **morphine** and **fentanyl**, induce dose-dependent respiratory depression and constipation in β-arrestin-2 knock-out mice, similar to what is observed in wild-type mice.[29−31] Subsequent pharmacological evaluation has also shown that MOR G-protein-biased agonists still have abuse potential.[29,32−34] It is still unclear whether the optimal outcome and pharmacotherapeutic potential of MOR agonists can be gained through selective activation of a particular downstream signaling pathway (functional selectivity) or whether an optimal level partial agonism at multiple pathways may instead provide a route for the development of safer opioids.[31,35] Independent of the signaling pathways and cellular mechanisms associated with respiratory depression and constipation, abuse liability remains as a serious concern that must be addressed with different drug design approaches.

The recognition of D_3R antagonism/partial agonism as an alternative and nonopioid approach for treatment of OUD, modulating the abuse potential of common prescription opioids (*e.g.*, oxycodone),[12,13,15] combined with the well-established antinociceptive properties of MOR agonists, prompted the idea of generating a novel class of dual-target ligands directed to both the MOR and D_3R (Figure 1). In theory, compounds that are both MOR agonists/partial agonists and D_3R antagonist/partial agonists would have analgesic activity without concomitant abuse liability. Our approach aimed at maintaining the analgesic effects of the classic MOR agonists, while reducing the rewarding properties and subsequent abuse liability as a result of D_3R antagonism. This drug design may lead to the development of safer dual-target drugs, bridging the most promising pharmacological effects of two classes of molecules/targets previously developed independently. Of note, our drug design was to develop new small molecules endowed with differing ranges of affinities for both targets, independently modulating their physiology/pharmacology rather than toward simultaneous binding of the MOR and D_3R when in close proximity or in a heteromeric conformation. Nevertheless, if MOR−D_3R heteromers are demonstrated to exist and are physiologically relevant, these molecules may be interesting tools to probe their pharmacology.

Furthermore, several well-known MOR agonists, such as **loperamide** (**3**) (peripherally limited potent MOR agonist, FDA-approved for antidiarrhea treatment) and **diphenoxylate** (**4**), share similar structural motifs with the highly potent nonselective D_2R/D_3R antagonist **haloperidol** (**5**) (Figure 1).[36] Substituted phenyl-piperazine and/or phenyl-piperidine synthons, common to both classes of ligands, can exploit the structural similarities between MOR and D_3R proteins, thus achieving dual-target binding. Of note, a similar approach was taken previously toward more effective peripherally limited analgesics, based on loperamide, although implementing a bivalent or bitopic drug design or binding to the D_3R was not described or presumably intended.[37]

Moreover, **methadone** (**6**) (Figure 1) also showed low micromolar D_2R and D_3R affinity in our binding assays (Table 1), supporting the hypothesis that some of its structural fragments could be used to target not only the MOR orthosteric binding site (OBS) but the D_2R and D_3R as well. Unlike **6**, the synthetic opioid **fentanyl**, with its completely different structural features, showed an interesting moderate affinity for the dopamine D_4R subtype but total lack of recognition for either the D_2R or D_3R (Table 1). This template was not considered in our drug design for this reason and also because, recently, bivalent ligands using fentanyl have been reported to lack antinociceptive activity.[38,39]

Due to the limited availability of reported structure−activity relationships (SARs) for dual-target MOR−D_3R ligands,[38,40−42] we used a fragment-based drug design approach, supported by molecular docking, computer-aided drug design (CADD), and extensive *in vitro* pharmacology to guide SAR, hit optimization, and lead identification.

Herein, we refer to bivalent dual-target analogues when an MOR agonist primary pharmacophore (PP) is tethered with a D_3R antagonist PP; both can bind their respective OBS, eliciting their corresponding opioid agonist and dopaminergic antagonist effects. Consistent with our definition of bitopic ligands,[43] we classify these new analogues as bitopic when they incorporate an MOR agonist PP, targeting its corresponding OBS that also has structural features suitable for D_3R OBS recognition, tethered to a D_3R secondary pharmacophore (SP), identifying the D_3R secondary binding pocket (SBP).[44] Of note, this D_3R SP may also elicit binding interactions within the MOR SBP. All new compounds represent carefully designed linkers, as tethering fragments, with specific SAR focusing on the linkers' regiochemistry, stereochemistry, and substituents.[43]

All newly synthesized analogues were tested for their on-target and off-target affinities at the MOR, D_2R, D_3R, and D_4R, in a combination of agonist and antagonist radioligand competition binding assays. Compounds selected as hits, for their promising dual-target and sub-micromolar affinities, were further evaluated in functional bioluminescence resonance energy transfer (BRET) studies to assess their agonist and/or antagonist potencies for the target of interest and possible functional selectivity (biased agonism) for specific signaling pathways.

RESULTS AND DISCUSSION

Chemistry. This novel class of compounds can be subdivided, as depicted in Figure 1A−C, in three general templates: (A) the *N*,*N*-dimethyl-2,2-diphenylacetamide, 2,2-diphenylacetonitrile, and 1,1-diphenylbutan-2-one MOR PPs, derived from **3**, **4**, and **6**, respectively (Figure 1), were tethered with suitably substituted PPs, inspired by selective and nonselective D_3R antagonists [*e.g.*, **1**, **2**, **PG648** (**7**), **eticlopride** (**8**) and **SB269,652** (**9**); Figure 1], *via* a short ethyl linker chain; (B) the same MOR OBS-binding agonist PPs were linked with D_3R OBS antagonist PPs *via* a longer and more complex butyl linker, substituted with a 3-hydroxyl group, or the piperazine or pyrrolidine basic function in several regiochemical combinations; and (C) the MOR agonist PPs were replaced with the more rigid, stereochemically complex, and hindered ethyl-2-(-5-(3-hydroxyphenyl)-2-azabicyclo[3.3.1]nonan-9-ylidene)acetate and 5-(3-hydroxy-

https://doi.org/10.1021/acs.jmedchem.1c00611
J. Med. Chem. 2021, 64, 7778−7808

Scheme 1[a]

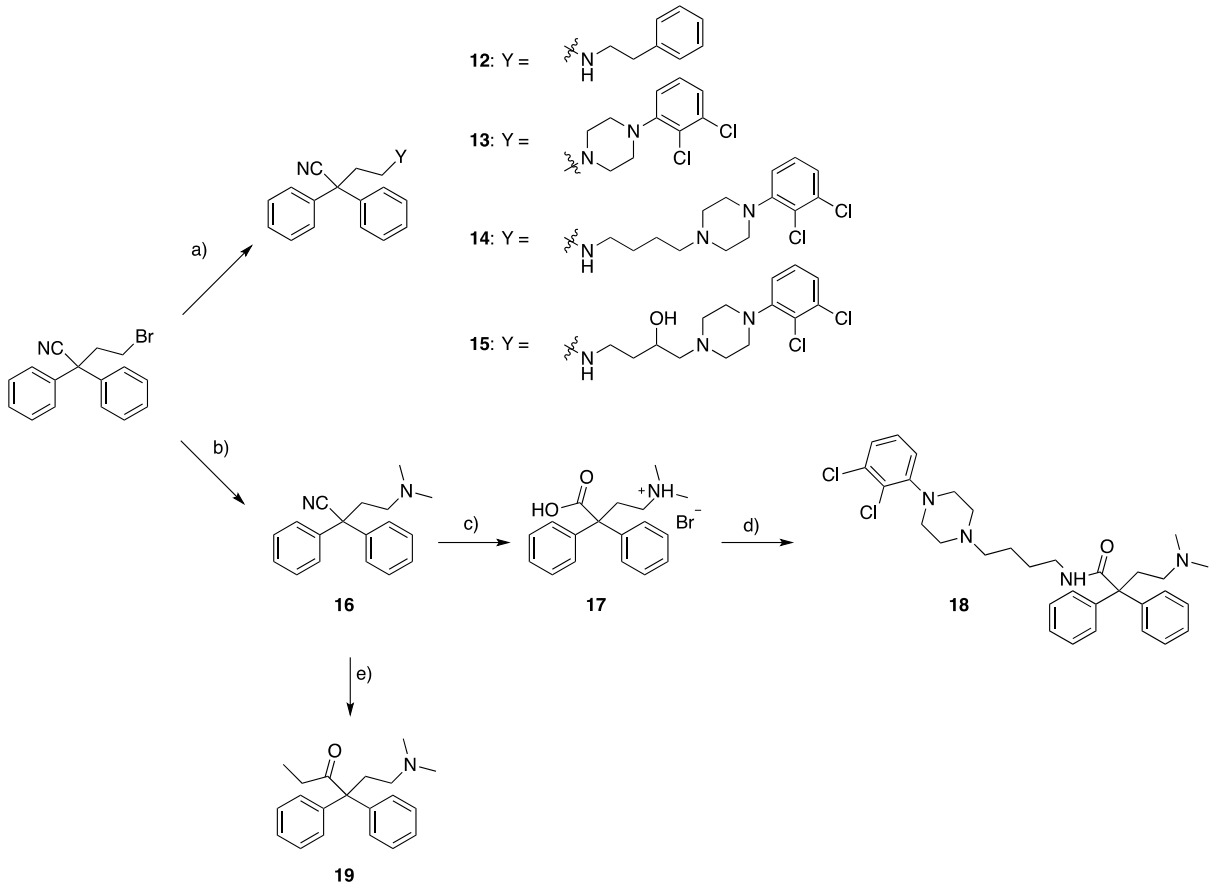

[a](a) Appropriate primary or secondary amine, K_2CO_3, and acetonitrile (ACN), 130 °C, overnight, 8−53%; (b) $Me_2NH{\cdot}HCl$, K_2CO_3, and ACN, 130 °C, overnight, 79%; (c) HBr 48% in H_2O, 100 °C, overnight; (d) *N*-(3-dimethylaminopropyl)-*N*′-ethylcarbodiimide hydrochloride (EDC), 1-hydroxybenzotriazole hydrate (HOBt), 4-(4-(2,3-dichlorophenyl)piperazin-1-yl)butan-1-amine,[47] *N*,*N*-diisopropylethylamine (Hünig's base, DIPEA), and dichloromethane (DCM), 25 °C, overnight, 6%; and (e) ethyl magnesium bromide (EtMgBr) 3 M in diethyl ether (Et_2O), toluene, 0 to 110 °C, 3 h, 59%.

Scheme 2[a]

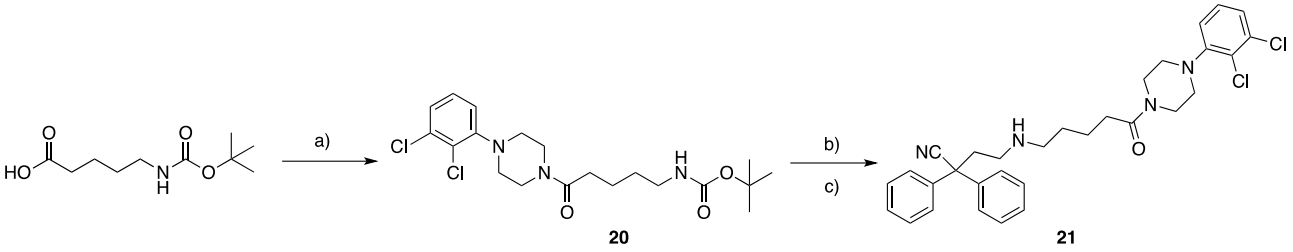

[a](a) 1-(2,3-Dichlorophenyl)piperazine, 2-(6-chloro-1-*H*-benzotriazole-1-yl)-1,1,3,3-tetramethylaminium hexafluorophosphate (HCTU), and DCM, 25 °C, 3 h, 59%; (b) trifluoroacetic acid (TFA) and DCM, 25 °C, 24 h; and (c) 4-bromo-2,2-diphenylbutanenitrile, K_2CO_3, and ACN, 82 °C, overnight, 3% (over two steps).

phenyl)-2-azabicyclo[3.3.1]nonan-9-ol PP (**10** and **11**; Figure 1), with structural features reminiscent of previously published D_3R ligands[45,46] that we have found to have low micromolar affinity for the MOR as well. This new MOR PP presented key functional groups for extending linkers of multiple lengths, substitutions, rigidity and chirality, and tethering D_3R PPs (for bivalent dual-target compounds) or D_3R SPs (*e.g.*, 2-indoleamide for bitopic dual-target compounds). When possible and appropriate, a complete resolution of the chiral centers at PP, SP, or linkers was performed, and the stereochemical properties of the new analogues have been taken into consideration when generating detailed SAR.

The first series of compounds with the 2,2-diphenylbutanenitrile as the MOR PP, inspired by **4**, were prepared as depicted in Scheme 1. Starting from the commercially available 4-bromo-2,2-diphenylbutanenitrile, simple N-alkylation under basic conditions yielded the first group of bivalent MOR−D_3R hybrids, where the D_3R PP was represented by 2-phenylethan-1-amine (**12**), 1-(2,3-dichlorophenyl)piperazine (**13**), 4-(4-(2,3-dichlorophenyl)piperazin-1-yl)butan-1-amine (**14**), and 4-amino-1-(4-(2,3-dichlorophenyl)piperazin-1-yl)butan-2-ol

https://doi.org/10.1021/acs.jmedchem.1c00611
J. Med. Chem. 2021, 64, 7778−7808

Scheme 3[a]

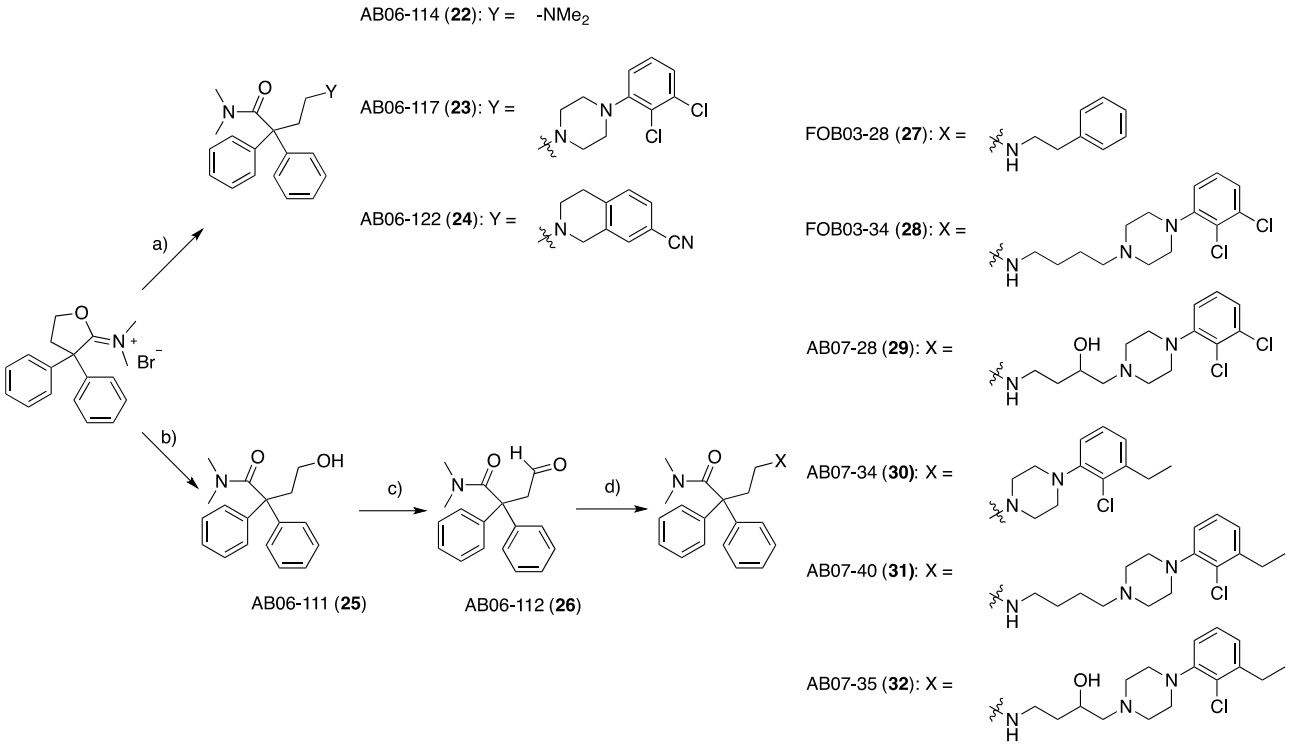

[a](a) Appropriate secondary amine, K_2CO_3, DIPEA (for **23** and **24**), ACN, and *tert*-butyl methyl ether (TBME), reflux, 24 h, 16−91%; (b) 2 N NaOH in H_2O, 25 °C, 5 min, 100%; (c) Dess−Martin periodinane (DMP), DCM, 0 to 25 °C, 1 h, 60%; and (d) appropriate primary or secondary amine, catalytic acetic acid (cat. AcOH), sodium triacetoxyborohydride (STAB), and 1,2-dichloroethane (DCE), 25 °C, 2.5 h, 12−100%.

Scheme 4[a]

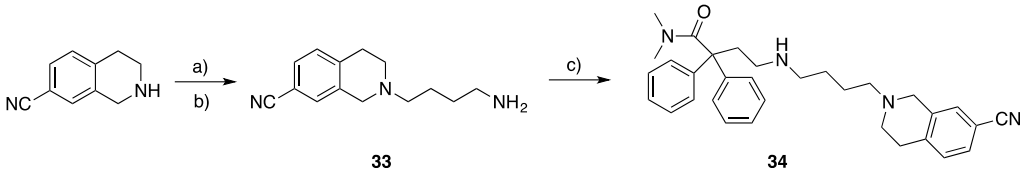

[a](a) *N*-(4-Bromobutyl)phthalimide, K_2CO_3, cat. KI, ACN, 82 °C, overnight; (b) hydrazine (NH_2NH_2) and ethanol (EtOH), 80 °C, 3 h, 94% (over 2 steps); and (c) *N*,*N*-dimethyl-4-oxo-2,2-diphenylbutanamide (**26**), cat. AcOH, STAB, and DCE, 25 °C, 2.5 h, 46%.

(**15**). This provided initial SAR deduction, by increasing the structural complexity of the D_3R PP and simultaneously modifying the linker length and substitution. To investigate the optimal regiochemistry for introducing the linker and D_3R PP, compound **18** was prepared, where the butyl-4-(2,3-dichlorophenyl)piperazine synthon was introduced to replace the nitrile, while maintaining the MOR 4-(dimethylamino)-2,2-diphenylbutanamide moiety, as seen in both **3** and **6** (Figure 1). In detail, 4-bromo-2,2-diphenylbutanenitrile was first N-alkylated with dimethylamine hydrochloride ($Me_2NH\cdot HCl$) under basic conditions, followed by hydrolysis of the nitrile in the presence of 48% HBr (aq solution) to yield the HBr salt of amino acid **17**. Subsequent amidation mediated by EDC, HOBt, and 4-(4-(2,3-dichlorophenyl)piperazin-1-yl)-butan-1-amine[47] yielded the desired product **18**. Despite the importance of the α-methyl group of **6** being well reported in the literature,[48] favoring the optimal binding pose within the MOR OBS, we decided to study the SAR of structurally simplified analogues. Thus, *via* simple Grignard addition to the nitrile **16**, we prepared the desmethyl-methadone **19**.

In Scheme 2, in order to investigate the structural requirement of the D_3R pharmacophore, in particular, the effect of replacing the basic butyl-4-(2,3-dichlorophenyl)-piperazine, with the corresponding amide analogue, HCTU mediated amide coupling of 5-((*tert*-butoxycarbonyl)amino)-pentanoic acid, followed by removal of the Boc-protecting group, and consequent mono N-alkylation with 4-bromo-2,2-diphenylbutanenitrile afforded the desired product **21**. The longer 5 carbon atom linker, instead of the canonical butyl chain, was chosen because of the increased rigidity of the cyclic amide function and need for extending the tethered PP to an optimal distance.

The switch from 2,2-diphenylbutanenitrile (**4**-like analogues) to *N*,*N*-dimethyl-2,2-diphenylbutanamide (**3**-like analogues) as the MOR PP was achieved, as described in Scheme 3. Starting from the commercially available *N*-(3,3-diphenyldihydrofuran-2(3*H*)-ylidene)-*N*-methylmethanaminium bromide, simple ring opening with the appropriate primary or secondary amines afforded compounds **22**, presenting the **6**-like dimethylamino function, **23**, where the 2,3-dichlorophenyl piperazine D_3R scaffold was introduced, as well as **24**, whose

https://doi.org/10.1021/acs.jmedchem.1c00611
J. Med. Chem. 2021, 64, 7778−7808

Scheme 5[a]

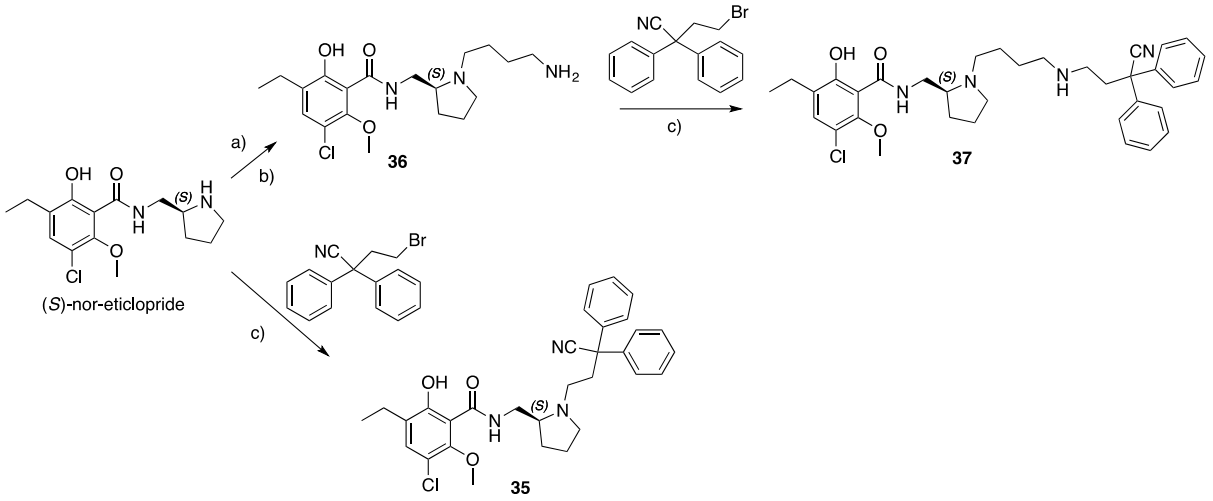

[a](a) *N*-(4-Bromobutyl)phthalimide, K_2CO_3, and ACN, 82 °C, overnight; (b) NH_2NH_2 and EtOH, 80 °C, 3 h, 36% (over two steps); and (c) K_2CO_3 and ACN, 130 °C, overnight, 10−23%.

Scheme 6[a]

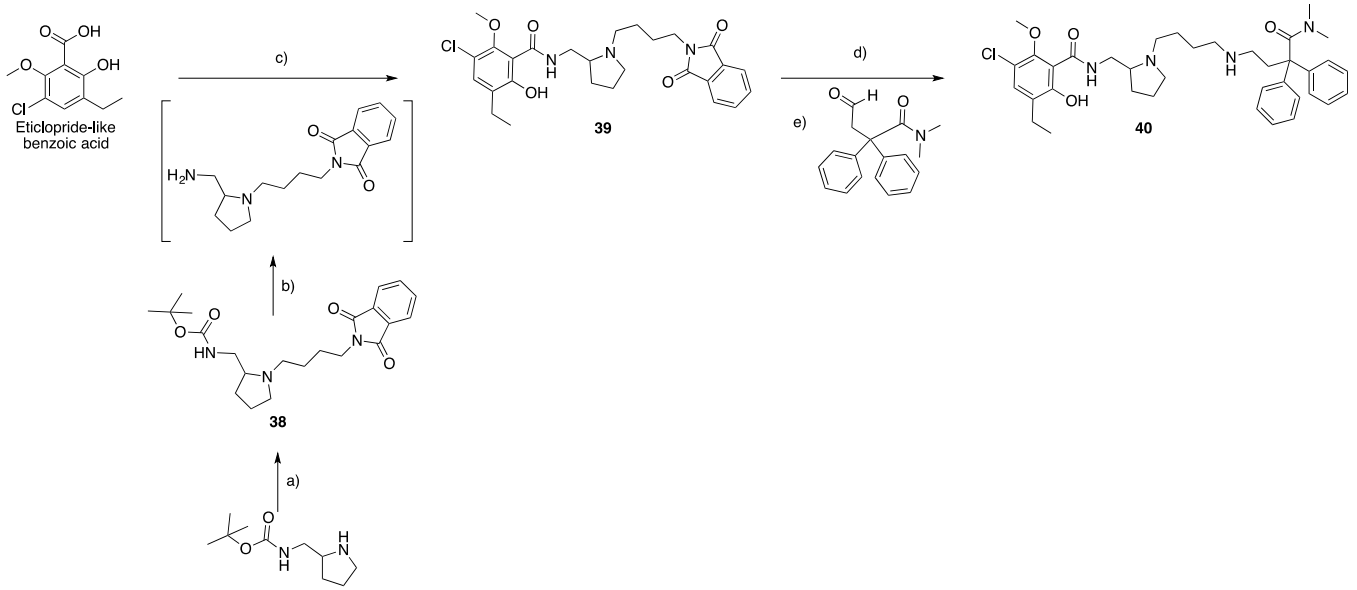

[a](a) *N*-(4-Bromobutyl)phthalimide, K_2CO_3, and ACN, 82 °C, overnight, 85%; (b) TFA and DCM, 25 °C, 3 h; (c) HCTU and DCM, 25 °C, 48 h, 26%; (d) NH_2NH_2 and EtOH, 80 °C, 3 h; and (e) cat. AcOH, STAB, and DCE, 25 °C, 12 h, 21% (over two steps).

1,2,3,4-tetrahydroisoquinoline-7-carbonitrile is another common D_2R/D_3R antagonist PP fragment, present in well-characterized ligands, such as **9**.[49−52]

To investigate the effect of the linker length and substitution on the bivalent hybrid analogues, *N*-(3,3-diphenyldihydrofuran-2(3*H*)-ylidene)-*N*-methylmethanaminium bromide was simply washed with 2 N NaOH in H_2O and extracted with DCM to obtain the alcohol intermediate **25**, which was then oxidized to the aldehyde using DMP and then mono-N-alkylated *via* reductive amination conditions with the appropriate primary and secondary amines. This small library of compounds (**27**, **28**, **29**, **30**, **31**, and **32**) covered a large structural variety of canonical D_3R antagonist PPs, as well as butyl and hydroxyl substituted linkers, known for increasing D_3R subtype selectivity.[53]

Compound **34**, containing the 1,2,3,4-tetrahydroisoquinoline-7-carbonitrile pharmacophore was synthesized according to Scheme 4, *via* preparation of intermediate **33** and reductive amination with **26**.

In order to expand the library toward different D_3R PPs, the canonical piperazine and 1,2,3,4-tetrahydroisoquinoline, inspired by selective D_3R antagonists and partial agonists (**1**, **2**, **7**, and **9**; Figure 1) were replaced in Scheme 5 with the highly decorated phenyl-*N*-(pyrrolidin-2-ylmethyl)benzamide derived from the eticlopride pharmacophore (**8**, Figure 1). Alkylation of (*S*)-nor-eticlopride (obtained from the NIDA Drug Supply Program) with 4-bromo-2,2-diphenylbutanenitrile yielded compound **35**, introducing the 2,2-diphenyl-nitrile MOR PP, tethered by an ethyl linker. Meanwhile, the formation of intermediate **36** allowed the synthesis of analogue **37**, tethered *via* the longer butyl-amino linker.

https://doi.org/10.1021/acs.jmedchem.1c00611
J. Med. Chem. 2021, 64, 7778−7808

Scheme 7[a]

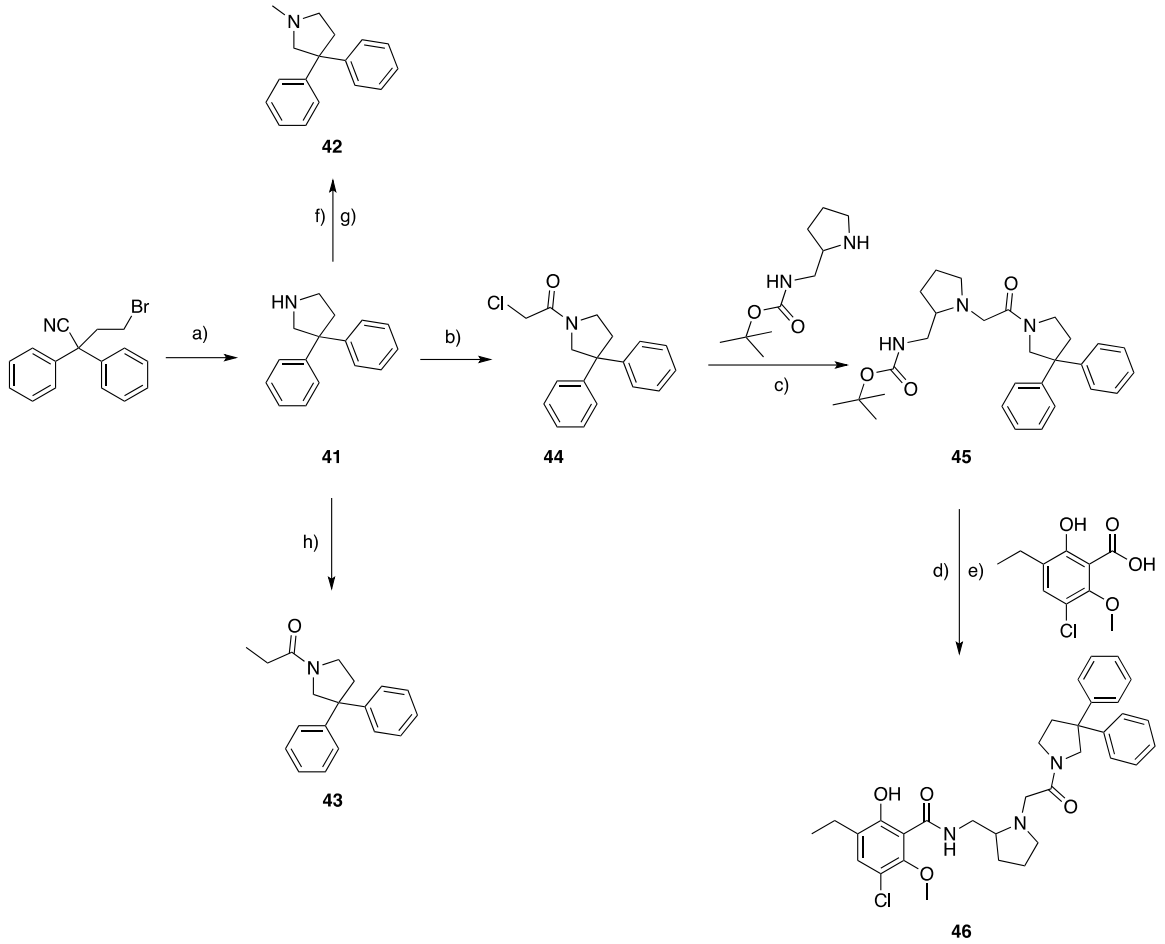

[a](a) LAH and tetrahydrofuran (THF), 0 to 25 °C, 15 h, 40%; (b) 2-chloroacetyl chloride, DIPEA, and THF, 0 to 25 °C, 1 h; (c) cat. KI, K_2CO_3 and ACN, 82 °C, 3 h, 74% (over two steps); (d) TFA and DCM, 25 °C, 2 h; (e) HCTU, DIPEA, and DCM, 25 °C, 3 h, 15% (over two steps); (f) methyl chloroformate, DIPEA, and DCM, 25 °C, 1 h; (g) LAH and THF, 0 to 25 °C, 56% (over two steps); and (h) propionyl chloride, DIPEA, and DCM, 40 °C, overnight, 29%.

Scheme 8[a]

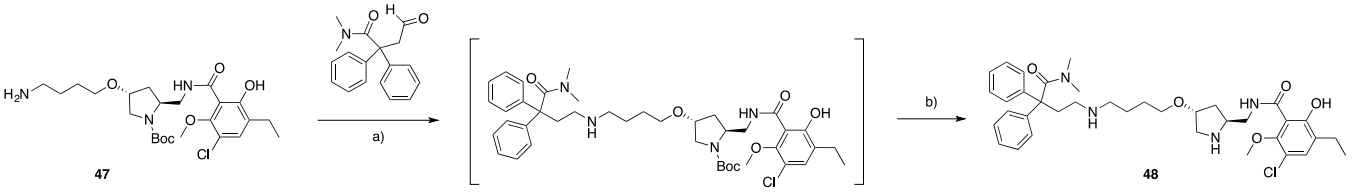

[a](a) Cat. AcOH, STAB, and DCE, 25 °C, 4 h; (b) TFA and DCM, 25 °C, overnight, 8.5% (over two steps).

Analogous to the approach described above for the phenylpiperazine series, we investigated the replacement of the diphenyl nitrile MOR PP, with the **3**-like *N*,*N*-dimethylamide functional group for the **8**-based bivalent analogues. In Scheme 6, the substituted benzoic acid intermediate was prepared following previous literature procedures.[14,54] The benzoic acid was coupled with 2-(4-(2-(aminomethyl)pyrrolidin-1-yl)butyl)isoindoline-1,3-dione, which was freshly prepared *in situ via* selective Boc-deprotection of **38**, prior to the HCTU-mediated amide coupling. The phthalimide group in intermediate **39** was removed, and the resulting primary amine was mono-*N*-alkylated *via* reductive amination to yield **40** as the racemic mixture.

In this case, we decided to synthesize the racemic mixture, starting from the commercially available *tert*-butyl (pyrrolidin-2-ylmethyl)carbamate, because although **8** favors the (*S*) absolute configuration at the pyrrolidine ring, we did not want to exclude the possibility of different stereochemical requirements for this bivalent analogue, as we have seen in another series of bivalent/bitopic D_3R ligands.[46]

SAR for an alternative MOR PP, with a 3,3-diphenyl substituted pyrrolidine, was investigated through the synthesis of analogues in Scheme 7. The common starting material 4-bromo-2,2-diphenylbutanenitrile was reacted with lithium

https://doi.org/10.1021/acs.jmedchem.1c00611
J. Med. Chem. 2021, 64, 7778−7808

Scheme 9[a]

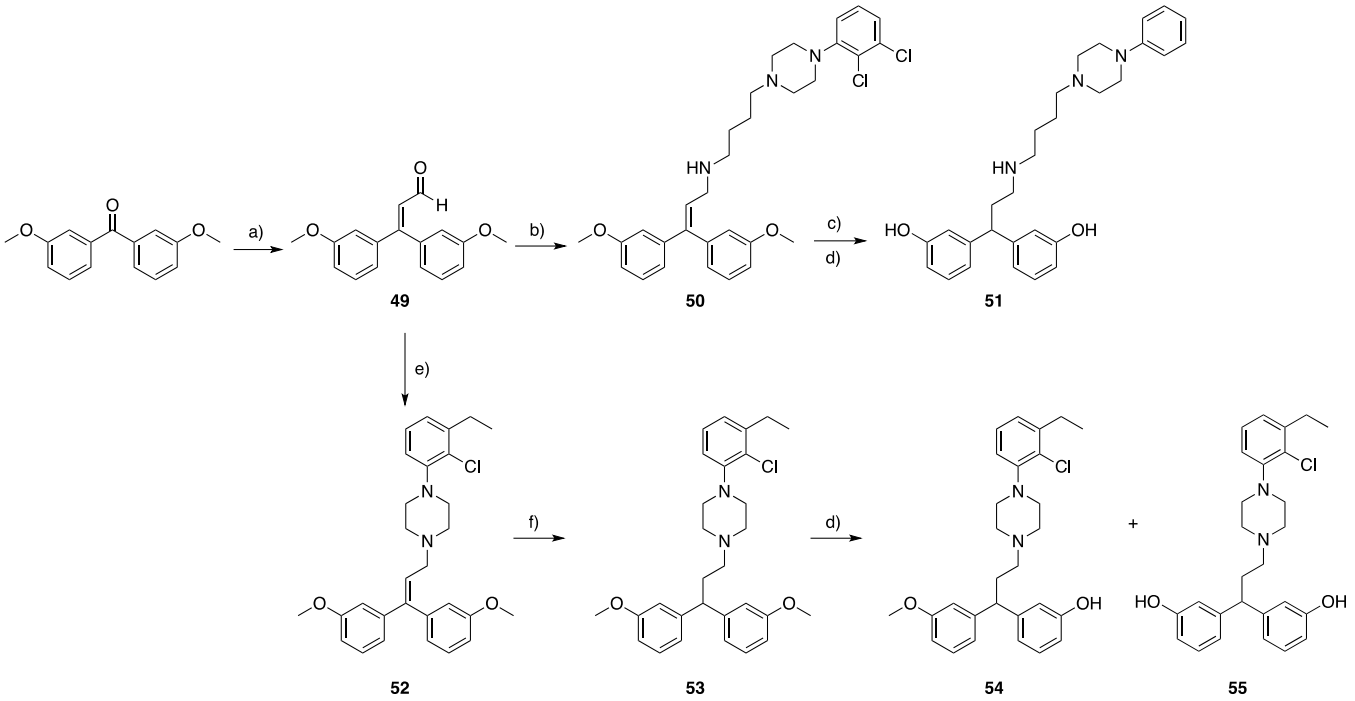

[a](a) Titanium tetrachloride ($TiCl_4$), triethylamine (TEA), and DCM, 0 to 25 °C, overnight, 58%; (b) 4-(4-(2,3-dichlorophenyl)piperazin-1-yl)butan-1-amine, cat. AcOH, STAB, and DCE, 25 °C, 4 h, 88%; (c) H_2 (50 psi), Pd/C (20% wt), and EtOH, 25 °C, 12 h; (d) HBr 33% in AcOH; 118 °C, 48 h, 13−31%; (e) 1-(2-chloro-3-ethylphenyl)piperazine,[14] cat. AcOH, STAB, and DCE, 25 °C, 4 h, 88%; and (f) H_2 (30 psi), Pd/C (20% wt), and EtOAc/EtOH (2:1), 25 °C, 3 h, 75%.

aluminum hydride (LAH) to give the primary amine and consequent ring-closure in a one-pot step. Intermediate **41** was either methylated *via* treatment with methyl chloroformate followed by *in situ* LAH reduction to afford **42** or reacted with propionyl chloride to yield the cyclic amide synthon **43**. This rather simple PP allowed us to evaluate the effect of structural rigidity in **6**- and **3**-like MOR PPs and the effect of replacing the protonatable cyclic amine to a cyclic amide. To prepare the bivalent analogue **46**, **41** was initially acylated with 2-chloroacetyl chloride. Subsequent alkylation of racemic *tert*-butyl (pyrrolidin-2-ylmethyl)carbamate yielded **45**. Finally, Boc-deprotection and amide coupling afforded the desired product.

As consistently observed in previous work,[43] when generating bitopic or bivalent ligand SAR, it is essential to study structural requirements not only for the PP and/or SP but also for regiochemistry and stereochemistry of the linkers, which can play a crucial role in their biological activity.

In Scheme 8, we approached a modification of the regiochemistry for the pyrrolidine D_3R PP scaffold. The final compound **48** presents the MOR diphenyl-*N*,*N*-dimethyl amide PP tethered to the D_3R PP, *via* a butyl ether linker fused in position-4 of the pyrrolidine nucleus, in a rel-trans stereochemistry configuration with respect to the **8** amide PP appended in position-2. This was easily introduced as shown in Scheme 8, starting from **47** *via* reductive amination and Boc-deprotection to ultimately yield **48**.

Extensive *in silico* docking studies and optimization (see the section below) were directed toward improving the dual-target affinity of these new MOR−D_3R analogues and guided us to the synthesis of **51** (Scheme 9). In particular, the hydroxy substitution of the MOR diphenyl PP was based on the *in silico* observation that the *meta*-hydroxy groups will engage a water-mediated hydrogen bond network observed in several known opioid ligands while being well tolerated by the D_3R SP binding site.

Homologation of the commercially available bis(3-methoxyphenyl)methanone in the presence of $TiCl_4$ and TEA[55] allowed the formation of the α,β-unsaturated aldehyde **49**. Reductive amination in the presence of 2,3-dichlorophenyl piperazine yielded **50**, which was hydrogenated in the presence of Pd/C. The crude mixture was then subsequently O-demethylated with 33% HBr in AcOH (Scheme 9).

High-resolution mass spectroscopy (HRMS) and NMR analyses revealed the loss of both chlorine atoms in final product **51**. Retrospective analyses of the previous synthetic steps and intermediates showed that the loss of both chlorine atoms occurred during hydrogenation while reducing the styrenyl olefin. Unfortunately, dehalogenation and concomitant hydrogenation appear to occur faster than the reduction of the desired olefin. Despite replacing Pd/C with PtO_2, the solvent (from EtOH to EtOAc), and H_2 pressure (from 50 to 15−20 psi), the same reaction outcome was observed. Nevertheless, we proceeded in testing **51**, as a proof of concept to validate the biological activity of the newly proposed bis-phenol PP to target the MOR.

The 1-(2-chloro-3-ethylphenyl)piperazine scaffold proved to be resistant to hydrogenation conditions[14] and was introduced as the D_3R PP tethered to the MOR bis-phenol scaffold (Scheme 9). Intermediate **52** was readily prepared by reductive amination, followed by milder hydrogenation conditions (30 psi H_2, using a mixture of EtOAc/EtOH 3:1 as a solvent, for 3 h of total reaction time) to obtain the saturated analogue **53**. Partial and total O-demethylation was again achieved in the

https://doi.org/10.1021/acs.jmedchem.1c00611
J. Med. Chem. 2021, 64, 7778−7808

Scheme 10[a]

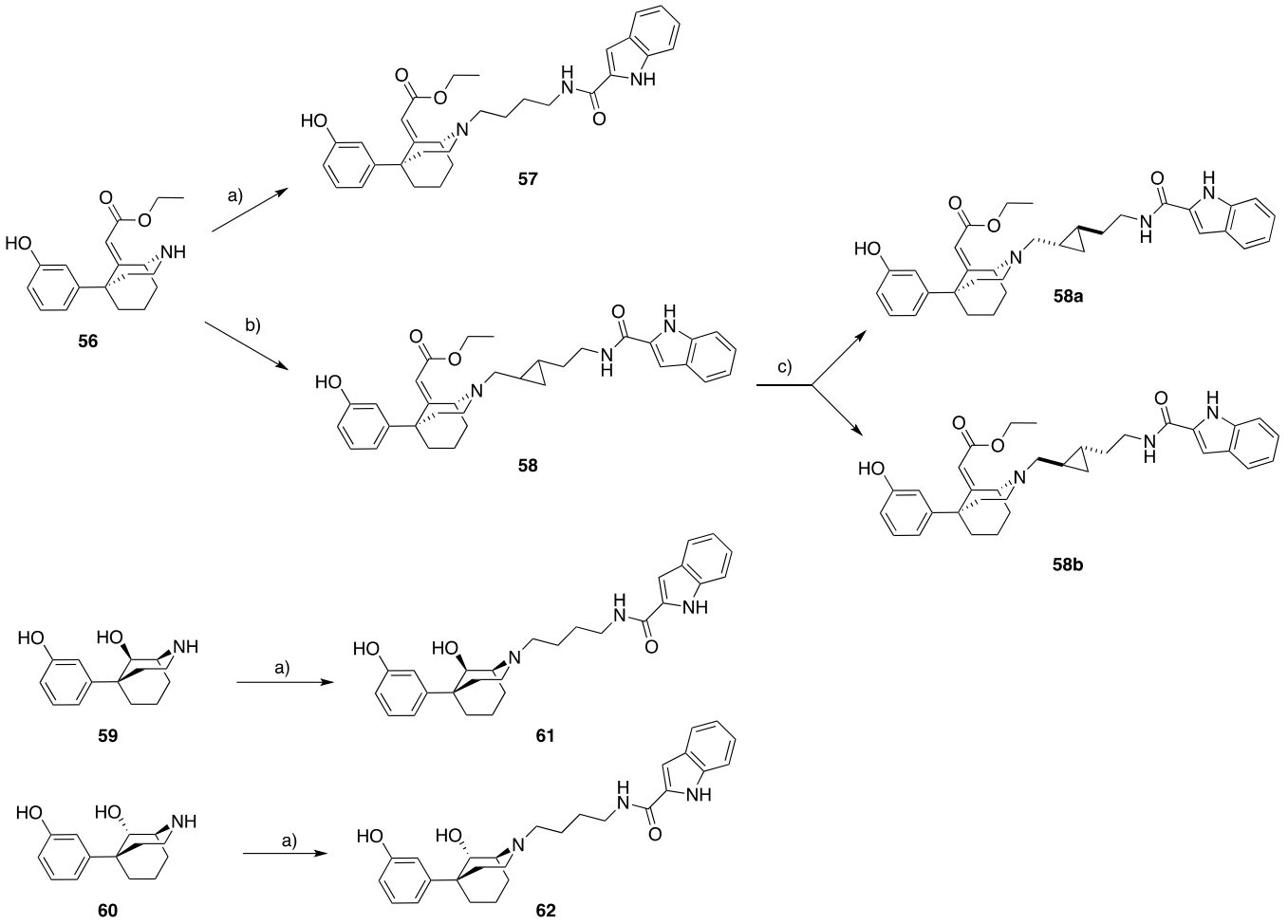

[a](a) *N*-(4-Oxobutyl)-1*H*-indole-2-carboxamide,[57] cat. AcOH, STAB, and DCE, 25 °C, 1.5 h, 26−88%; (b) *trans*-*N*-(2-(2-formylcyclopropyl)-ethyl)-1*H*-indole-2-carboxamide,[45] cat. AcOH, STAB, and DCE, 25 °C, 1.5 h, 65%; and (c) preparative enantioselective high-performance liquid chromatography (HPLC), ChiralPak AD-H column.

presence of 33% HBr in AcOH, and respective products **54** (obtained and tested as the racemic mixture) and **55** were isolated and tested *in vitro*.

To further expand SAR on the MOR PP, in Scheme 10, we synthesized a new library of bitopic analogues presenting different phenylmorphan nuclei as PPs to target the MOR and the well-known 2-indoleamide SP to target D_3R SBP. We were motivated to use this combination of pharmacophores because phenylmorphans are a well-characterized scaffold for obtaining highly potent and selective MOR ligands,[56] and they also structurally resemble phenyl/pyridine morpholino moieties that we extensively studied as D_3R OBS ligands.[45] Moreover, we recently demonstrated how the pyridine morpholine scaffold designed as a D_3R PP can also be structurally tweaked *via* the bitopic approach and linker tethering to target other families of GPCRs, including the MOR.[46] This suggested that simple structural modification of the phenylmorphan scaffold might also exploit affinity for both targets and ultimately be suitable for the generation of bitopic and bivalent hybrids for both the MOR and D_3R.

In Scheme 10, **56** was N-alkylated *via* reductive amination with *N*-(4-oxobutyl)-1*H*-indole-2-carboxamide[57] and *trans*-*N*-(2-(2-formylcyclopropyl)ethyl)-1*H*-indole-2-carboxamide,[45] to obtain **57** and **58**, respectively. We have previously published[45] the importance of the rigid cyclopropyl linker to achieve unique pharmacological profiles, and its stereochemistry is essential in modulating favorable poses for D_3R target recognition, binding affinity, selectivity, and functional efficacy. Thus, both trans enantiomers of **58** were resolved *via* preparative chiral HPLC (**58a** and **58b**) and pharmacologically evaluated. Due to the lack of significant differences between their biological profiles we did not proceed any further in assigning the absolute configuration of each *trans*-cyclopropyl enantiomers for these analogues.

In silico docking predicted that replacing the ethyl acrylate on the phenylmorphan ring with a less sterically hindered group (*e.g.*, ketone or hydroxyl group) would be tolerated within the MOR OBS and could increase the affinity of the new hybrids for the D_3R. Moreover, since the bitopic analogues **57** and **58** showed high affinity for the MOR, but moderate to low binding at D_2-like receptors (Table 2), we aimed to study and invert the stereochemistry of the phenylmorphan ring, while simultaneously evaluating all the possible stereochemical combinations with the hydroxyl group. We synthesized both diastereoisomers **61** and **62**, starting from the fully resolved **59** and **60**, to study not only the effect of the hydroxyl substitution but of its stereochemistry too, in the dual-target binding profile.

https://doi.org/10.1021/acs.jmedchem.1c00611
J. Med. Chem. 2021, 64, 7778−7808

Scheme 11[a]

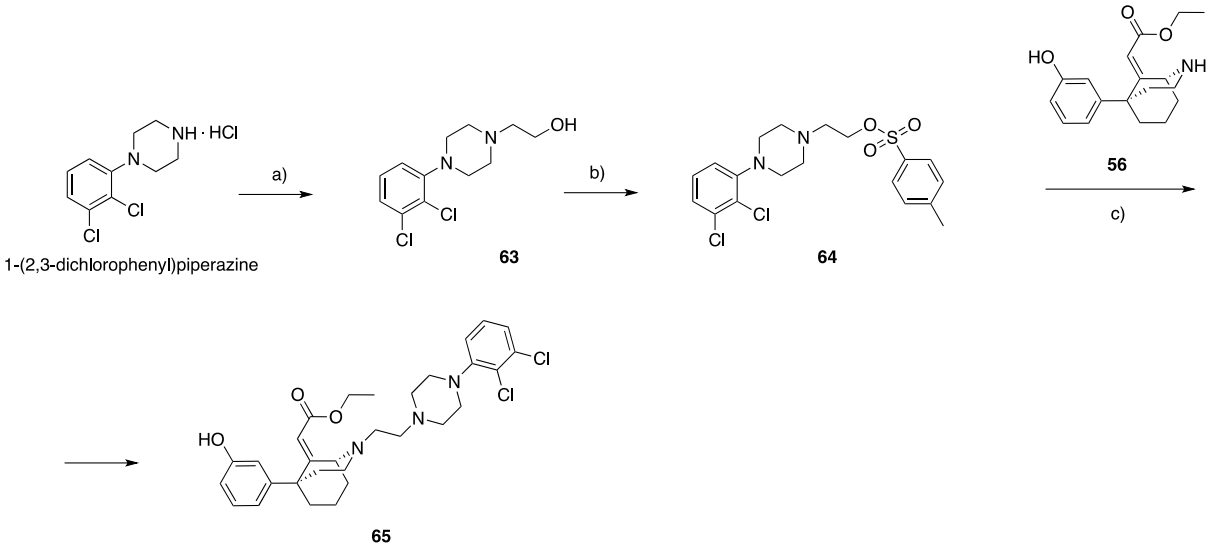

[a](a) 2-Bromoethan-1-ol, K_2CO_3, cat. KI, and ACN, 82 °C, overnight, 60%; (b) *p*-toluenesulfonyl chloride (*p*-TsCl), DIPEA, and DCM, 25 °C, overnight, 36%; (c) $NaHCO_3$ and ACN, 82 °C, 6 h, 43%.

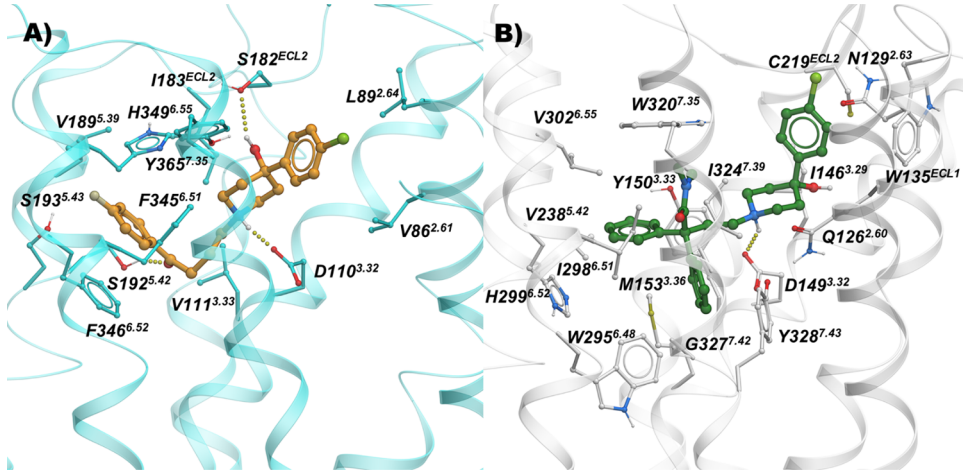

Figure 2. Binding mode of **5** (orange sticks) inside the (A) D_3R (cyan; PDB: 3PBL) and (B) binding mode of **3** (green sticks) inside the MOR (white; PDB: 5C1M).

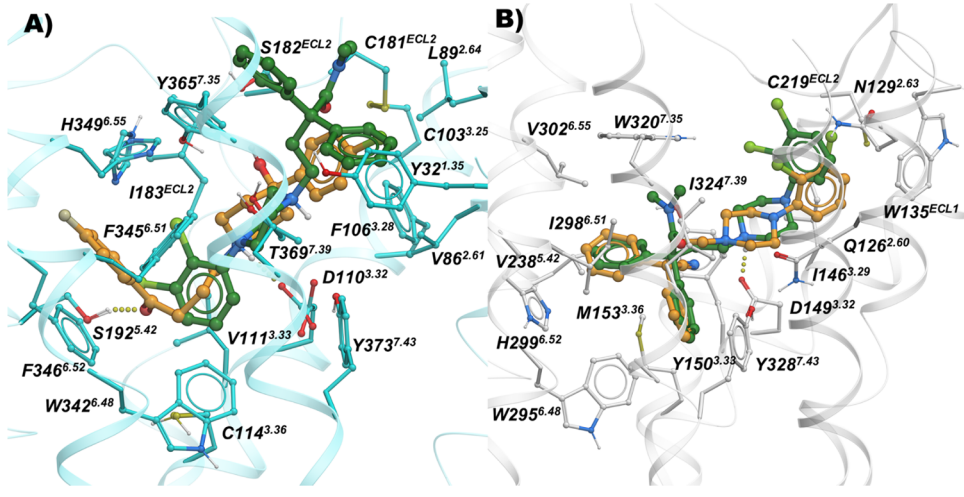

Figure 3. Binding modes of **23** (green) and **5** (orange) inside the (A) D_3R (cyan; PDB: 3PBL) and (B) docking mode of **23** (green) and **13** (orange) inside the MOR (white; PDB: 5C1M).

https://doi.org/10.1021/acs.jmedchem.1c00611
J. Med. Chem. 2021, 64, 7778−7808

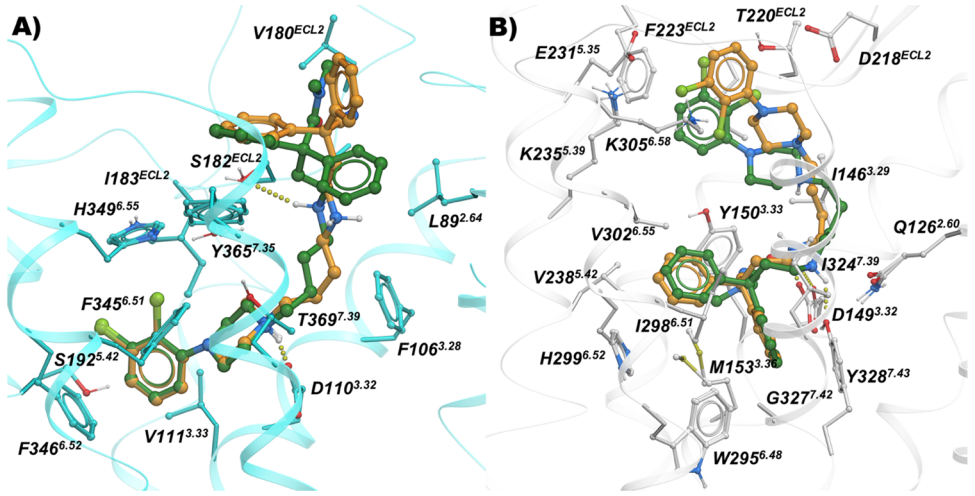

Figure 4. Binding mode of **14** (orange sticks) and **28** (green sticks) inside the (A) D_3R (cyan; PDB: 3PBL) and (B) MOR (white; PDB: 5C1M).

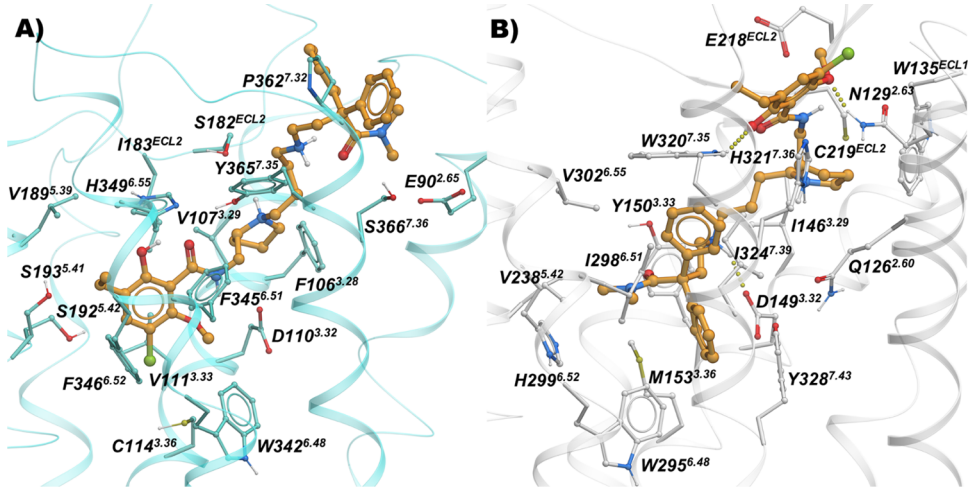

Figure 5. Binding mode of **40** (orange sticks) inside the (A) D_3R (cyan; PDB: 3PBL) and (B) MOR (white; PDB: 5C1M).

Finally, as shown in Scheme 11, we prepared the bivalent analogue of this phenylmorphan series, **65**, presenting both the MOR PP and the canonical D_3R PP 2,3-dichlorophenyl piperazine for D_3R OBS, instead of the 2-indoleamide for SBP binding. The alcohol intermediate **63** was prepared starting from 1-(2,3-dichlorophenyl)piperazine hydrochloride and 2-bromoethan-1-ol, under basic conditions. Tosylation of the hydroxy group and subsequent nucleophilic substitution with **56** yielded the desired product **65**.

Molecular Docking and CADD. We employed structure-based molecular modeling methods to guide the rational design of our dual-target compounds. All atom docking studies on the inactive-state D_3R (PDB: 3PBL)[44] and active-state MOR (PDB: 5C1M)[58] were performed, followed by local optimization of receptor−ligand interactions *via* energy-based Monte Carlo minimization protocols[59] using ICM-Pro (Molsoft LLC). Figure 2 shows optimized binding modes of **5** and **3** inside the D_3R and MOR, respectively, indicating salt bridge interactions between basic nitrogen and conserved $D^{3.32}$ of the receptors. The fluorophenyl butanone moiety of **5** occupies the OBS between TM3, TM5, and TM6 in the D_3R, lined by hydrophobic residues such as $V111^{3.33}$, $V189^{5.39}$, $F345^{6.51}$, $F346^{6.52}$, and $H349^{6.55}$. In the MOR, the diphenyl butanamide moiety of **3** also occupies the OBS pocket similar to canonical MOR ligands such as morphine and methadone, interacting with residues $Y150^{3.33}$, $M153^{3.35}$, $V238^{5.42}$, $W295^{6.48}$, $I298^{6.51}$, $H299^{6.52}$, $V302^{6.55}$, $W320^{7.35}$, $I324^{7.39}$, and $Y328^{7.43}$. Although the chlorophenyl and hydroxy substituents on the piperidine rings are common for both **5** and **3**, these moieties occupy distinct SBPs and interact with different residues in their cognate receptors. Attempts at cross-docking these ligands, that is, dock **5** to the MOR and **3** to the D_3R, were unsuccessful, corroborating selectivity of the PPs to their corresponding OBS pockets.

Figure 3 shows an overlay of MOR and D_3R docking modes of **23**, a compound with the *N*,*N*-dimethyl-diphenylbutanamide PP of the MOR tethered to a 2,3-dichlorophenyl-piperazine PP of canonical D_3R antagonists/partial agonists. In docking to the MOR (Figure 3B), we observed a perfect fit of the MOR PP in the corresponding OBS, while the D_3R PP of **23** was accommodated in the secondary site of the MOR. In the D_3R, the lack of flexibility of the N-linked 2,3-dichlorophenyl of **23** prevented this D_3R PP from reaching its OBS site (Figure 3A). However, the 2,3-dichlorophenyl moiety still comfortably fits the hydrophobic pocket lined by $V111^{3.33}$, $W342^{6.48}$, $F345^{6.51}$, $F346^{6.52}$, and $H349^{6.55}$. The MOR PP moiety of **23**, *N*,*N*-dimethyl-diphenylbutanamide, is placed in a hydrophobic region of the D_3R surrounded by $V86^{2.61}$,

https://doi.org/10.1021/acs.jmedchem.1c00611
J. Med. Chem. 2021, 64, 7778−7808

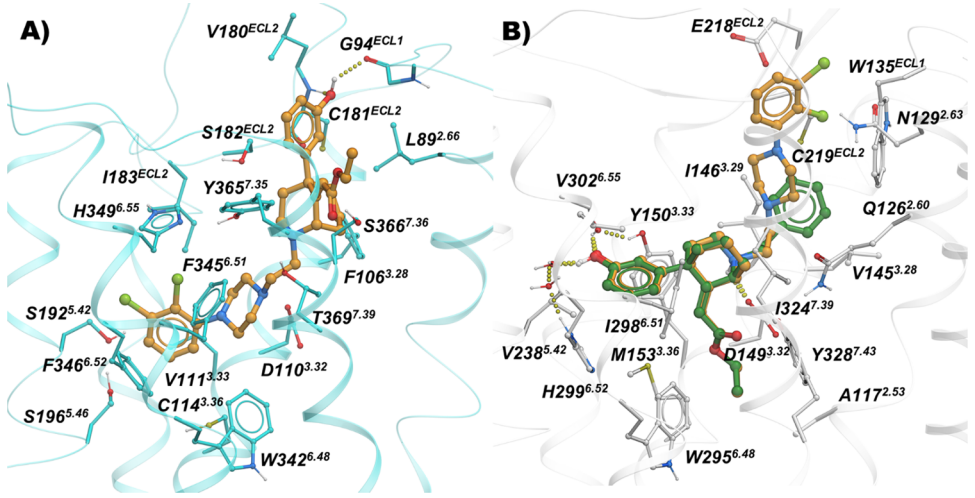

Figure 6. Binding mode of **65** (orange sticks) and **10** (green sticks) inside the (A) D_3R (cyan; PDB: 3PBL) and (B) MOR (white; PDB: 5C1M).

L89$^{2.64}$, C103$^{3.25}$, F106$^{3.28}$, C181^{ECL2}, Y365$^{7.35}$, and T369$^{7.39}$ and makes additional interactions resulting in comparable docking scores for the MOR and D_3R, supporting the synthesis of this compound.

In contrast, despite D_3R SAR that supported introduction of the butyl linker between the tethered *N*,*N*-dimethyl-diphenylbutanamide or 2,2-diphenylbutanenitrile MOR PP and the 2,3-dichlorophenyl-piperazine, as seen in compounds such as **14** and **28**, this design had no effect on the placement of the compounds in the OBS of the D_3R, while the corresponding SP motif moves further toward the extracellular region, away from the hydrophobic residues of TM2, TM3, and ECL2 (Figure 4).

The *meta*-hydroxy compounds were designed to avail the water-mediated hydrogen bonding network close to H299$^{6.52}$ and Y150$^{3.33}$ in the MOR, such as **51**, **54**, and **55** indeed indicate the presence of those predicted hydrogen bonds, while the 2-chloro-3-ethyl-substituted phenyl-piperazine D_3R PP motif is tolerated in the voluminous and solvent-accessible MOR pocket (Figure S1). Furthermore, the highly decorated **8**-based D_3R PP of compounds **40** and **48** are placed expectedly in the OBS of the D_3R, and like the substituted phenyl analogues, the *N*,*N*-dimethyl-diphenylbutanamide motif occupies hydrophobic subpockets between TM2, TM3, ECL2, and TM7 (Figure 5).

The conformationally restricted ethyl-2-(-5-(3-hydroxyphenyl)-2-azabicyclo[3.3.1]nonan-9-ylidene)acetate MOR PP motif of **10** expectedly docks in the MOR hydrophobic pocket formed between TM3−TM5−TM6−TM7, and 3-hydroxyphenyl forms water-mediated hydrogen bonding interactions with H299$^{6.52}$ and Y150$^{3.33}$. The ethyl phenyl tail of **10** shares the same hydrophobic subpocket between TM2 and TM3 engaged by **fentanyl**-like compounds. The docking mode of **65** overlaps completely with the binding mode of **10**, except the fact that extended 2,3-dichlorophenyl piperazine of **65** moves slightly toward the extracellular region and is placed in the subpocket between TM2−TM3−ECL2. The 2,3-dichlorophenyl piperazine of **65** is docked in the OBS of the D_3R, while the ethyl-2-(-5-(3-hydroxyphenyl)-2-azabicyclo[3.3.1]-nonan-9-ylidene)acetate moiety is placed in the hydrophobic SBP region (Figure 6).

Binding Studies and SARs. All the newly synthesized compounds were tested for their binding affinities at the hMOR (in competition with [^{3}H]-DAMGO), hD_2R, hD_3R, and hD_4R [in competition with [^{3}H]-*N*-methylspiperone ([^{3}H]-NMSP) for all the hD_2-like subtypes]. Moreover, a subset of selected hits were further studied at hD_2R and hD_3R using the agonist [^{3}H]-(*R*)-(+)-7-OH-DPAT as the competing radioisotope. We have previously observed and reported that differences in affinity due to the radioligand being an agonist or antagonist can predict functional efficacy profiles for the tested compounds.[45,60]

In Table 1, the binding data are reported for the first series of MOR−D_3R hybrid analogues, based on, **3**-, **4**-, and **6**-like PPs. Reference compounds, including **fentanyl**, **3**, **4**, **5**, and **6**, are reported in the table for useful comparisons. Among the reference compounds, it was interesting to observe how **3**, a well-known potent MOR agonist, despite presenting an SP identical to the D_2-like antagonist **5** (Figure 1), binds with low micromolar affinity to all the D_2-like subtypes, as predicted in the CADD studies. **Fentanyl**, **4**, and **6** all have low nanomolar affinities for the MOR, as expected and consistent with the literature.[61,62] **Fentanyl**, however, presents moderate affinity for D_4R (K_i = 554 nM), while being inactive at both the D_2R and D_3R (K_is > 10,000 nM); meanwhile, **6** is endowed with a preferential low micromolar affinity for the D_3R, being completely inactive at D_2R and >10-fold selective over D_4R. These data highlight how subtle structural changes in well-characterized MOR agonists can induce different binding profiles and subtype selectivity for the D_2-like dopamine receptors and that binding affinities can be directed toward dual-target profiles with well-designed structural modifications.

The docking studies showed that the MOR PP motifs (*N*,*N*-dimethyl-diphenylbutanamide and 2,2-diphenylbutanenitrile) occupy primarily hydrophobic pockets in both the D_3R and MOR. In the case of the MOR, this pocket formed between TM3, TM5, TM6, and TM7 is an accumulation of three subpockets lined by (a) V238$^{5.42}$, M153$^{3.33}$, H299$^{6.52}$, I298$^{6.51}$, and V302$^{6.55}$, (b) M153$^{3.33}$, W295$^{6.48}$, and Y328$^{7.43}$, and (c) W320$^{7.35}$, I324$^{7.39}$, I298$^{6.51}$, and V302$^{6.55}$. In the D_3R, these MOR PP motifs occupy a hydrophobic SBP between TM2, TM3, and ECL2 (Figures 3 and 4). In general, replacing the nitrile group with the **3**-like *N*,*N*-dimethylamide synthon significantly increased the affinity profiles of all the analogues. In particular, **23** presents one of the highest MOR affinities among all the new analogues (MOR K_i = 0.832 nM), and

https://doi.org/10.1021/acs.jmedchem.1c00611
J. Med. Chem. 2021, 64, 7778−7808

Table 1. Radioligand Competition Binding Affinity Data for All the MOR Diphenyl PP Analogues Based on 3, 4, and 6 at hMOR and hD$_2$-like Receptor Subtypes[a]

Compound	Structure	[^{3}H]-DAMGO	[^{3}H]-*N*-methylspiperone			[^{3}H]-(R)-(+)-7-OH-DPAT	
		MOR K_i ± SEM (nM)	D_2R K_i ± SEM (nM)	D_3R K_i ± SEM (nM)	D_4R K_i ± SEM (nM)	D_2R K_i ± SEM (nM)	D_3R K_i ± SEM (nM)
Fentanyl	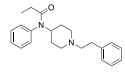	5.23 ± 0.266 (n=5)	21000 ± 1760 (n=3)	26200 ± 3830 (n=4)	554 ± 17.7 (n=3)	ND	ND
Loperamide (3)	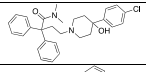	0.268 ± 0.0227 (n=3)	5790 ± 366 (n=4)	1940 ± 78.8 (n=3)	1850 ± 291 (n=4)	ND	ND
Diphenoxylate (4)	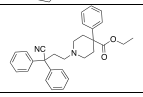	12.37[c]	ND	ND	ND	ND	ND
Haloperidol (5)	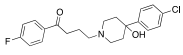	2470 ± 236 (n=3)	3.55 ± 0.296 (n=3)	4.40 ± 0.202 (n=4)	1.43 ± 0.229 (n=3)	ND	ND
Methadone (6)		13 ± 1.11 (n=5)	>100000[b]	2110 ± 167 (n=3)	26200 ± 11900 (n=3)	ND	ND
12	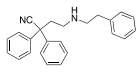	1170 ± 158 (n=3)	17600 ± 1400 (n=4)	8960 ± 901 (n=3)	13900 ± 5930 (n=3)	ND	ND
13	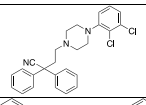	266 ± 50.9 (n=3)	2630 ± 259 (n=3)	2240 ± 1040 (n=5)	8490 ± 3610 (n=3)	ND	ND
14	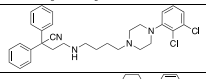	490 ± 64.2 (n=5)	149 ± 9.80 (n=3)	132 ± 26.3 (n=5)	25.9 ± 7.17 (n=4)	36.3 ± 11.9 (n=3)	67.9 ± 13 (n=5)
15	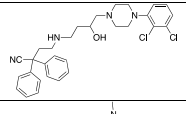	63.5 ± 6.60 (n=3)	903 ± 362 (n=3)	460 ± 148 (n=4)	426 ± 84.5 (n=3)	ND	ND
16		3910 ± 669 (n = 4)	17900 ± 410 (n=3)	16100 ± 734 (n=3)	23200 ± 3280 (n=3)	ND	ND
18	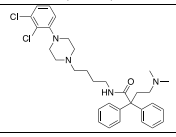	1470 ± 222 (n=4)	42.7 ± 7.04 (n=4)	11.8 ± 1.83 (n=3)	466 ± 85.7 (n=3)	ND	ND
19		35.9 ± 5.34 (n=3)	34900 ± 8520 (n=3)	4270 ± 302 (n=3)	>100000[b]	ND	ND
21	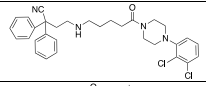	60.8 ± 10.8 (n=3)	1940 ± 308 (n=3)	1360 ± 373 (n=3)	3930 ± 244 (n=3)	ND	ND
22		649 ± 68.9 (n=3)	>100000[b]	36900 ± 5000 (n=3)	20200 ± 2340 (n=3)	ND	ND
23	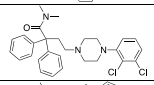	0.832 ± 0.121 (n=3)	74.7 ± 7.50 (n=3)	171 ± 49.2 (n=5)	102 ± 19.2 (n=3)	31.3 ± 1.14 (n=3)	316 ± 67.4 (n=5)
24	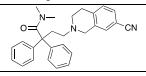	18.2 ± 1.7 (n=4)	2270 ± 243 (n=3)	1630 ± 262 (n=4)	18000 ± 1650 (n=3)	ND	ND
27	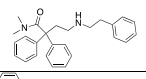	50.4 ± 7.84 (n=3)	3650 ± 1210 (n=3)	2080 ± 317 (n=3)	12600 ± 5030 (n=3)	ND	ND
28	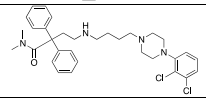	23.8 ± 4.91 (n=3)	43.9 ± 9.04 (n=3)	39.2 ± 11.3 (n=5)	378 ± 80.3 (n=4)	23.1 ± 8.62 (n=3)	33.9 ± 4.20 (n=5)
29	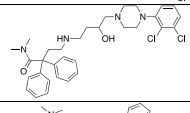	58.8 ± 9.03 (n=3)	700 ± 97.6 (n=3)	572 ± 65.6 (n=4)	2780 ± 531 (n=3)	167 ± 24.4 (n=3)	209 ± 32 (n=3)
30	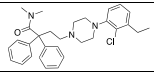	0.842 ± 0.192 (n=3)	43.0 ± 9.26 (n=3)	69.0 ± 6.20 (n=4)	64.8 ± 13.6 (n=3)	20.3 ± 3.93 (n=3)	197 ± 20.1 (n=3)

https://doi.org/10.1021/acs.jmedchem.1c00611
J. Med. Chem. 2021, 64, 7778−7808

Table 1. continued

Compound	Structure	[^{3}H]-DAMGO	[^{3}H]-*N*-methylspiperone			[^{3}H]-(R)-(+)-7-OH-DPAT	
		MOR K_i ± SEM (nM)	D_2R K_i ± SEM (nM)	D_3R K_i ± SEM (nM)	D_4R K_i ± SEM (nM)	D_2R K_i ± SEM (nM)	D_3R K_i ± SEM (nM)
31	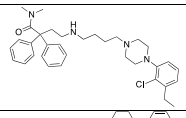	264 ± 56.7 (n=3)	62.1 ± 14.7 (n=3)	17.8 ± 2.80 (n=4)	503 ± 66.6 (n=3)	44.2 ± 14 (n=3)	38.3 ± 5.89 (n=3)
32	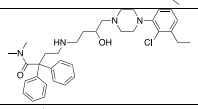	330 ± 22.1 (n=3)	457 ± 18.8 (n=3)	123 ± 6.37 (n=4)	1260 ± 267 (n=3)	114 ± 15.6 (n=3)	123 ± 6.57 (n=3)
34	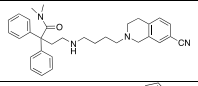	150 ± 22.3 (n=3)	1240 ± 66.1 (n=3)	1060 ± 113 (n=4)	58900 ± 10400 (n=3)	ND	ND
35	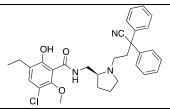	11100 ± 2040 (n=5)	12400 ± 3620 (n=5)	1550 ± 286 (n=5)	>100000[b]	ND	ND
37	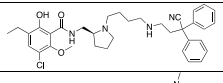	866 ± 144 (n=5)	1730 ± 585 (n=5)	260 ± 111 (n=5)	6610 ± 2460 (n=3)	ND	ND
40	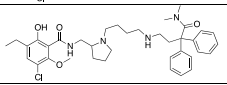	106 ± 3.25 (n=3)	502 ± 32 (n=3)	135 ± 13.2 (n=3)	3420 ± 436 (n=3)	93.7 ± 19.4 (n=3)	146 ± 16.1 (n=5)
42		8500 ± 1070 (n=3)	>100000[b]	>100000[b]	35400 ± 7800 (n=3)	ND	ND
43		15000 ± 817 (n=3)	>100000[b]	>100000[b]	>100000[b]	ND	ND
46	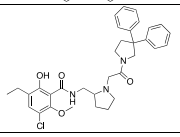	14200 ± 701 (n=3)	2380 ± 430 (n=3)	288 ± 53.1 (n=3)	31000 ± 16400 (n=3)	ND	ND
48	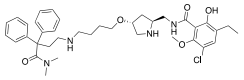	559 ± 76.3 (n=3)	9.41 ± 2.26 (n=3)	2.21 ± 0.762 (n=3)	674 ± 73.2 (n=3)	ND	ND
50	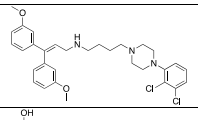	10100 ± 2700 (n=4)	5240 ± 445 (n=3)	342 ± 30.9 (n=4)	26100 ± 3310 (n=3)	ND	ND
51	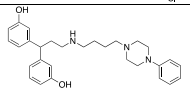	213 ± 6.78 (n=4)	987 ± 8.09 (n=3)	249 ± 29.8 (n=3)	422 ± 72 (n=3)	ND	ND
53	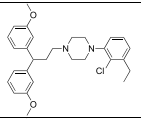	3880 ± 7986 (n=3)	170 ± 8.04 (n=3)	93.8 ± 3.37 (n=3)	63.4 ± 10.7 (n=3)	ND	ND
54	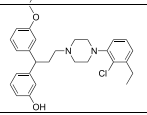	238 ± 10.6 (n=3)	190 ± 16.5 (n=3)	235 ± 14.1 (n=3)	38.5 ± 5.46 (n=3)	ND	ND
55	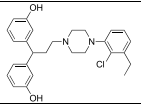	327 ± 26 (n=3)	187 ± 27 (n=3)	200 ± 26.2 (n=3)	19.2 ± 0.431 (n=3)	ND	ND

[a]All the affinity values are expressed as K_i ± standard error of the mean (SEM), derived from IC_{50} values using the Cheng–Prusoff equation,[63] and calculated as the mean of at least three independent experiments (n = number of independent experiments), each performed in triplicate. ND = not determined. [b]No inhibition of specific radioligand binding was observed at the highest tested concentration in one to three independent experiments, each performed in triplicate. [c]K_i value obtained from ref 61.

despite the shorter linker, which is generally less favorable for D_2-like receptors affinity, we still obtained a potent D_2-like ligand (D_2R K_i = 74.7 nM, D_3R K_i = 171 nM, and D_4R K_i = 102 nM). A similar nanomolar binding profile across the D_2R and D_3R was also confirmed when **23** was tested in the presence of [^{3}H]-(*R*)-(+)-7-OH-DPAT. The analogous nitrile compound, **13**, showed reduced MOR binding (~320-fold; K_i

https://doi.org/10.1021/acs.jmedchem.1c00611
J. Med. Chem. 2021, 64, 7778−7808

Table 2. Radioligand Competition Binding Affinity Data, for All the MOR-Substituted Phenylmorphan PP Analogues, at the hMOR and hD$_2$-like Receptor Subtypes[a]

Compound	Structure	[^{3}H]-DAMGO	[^{3}H]-*N*-methylspiperone			[^{3}H]-(R)-(+)-7-OH-DPAT	
		MOR K_i ± SEM (nM)	D$_2$R K_i ± SEM (nM)	D$_3$R K_i ± SEM (nM)	D$_4$R K_i ± SEM (nM)	D$_2$R K_i ± SEM (nM)	D$_3$R K_i ± SEM (nM)
10	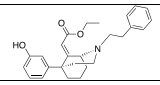	0.633 ± 0.0335 (n=3)	636 ± 63.8 (n=3)	1720 ± 125 (n=3)	5470 ± 304 (n=3)	186 ± 14.7 (n=3)	2300 ± 236 (n=3)
11	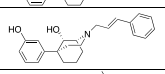	0.377 ± 0.0122 (n=3)	7380 ± 123 (n=3)	15700 ± 569 (n=3)	36900 ± 2260 (n=3)	2790 ± 758 (n=3)	20000 ± 1930 (n=3)
56	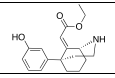	474 ± 140 (n=5)	>100000[b]	>100000[b]	>100000[b]	ND	ND
57	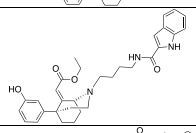	57.2 ± 3.93 (n=4)	2950 ± 507 (n=4)	13700 ± 7370 (n=3)	13800 ± 3140 (n=3)	ND	ND
58	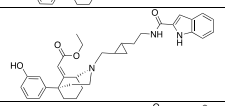	19.7 ± 1.76 (n=4)	3890 ± 896 (n=4)	4350 ± 623 (n=3)	23400 ± 11100 (n=3)	ND	ND
***rel*-58a**	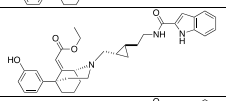	13.5 ± 2.05 (n=3)	2860 ± 624 (n=3)	1290 ± 165 (n=3)	29200 ± 15700 (n=3)	ND	ND
***rel*-58b**	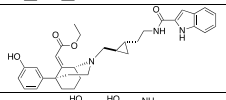	56.2 ± 6.77 (n=3)	4860 ± 1320 (n=3)	2300 ± 916 (n=3)	17600 ± 7880 (n=3)	ND	ND
59	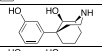	3200 ± 212 (n=3)	>100000[b]	>100000[b]	>100000[b]	>100000[b]	>100000[b]
60	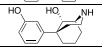	172 ± 9.78 (n=3)	>100000[b]	>100000[b]	>100000[b]	>100000[b]	>100000[b]
61	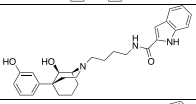	988 ± 336 (n=3)	4530 ± 1640 (n=3)	232 ± 53.3 (n=3)	5630 ± 1640 (n=3)	ND	ND
62	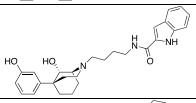	464 ± 219 (n=4)	1310 ± 469 (n=3)	79.6 ± 25.6 (n=3)	3810 ± 291 (n=3)	ND	ND
65	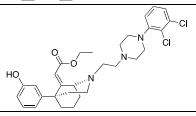	92.7 ± 22.4 (n=3)	51.6 ± 19.7 (n=3)	139 ± 37.7 (n=3)	1600 ± 62.8 (n=3)	ND	ND

[a]All the affinity values are expressed as K_i ± SEM, derived from IC_{50} values using the Cheng−Prusoff equation,[63] and calculated as the mean of at least three independent experiments (n = number of independent experiments), each performed in triplicate. ND = not determined. [b]No inhibition of specific radioligand binding was observed at the highest tested concentration in one to three independent experiments, each performed in triplicate.

= 266 nM) and reduced D$_3$R binding (~13-fold; K_i = 2240 nM).

The docking studies of butyl-linked compounds show that in the D$_3$R, the *N*,*N*-dimethyl-diphenylbutanamide and 2,2-diphenylbutanenitrile MOR PP motifs move further toward the extracellular region, away from the hydrophobic residues of TM2, TM3, and ECL2 (Figure 4). Perhaps, because of this conformational change, *N*,*N*-dimethylamide to cyano substitutions on the extended linker molecules such as **14** (D$_2$R K_i = 149 nM and D$_3$R K_i = 132 nM) are better tolerated at the D$_3$R than the shorter linker compounds such as **13** (D$_2$R K_i = 2630 nM and D$_3$R K_i = 2240 nM). As in the D$_3$R, the extended linker compounds are reasonably well tolerated inside the MOR. However, in contrast to its binding profile at the D$_3$R, even the extended linker molecule with nitrile substitutions **14** shows reduced MOR binding (K_i = 490 nM). This was also observed with the nitrile analogues, **35** and **37**. Compound **28**, an analogous compound with substituted *N*,*N*-dimethylamide in the MOR PP motif, shows significant improvement in both D$_3$R affinity (K_i = 39.2 nM) and MOR binding (K_i = 23.8 nM). This was the first hit analogue in this series to show a low nanomolar dual-target affinity for both the MOR and the D$_2$-like receptors. In contrast, compound **18** showed similarly high affinity for the D$_2$-like receptors, but MOR affinity was diminished (K_i = 1470 nM), whereas compounds **15**, **19**, **21**, **24**, and **27** showed the opposite profile, having higher affinities for the MOR than the D$_2$R or D$_3$R. Compounds **16** and **22** were poorly active at all receptors tested, reflecting an inability to bind the OBS of either MOR or the D$_2$-like receptors.

Introduction of the hydroxy substituent in the butylamine linker (compounds **29** and **32**), as well as replacement of the 2,3-dichlorophenyl piperazine, with the 2-chloro-3-ethylphenylpiperazine (compounds **31** and **32**) either maintained or slightly decreased the overall affinity for all the D$_2$-like

https://doi.org/10.1021/acs.jmedchem.1c00611
J. Med. Chem. 2021, 64, 7778−7808

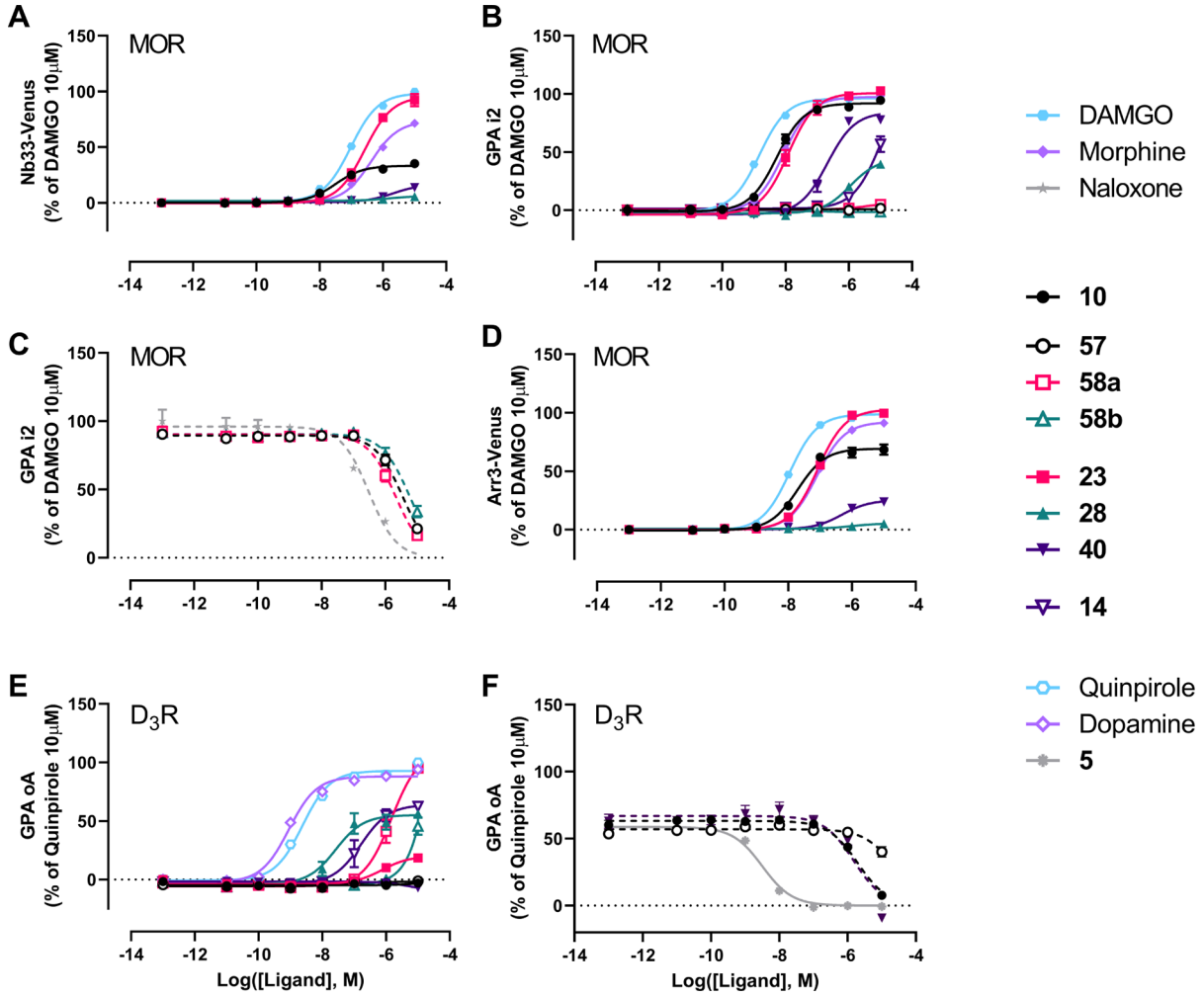

Figure 7. Functional profiles of selected MOR−D_3R hybrids. Each panel shows a different signaling readout: (A) Nb33 recruitment at the MOR, (B) MOR-mediated $G\alpha_{i2}$ protein activation, (C) antagonism at the MOR using GPA in the presence of 100 nM DAMGO, (D) arrestin-3 recruitment at the MOR in the presence of overexpressed GRK2, (E) D_3R-mediated $G\alpha_{oA}$ protein activation, and (F) antagonism at the D_3R using GPA in the presence of 3 nM quinpirole. In order to ensure that test ligands achieved maximal receptor occupancy possible before agonist addition, all ligands were added to the cells 3 h prior to activating the D_3R with quinpirole and measuring BRET signals with the exception of **5**. Dotted lines represent fits where the bottom asymptote was constrained to be 0%.

receptor subtypes, when compared to **28** and shown in Figure S2. The introduction of 1,2,3,4-tetrahydroisoquinoline-7-carbonitrile as the D_3R PP (**34**) decreased affinity for the D_2-like receptors into the micromolar range. None of the diphenyl-pyrrolidine analogues (compounds **42**, **43**, and **46**) were active. However, the only bivalent compound **46** did have moderate affinity for the D_3R (K_i = 288 nM).

Removal of either nitrile or amide functions from the diphenyl MOR PP and introduction of the *meta*-hydroxy substituents to the bis-phenyl system, **51**, were tolerated as suggested from the docking predictions (Figure S1). Despite the presence of a simple unsubstituted phenylpiperazine pharmacophore, **51** still maintained moderate affinities at both the MOR (K_i = 213 nM) and D_3R (K_i = 249 nM).

When the bis-*meta*-phenol MOR PP was used in combination with the 2-chloro,3-ethyl-phenylpiperazine D_3R PP, tethered *via* the shorter (two methylene units) linker (**55**), moderate affinity for all the targets of interest was maintained, but this analogue was not significantly different from the longer linker analogue **51**. The presence of the *meta*-hydroxy substituents also retained D_2-like affinity for **55**, similar to that observed for **23** and **30** (containing the **3**-like MOR PP). In a continuation of a trend noted previously, we observed a significant loss of affinity at the MOR, with **55** presenting a binding K_i >300-fold less than **30** and **23**. These results suggest that while the bis-phenol MOR PP is well tolerated as an alternative to the more canonical **3**-like di-phenyl-*N*,*N*-dimethylamide, the binding profile is still dependent on the linker length, rigidity, and overall substitutions on the D_3R PP as well.

In agreement with the CADD, the meta-substitutions in bis-phenyl-containing compounds are important for MOR recognition. The methoxy analogues result in partial loss of MOR affinity with a general binding profile of **53** (di-methoxy) < **54** (mono-methoxy) ∼ **55** (di-hydroxy). This, however, does not apply for D_2-like binding, where all three analogues show moderate affinities for all the subtypes independent of *meta*-methoxy or *meta*-hydroxy substitutions on the bis-phenyl rings, interestingly with higher affinities at D_4R.

Shifting from a phenylpiperazine-based D_3R PP to a highly decorated **8**-based D_3R PP, to develop SAR around the pyrrolidine scaffold, **40**, containing a racemic pyrrolidin-2-

https://doi.org/10.1021/acs.jmedchem.1c00611
J. Med. Chem. 2021, 64, 7778−7808

Table 3. Potencies and Efficacies at the MOR and D_3R[a]

	MOR Nb33 recruitment		MOR G_{i2} activation			MOR arr3 recruitment (+GRK2)		D_3R G_{oA} activation		
compound	pEC_{50} ± SEM [nM]	E_{max} ± SEM (%)	pEC_{50} ± SEM [nM]	E_{max} ± SEM (%)	pIC_{50} ± SEM [nM]	pEC_{50} ± SEM [nM]	E_{max} ± SEM (%)	pEC_{50} ± SEM [nM]	E_{max} ± SEM (%)	pIC_{50} ± SEM [nM]
DAMGO	7.02 ± 0.04 [95.9] (n = 3)	100	8.83 ± 0.03 [1.50] (n = 9)	100		7.97 ± 0.03 [11.1] (n = 3)	100			
morphine	6.38 ± 0.05 [416] (n = 3)	73.4 ± 1.7	8.06 ± 0.03 [8.66] (n = 6)	97.4 ± 1.1		7.10 ± 0.04 [79.8] (n = 3)	92.1 ± 1.4			
naloxone					6.52 ± 0.1 [305] (n = 3)					
quinpirole								8.62 ± 0.05 [2.39] (n = 7)	100	
dopamine								9.05 ± 0.05 [0.896] (n = 3)	88.0 ± 1.3	
haloperidol (5)										8.46 ± 0.07 [3.49] (n = 3)
10	7.51 ± 0.10 [31.3] (n = 3)	33.3 ± 1.2	8.28 ± 0.05 [5.29] (n = 9)	91.9 ± 1.3		7.70 ± 0.07 [20.0] (n = 3)	69.3 ± 1.7	NA	NA	5.70 ± 0.06 [1997] (n = 3)
14	NA	NA	4.98 ± 0.29 [10,530] (n = 6)	114.9 ± 39.2		NA	NA	6.78 ± 0.15 [165] (n = 4)	63.8 ± 4.2	
23	6.58 ± 0.06 [266] (n = 3)	95.5 ± 2.7	7.91 ± 0.06 [12.3] (n = 3)	100.8 ± 2.1		7.08 ± 0.03 [83.3] (n = 3)	102.7 ± 1.3	6.13 ± 0.16 [747] (n = 3)	20.2 ± 2.1	
28	NA	NA	5.96 ± 0.09 [1107] (n = 3)	44.5 ± 2.4		NA	NA	7.58 ± 0.16 [26.4] (n = 3)	55.0 ± 3.2	
40	5.67 ± 0.20 [2136] (n = 3)	16.6 ± 2.1	6.68 ± 0.08 [211] (n = 3)	84.4 ± 2.9		6.32 ± 0.11 [484] (n = 3)	25.3 ± 1.3	NA	NA	5.82 ± 0.15 [1515] (n = 3)
57	NA	NA	NA	NA	5.45 ± 0.05 [3522] (n = 5)	NA	NA	NA	NA	>5 (n = 3)
58a	NA	NA	NA	NA	5.68 ± 0.05 [2102] (n = 6)	NA	NA	5.83 ± 0.08 [1498] (n = 4)	110.6 ± 6.0	
58b	NA	NA	NA	NA	5.24 ± 0.06 [5770] (n = 6)	NA	NA	45.6% of DA at 10 μM (n = 4)	ND	

[a]All data represent the mean of at least three independent experiments (n = number of independent experiments), each performed in duplicate. Potency values are expressed as pEC_{50} ± SEM with the corresponding EC_{50} in nM in brackets. Efficacy values are calculated as a percentage of a reference ligand (DAMGO or quinpirole for the MOR and D_3R, respectively) and expressed as E_{max} ± SEM (%). NA = not active, and the compound presents no agonist activity at the highest tested concentration.

https://doi.org/10.1021/acs.jmedchem.1c00611
J. Med. Chem. 2021, 64, 7778−7808

ylmethyl-amide linker, and **48**, presenting a butyl ether linker chain in position 4 of the *trans*-pyrrolidine nucleus, were synthesized. Compound **48** showed the highest D_2R/D_3R affinity among all the new analogues (D_2R K_i = 9.41 nM; D_3R K_i = 2.21 nM); however, the regio- and stereochemistry of the substituted pyrrolidine ring was detrimental for MOR binding, with a K_i of 559 nM. On the other hand, **40** emerged as our third lead, alongside **23** and **28**, with its almost identical affinities for both the MOR (K_i = 106 nM) and D_3R (K_i = 135 nM), ∼4- and ∼25-fold selectivity over D_2R and D_4R, respectively. This profile distinguished **40** as one of the most promising dual-target MOR−D_3R compounds in the series.

The binding data for the phenylmorphan analogues are reported in Table 2. Compounds **10**, **11**, and the nor-analogues **56**, **59**, and **60** were tested as reference compounds, since most of them were key MOR PP building blocks for our bivalent and bitopic drug design. Compound **10** showed the highest MOR affinity as an OBS PP, with K_i = 0.633 nM, similar to the affinities of **3** and the hybrid bivalent analogue, **23**. Interestingly, **10** also showed moderately low micromolar and sub-micromolar affinities for the D_2R and D_3R, supporting the hypothesis that the phenylmorphan ring structurally resembles more flexible phenyl-morpholino moieties, canonical scaffolds for D_3R ligands.[45]

Docking studies suggested that the steric clash between the ethyl acrylate group and the backbone of the D_3R receptor would limit and potentially challenge the development of bitopic ligands **57** and **58** targeting D_3R, despite being tolerated in the MOR OBS. Indeed, bitopic analogues **57** and **58** and the resolved enantiomers **58a** and **58b** all showed high affinities at the MOR (K_is ranging from 13.5 to 57 nM) but micromolar K_is for all the D_2-like subtypes, independent of linker rigidity or stereochemistry. The shorter bivalent analogue **65** with a simple ethyl linker chain (n = 2) was predicted by docking studies to be the optimal spacer to resolve steric clashes of the MOR PP motif in the D_3R; Figure 6. Indeed, tethering the MOR phenylmorphan PP and the D_3R 2,3-dichlorophenyl piperazine PP presented one of the most interesting dual-target candidates (**65**) with equivalent affinities at the MOR (K_i = 92.7 nM) and D_3R (K_i = 139 nM).

Replacement of the sterically hindered ethyl acrylate group with a smaller hydroxy substituent allowed validation of the docking observation that a small substituent would significantly improve D_3R binding. Overall, **61** and **62** adopt the same docking as **65** inside the MOR but lose hydrophobic interactions of the ethyl acrylate moiety with $M153^{3.36}$ and $Y328^{7.43}$ (Figure S3). The hydrogen-bonding interactions between the 9-OH and $Y328^{7.43}$ provide limited compensation for **62**. However, for **61**, this hydrogen bond is accompanied by negative interactions due to proximity of the carboxylate oxygen of $D149^{3.32}$ (3.2 Å compared to 4.5 Å of S-chiral **62**). Furthermore, **61** and **62** adopt an interesting conformation inside the D_3R with the indole carboxamide ring situated in the OBS. In the absence of positively charged nitrogen, the nitrogen of the amide forms a hydrogen bond with the $D110^{3.32}$ residue. Interestingly, the 9-OH is placed very close to the backbone of TM7 for **62** and TM2 for **61**. Therefore, the substitution of this position with ethyl acrylate would cause steric clashes with the D_3R, as indicated by the loss of affinity of **57**. Bitopic analogue **62**, with all the resolved stereochemical configurations around the phenylmorphan moiety inverted with respect to **57**, showed a D_3R K_i of 79.6 nM, ∼172-fold improved affinity with respect to the ethyl acrylate analogue **57**, maintaining a moderate affinity (K_i = 464 nM) for the MOR.

Across all the tested compounds, no significant differences were observed in the D_2-like affinities determined using [^{3}H]-NMSP, and [^{3}H]-(*R*)-(+)-7-OH-DPAT binding assays were observed, unlike our previous observations for efficacious agonist ligands,[43,45] consistent with our hypothesis that all the new analogues are likely antagonists or low-efficacy partial agonists at the D_3R.

Based on their binding profiles, a select group of hits were tested in functional assays to determine their agonist and antagonist potencies for the multiple GPCR-related signaling pathways, as well as to validate and confirm the MOR agonism and D_3R antagonism/partial agonism profile, we were seeking with these new hybrid molecules.

BRET Functional Studies at the MOR and D_3R. With the binding studies and SAR established, we then characterized the action of selected ligands to signal through both the MOR and D_3R; these results are shown in Figure 7 and Table 3. The action of these ligands was assessed through arrestin-3 (or β-arrestin-2) recruitment at MOR and G-protein activation (GPA) at MOR ($G\alpha_{i2}$) and D_3R ($G\alpha_{oA}$) assays. In addition, the ability of the ligands to induce the active state of the MOR was determined by measuring recruitment of a conformationally selective nanobody that recognizes and binds to the active conformation of the MOR, nanobody 33 (Nb33).[64] Seven of the newly synthesized MOR−D_3R hybrids (**14**, **23**, **28**, **40**, **57**, **58a**, and **58b**) were tested together with **10**. The efficacious agonists **DAMGO** (D-Ala2, N-MePhe4, and Gly5-ol-enkephalin), **quinpirole**, and **dopamine** were used as reference agonists to normalize data at the MOR and D_3R. We included the MOR partial agonist **morphine** to illustrate the relative coupling efficiency and amplification of the different assays (Figure 7A,B,D). Both known antagonists, **naloxone** (MOR) and **5** (D_3R), inhibited agonist-stimulated GPA in a concentration-dependent manner (Figure 7C,F).

The three substituted phenylmorphan MOR PP analogues (**57**, **58a**, and **58b**), despite showing improved affinities for the MOR compared to **56**, did not activate the MOR in any of the three pathways tested (Figure 7A,B,D). Thus, we tested the ability of these bitopic compounds to inhibit the action of 100 nM of **DAMGO** in the GPA i2 assay. As shown in Figure 7C, all three ligands were able to inhibit **DAMGO**-mediated GPA to the same extent as **naloxone** albeit with lower potencies. When tested at the D_3R, **57** failed to demonstrate any D_3R activity (up to 10 μM, Figure 7E,F), which is likely due to the low affinity of this compound for this receptor (Table 2). Compounds **58a** and **58b** showed agonist activity at the D_3R but with low (micromolar) potencies that reflect their affinity for the D_3R (Figure 7E, Table 3). Thus, these two phenylmorphan hybrids display MOR antagonism and D_3R agonism, rather than the MOR agonist/D_3R antagonist or partial agonist profile we targeted.

In contrast, all four MOR diphenyl PP analogues tested (**14**, **23**, **28**, and **40**) showed agonist activity at the MOR, with **23** being the most potent and efficacious compound. Compound **14** showed low-potency MOR agonism that could only be detected at the highest concentration used of 10 μM in the most amplified and sensitive GPA i2 assay. **40** displayed higher potency and efficacy in assays of MOR activation than **28**, with **28** displaying no detectable agonism in the less-amplified Nb33 and arrestin-3 recruitment assays but an E_{max} of 50% that of **DAMGO** in the GPA i2 assay. Compound **40** gave a robust

https://doi.org/10.1021/acs.jmedchem.1c00611
J. Med. Chem. 2021, 64, 7778−7808

response (E_{max} = 84.4% of DAMGO) but much weaker responses in the arrestin and Nb33 assays, indicating that it is a less-efficacious partial agonist than **morphine**. All four bivalent compounds share a similar MOR diphenyl PP based on **3** and **4**, the *N*,*N*-dimethyl-diphenylbutanamide PP being more favorable than the diphenylbutanenitrile PP for MOR agonism. The major structural differences are present in the D_3R PP and the type and length of the linker between the two pharmacophores: a shorter linker being more favorable for MOR agonism. In general, across the series of compounds and **morphine**, we observe higher maximal effects (E_{max}) and potencies in the GPA i2 assay as compared to that in the arrestin-3 recruitment and Nb33 assays. Such a behavior is consistent with the action of partial agonists at signaling endpoints with different levels of amplification and coupling efficiency of the pathway. In agreement with this, when these data were analyzed using the Black and Leff operational model of agonism and assessed for biased agonism using **DAMGO** as the reference ligand, none of the compounds displayed significant bias between these two pathways relative to the action of **DAMGO** (Table S2).

When these four MOR diphenyl PP ligands were tested for their ability to activate the D_3R (Figure 7E,F), **14** and **28** showed similar efficacies (64 and 55% of dopamine, respectively), with **28** being the most potent compound in agreement with their relative affinities (Table 1). Although **14** and **40** display similar affinities for D_3R, **40** acted as an antagonist with micromolar potency (IC_{50} = 1.5 μM), whereas **14** acted as a robust partial agonist (E_{max} = 63.8% of quinpirole). Finally, **23**, which was the most potent MOR agonist and shares the same D_3R PP structure as **28** but with a shorter linker, displayed weak partial agonism (E_{max} = 20% of quinpirole) at the D_3R and sub-micromolar potency consistent with its binding affinity.

CONCLUSIONS

The data obtained highlight a series of hit to lead candidates as MOR−D_3R dual-target ligands. We have synthesized multiple combinations of bivalent or bitopic ligands based on carefully designed structural modifications and *in silico*-guided SAR around the MOR PP, D_3R PP, and SP, as well as linkers, with a particular focus on regio- and stereochemistry. Importantly, we have identified compounds with a range of sub-nanomolar to sub-micromolar binding affinities for each receptor of interest and thus provide a new approach to modulate the pharmacological profiles of highly selective MOR agonists through concomitant dual-target D_3R antagonism.

The functional studies revealed three lead analogues, **23**, **28** and **40**, which are partial agonists at the MOR and partial agonists or antagonists at the D_3R. We and others have suggested that low intrinsic efficacy could explain the improved therapeutic window observed on the most recent MOR agonists, such as **PZM21** and **TRV-130**,[31] and our three lead compounds fit this desired functional profile with the added feature of D_3R low-efficacy partial agonism or antagonism, which may prove beneficial in avoiding the addictive liability of opioid receptor-targeted drugs. Furthermore, evaluation and thus a better understanding of the desired kinetic profiles at both targets for the optimal pharmacological effect will be crucial in the development of future generations of dual-target MOR−D_3R ligands. Indeed, current drug design is focused on improving drug-like characteristics and blood−brain barrier penetrability as the current lead compounds have central nervous system multiparameter optimization[65,66] scores of ∼2 and are predicted to be peripherally limited. This indeed was what Komoto and colleagues[37] found with their loperamide analogues, which is perhaps unsurprising. Nevertheless, with the proof-of-concept in hand, we have laid the groundwork for an alternative pharmacological approach, using bivalent drug design to engage both the MOR and D_3R in the pursuit of a novel class of opioid analgesics with lower abuse potential.

EXPERIMENTAL METHODS

Chemistry. All chemicals and solvents were purchased from chemical suppliers unless otherwise stated and used without further purification. All melting points were determined (when obtainable) on an OptiMelt automated melting point system and are uncorrected. Reactions were not yield optimized. The ^1H and ^{13}C NMR spectra were recorded on a Varian Mercury Plus 400 instrument. Proton chemical shifts are reported as parts per million (δ ppm) relative to tetramethylsilane (0.00 ppm) as an internal standard or to deuterated solvents. Coupling constants are measured in Hertz. Chemical shifts for ^{13}C NMR spectra are reported as parts per million (δ ppm) relative to deuterated $CHCl_3$ or deuterated MeOH ($CDCl_3$ 77.5 ppm and CD_3OD 49.3 ppm). Chemical shifts, multiplicities, and coupling constants (J) have been reported and calculated using VnmrJ Agilent-NMR 400MR or MNova 9.0 software. Gas chromatography−mass spectrometry (GC/MS) data were acquired (where obtainable) using an Agilent Technologies (Santa Clara, CA) 7890B GC equipped with an HP-5MS column (cross-linked 5% PH ME siloxane, 30 m × 0.25 mm i.d. × 0.25 μm film thickness) and a 5977B mass-selective ion detector in the electron-impact mode. Ultrapure-grade helium was used as the carrier gas at a flow rate of 1.2 mL/min. The injection port and transfer line temperatures were 250 and 280 °C, respectively, and the oven temperature gradient used was as follows: the initial temperature (70 °C) was held for 1 min and then increased to 300 °C at 20 °C/min and maintained at 300 °C for 4 min, with a total run time of 16.5 min. Column chromatography was performed using a Teledyne Isco CombiFlash RF flash chromatography system or a Teledyne Isco EZ-Prep chromatography system. Preparative thin-layer chromatography was performed on Analtech silica gel plates (1000 μm). When % DMA is reported as the eluting system, it stands for % of methanol in DCM, in the presence of 0.5−1% NH_4OH. Preparative chiral HPLC was performed using a Teledyne Isco EZ-Prep chromatography system with the diode array detector (DAD) and ELS detectors. HPLC analysis was performed using an Agilent Technologies 1260 Infinity system coupled with the DAD. For each analytical HPLC run, multiple DAD λ absorbance signals were measured in the range of 210−280 nm. Separation of the analyte, purity, and enantiomeric/diastereomeric excess determinations were achieved at 40 °C using the methods reported in each detailed reaction description. Preparative and analytical HPLC columns were purchased from Daicel Corporation or Phenomenex. HPLC methods and conditions are reported in the descriptions of the chemical reactions where they were applied. Microanalyses were performed by Atlantic Microlab, Inc. (Norcross, GA) and agree with ±0.4% of calculated values. HRMS (mass error within 5 ppm) and MS/MS fragmentation analysis were performed on an LTQ-Orbitrap Velos (Thermo Scientific, San Jose, CA) coupled with an ESI source in the positive-ion mode to confirm the assigned structures and regiochemistry. Unless otherwise stated, all the test compounds were evaluated to be >95% pure on the basis of combustion analysis, NMR, GC/MS, and HPLC-DAD. The detailed analytical results are reported in the characterization of each final compound.

*4-(Phenethylamino)-2,2-diphenylbutanenitrile (**12**).* A suspension of 4-bromo-2,2-diphenylbutanenitrile (500 mg, 1.67 mmol), 2-phenylethan-1-amine (605 mg, 5 mmol), and K_2CO_3 (230 mg, from 1.67 mmol up to 10 equiv) in ACN (50 mL) was heated at 130 °C in a sealed vessel overnight. The mixture was filtered, the solvent was removed under vacuum, and the residue was purified by flash

https://doi.org/10.1021/acs.jmedchem.1c00611
J. Med. Chem. 2021, 64, 7778−7808

chromatography eluting with 15% DMA. The desired product was obtained as colorless oil (300 mg, 53% yield). ^{1}H NMR (400 MHz, $CDCl_3$): δ 7.36−7.18 (m, 15H), 3.74 (t, J = 7.1 Hz, 2H), 3.07 (t, J = 6.2 Hz, 2H), 2.95 (t, J = 7.2 Hz, 2H), 2.60 (t, J = 6.2 Hz, 2H); ^{13}C NMR (101 MHz, $CDCl_3$): δ 171.34, 142.74, 139.55, 128.86, 128.57, 128.46, 128.38, 128.36, 128.12, 126.98, 126.18, 61.47, 53.40, 46.66, 46.18, 37.35, 33.47. The free base was converted into the corresponding oxalate salt. HRMS ($C_{24}H_{24}N_2$ + H^+): calcd, 341.20123; found, 341.20048 (error −0.7 ppm). CHN ($C_{24}H_{24}N_2$ + 1.5$H_2C_2O_4$ + H_2O) Calcd: C, 65.71; H, 5.92; N, 5.68. Found: C, 65.76; H, 5.77; N, 5.57. mp: salt too hygroscopic to determine the melting point.

*4-(4-(2,3-Dichlorophenyl)piperazin-1-yl)-2,2-diphenylbutanenitrile (**13**).* The reaction was performed following the same procedure described for **12**, starting from 1-(2,3-dichlorophenyl)piperazine (250 mg, 0.9 mmol) and 4-bromo-2,2-diphenylbutanenitrile (350 mg, 1.17 mmol). The desired product was purified by flash chromatography eluting with hexanes/ethyl acetate (hex/EtOAc 5:5) and obtained as colorless oil (30 mg, 7.5% yield). ^{1}H NMR (400 MHz, $CDCl_3$): δ 7.45−7.23 (m, 10H), 7.19−7.08 (m, 2H), 6.94 (dd, J = 6.8, 2.8 Hz, 1H), 3.04 (br s, 4H), 2.65 (dd, J = 10.5, 4.3 Hz, 6H), 2.57−2.49 (m, 2H). The free base was converted into the corresponding oxalate salt. CHN ($C_{26}H_{25}N_3Cl_2$ + $H_2C_2O_4$ + 0.25H_2O) Calcd: C, 61.71; H, 5.09; N, 7.71. Found: C, 61.67; H, 5.09; N, 7.85. mp: 202−207 °C.

*4-((4-(4-(2,3-Dichlorophenyl)piperazin-1-yl)butyl)amino)-2,2-diphenylbutanenitrile (**14**).* The reaction was performed following the same procedure described for **12**, starting from 4-(4-(2,3-dichlorophenyl)piperazin-1-yl)butan-1-amine (200 mg, 0.7 mmol) and 4-bromo-2,2-diphenylbutanenitrile (105 mg, 0.35 mmol). The desired product was purified by flash chromatography eluting with 15% DMA and obtained as colorless oil (58 mg, 31% yield). ^{1}H NMR (400 MHz, $CDCl_3$): δ 7.37−7.29 (m, 10H), 7.29−7.18 (m, 2H), 6.95 (dd, J = 6.4, 3.2 Hz, 1H), 4.84 (br s, 1H), 3.52 (t, J = 7.2 Hz, 2H), 3.26 (t, J = 6.2 Hz, 2H), 3.05 (t, J = 4.8 Hz, 4H), 2.71 (t, J = 6.2 Hz, 2H), 2.59 (br s, 4H), 2.44 (dd, J = 8.2, 6.7 Hz, 2H), 1.70−1.53 (m, 4H); ^{13}C NMR (101 MHz, $CDCl_3$): δ 171.46, 151.32, 142.37, 133.99, 128.51, 128.45, 127.48, 127.39, 127.15, 124.48, 118.56, 61.65, 58.24, 53.24, 51.31, 46.34, 44.72, 37.36, 25.14, 24.26. The free base was converted into the corresponding oxalate salt. HRMS ($C_{30}H_{34}N_4Cl_2$ + H^+): calcd, 521.22333; found, 521.22363 (error 0.3 ppm). CHN ($C_{30}H_{34}N_4Cl_2$ + 3$H_2C_2O_4$ + 0.5H_2O) Calcd: C, 54.01; H, 5.16; N, 7.00. Found: C, 53.97; H, 5.33; N, 7.15. mp: salt decomposes above 80 °C.

*4-((4-(4-(2,3-Dichlorophenyl)piperazin-1-yl)-3-hydroxybutyl)amino)-2,2-diphenylbutanenitrile (**15**).* The reaction was performed following the same procedure described for **12**, starting from 4-amino-1-(4-(2,3-dichlorophenyl)piperazin-1-yl)butan-2-ol[47] (223 mg, 0.7 mmol) and 4-bromo-2,2-diphenylbutanenitrile (105 mg, 0.35 mmol). The desired product was purified by flash chromatography eluting with 15% DMA and obtained as colorless oil (53 mg, 28% yield). ^{1}H NMR (400 MHz, $CDCl_3$): δ 7.48−7.32 (m, 6H), 7.24−7.10 (m, 6H), 6.95 (dd, J = 7.2, 2.3 Hz, 1H), 4.22−4.06 (m, 3H), 3.75−3.67 (m, 2H), 3.12 (br s, 4H), 2.96 (tt, J = 8.1, 4.2 Hz, 4H), 2.76 (d, J = 10.7 Hz, 2H), 2.67 (dd, J = 12.5, 3.2 Hz, 1H), 2.61−2.50 (m, 1H), 2.01 (s, 1H), 1.82 (ddd, J = 16.4, 13.9, 7.1 Hz, 1H); ^{13}C NMR (101 MHz, $CDCl_3$): δ 169.96, 150.78, 138.44, 138.40, 134.10, 129.50, 129.48, 128.91, 128.89, 127.88, 127.78, 127.58, 127.43, 124.83, 118.64, 64.45, 63.72, 62.31, 53.36, 50.83, 50.62, 45.63, 37.82, 31.51. HRMS ($C_{30}H_{34}ON_4Cl_2$ + H^+): calcd, 537.21824; found, 537.21935 (error 1 ppm). HPLC analysis method A: Chiralpak AD-H analytical column (4.5 mm × 250 mm—5 μm particle size); mobile phase: isocratic 30% 2-PrOH in hexanes; flow rate: 1 mL/min; injection volume: 20 μL; sample concentration: ∼1 mg/mL; multiple DAD λ absorbance signals measured in the range of 210−280 nm, Rt 4.944 min, purity >94.3% (absorbance at 254 nm). HPLC analysis method B: Chiralpak OZ-H analytical column (4.5 mm × 250 mm—5 μm particle size); mobile phase: isocratic 30% 2-PrOH in hexanes; flow rate: 1 mL/min; injection volume: 20 μL; sample concentration: ∼1 mg/mL; multiple DAD λ absorbance signals measured in the range of 210−280 nm, Rt 9.072 and 10.862 min, purity >95%, er 43:57 (absorbance at 254 nm).

*4-(Dimethylamino)-2,2-diphenylbutanenitrile (**16**).* The reaction was performed following the same procedure described for **12**, starting from dimethylamine hydrochloride (2.0 g, 25 mmol) and 4-bromo-2,2-diphenylbutanenitrile (5.0 g, 16.7 mmol). The desired product was purified by flash chromatography eluting with 5% DMA and obtained as colorless oil (3.5 g, 79% yield). ^{1}H NMR (400 MHz, $CDCl_3$): δ 7.66−6.75 (m, 10H), 2.68−2.50 (m, 2H), 2.50−2.33 (m, 2H), 2.25 (s, 6H). GC/MS (EI), Rt 10.499 min; 264.1 (M^+), purity >95%. The free base was converted into the corresponding oxalate salt. CHN ($C_{18}H_{20}N_2$ + $H_2C_2O_4$) Calcd: C, 67.78; H, 6.26; N, 7.90. Found: C, 67.66; H, 6.43; N, 7.96. mp: 163−169 °C.

*3-Carboxy-N,N-dimethyl-3,3-diphenylpropan-1-aminium Bromide (**17**).* Compound **16** (2 g, 7.6 mmol) was dissolved in 48% HBr aq solution (50 mL) and stirred under reflux overnight. The solution was concentrated to half-volume and decanted, and the residue was washed multiple times with Et_2O. The dried crude material was used in the next step without further purification.

*N-(4-(4-(2,3-Dichlorophenyl)piperazin-1-yl)butyl)-4-(dimethylamino)-2,2-diphenylbutanamide (**18**).* A solution of **17** (460 mg, 1.26 mmol), EDC hydrochloride (240 mg, 1.26 mmol), HOBt (170 mg, 1.26 mmol), and DIPEA (2.2 mL; 12.6 mmol) in DCM (20 mL) was stirred at room temperature (RT) for 1 h, followed by dropwise addition of 4-(4-(2,3-dichlorophenyl)piperazin-1-yl)butan-1-amine (380 mg, 1.26 mmol) in DCM (20 mL). The mixture was stirred at RT overnight, the solvent was evaporated under vacuum, and the residue was purified by flash chromatography eluting with 10% DMA. The desired product was obtained as yellow oil (40 mg, 6% yield). ^{1}H NMR (400 MHz, $CDCl_3$): δ 7.36−7.20 (m, 10H), 7.18−7.08 (m, 2H), 6.94 (dd, J = 6.6, 3.0 Hz, 1H), 6.74 (br s, 1H), 3.31−3.14 (m, 2H), 3.03 (br s, 4H), 2.62−2.53 (m, 6H), 2.40−2.27 (m, 2H), 2.19 (m, 8H), 1.53−1.36 (m, 4H); ^{13}C NMR (101 MHz, $CDCl_3$): δ 173.99, 151.26, 143.81, 133.99, 128.74, 128.25, 127.47, 127.40, 126.81, 124.51, 118.55, 60.22, 58.03, 55.98, 53.23, 51.28, 45.53, 45.42, 44.87, 39.71, 36.80, 29.40, 27.36, 24.09. The free base was converted into the corresponding oxalate salt. HRMS ($C_{32}H_{40}ON_4Cl_2$ + H^+): calcd, 567.26519; found, 567.26524 (error 1.3 ppm). CHN ($C_{32}H_{40}ON_4Cl_2$ + 2$H_2C_2O_4$ + 3H_2O) Calcd: C, 53.93; H, 6.29; N, 6.99. Found: C, 53.89; H, 5.90; N, 7.31. mp: salt too hygroscopic to determine melting point.

*6-(Dimethylamino)-4,4-diphenylhexan-3-one (**19**).* Ethyl magnesium bromide (3 M solution in diethyl ether, 10 mmol) was added dropwise to a solution of **16** (2.0 g, 7.5 mmol) in toluene (30 mL) at 0 °C. The mixture was slowly warmed to RT and then stirred at reflux for 3 h. The reaction was quenched with 10 mL of 2 N HCl (aq solution) at 0 °C and stirred at reflux for 30 min. The suspension was basified with 2 N NaOH at 0 °C, the toluene was removed under vacuum, and the aqueous phase was extracted with DCM/2-PrOH (3:1). The organic layers were combined, dried over Na_2SO_4, filtered, and dried under vacuum to afford the crude material, which was purified by flash chromatography eluting with 10% DMA. The desired product was obtained as colorless oil (1.3 g, 59%). ^{1}H NMR (400 MHz, $CDCl_3$): δ 7.51−7.06 (m, 10H), 2.52 (m, 2H), 2.30 (m, 2H), 2.15 (d, J = 0.9 Hz, 6H), 1.95 (m, 2H), 0.88 (td, J = 7.3, 0.9 Hz, 3H); ^{13}C NMR (101 MHz, $CDCl_3$): δ 211.02, 141.48, 129.14, 128.26, 126.94, 65.04, 55.67, 45.52, 35.41, 32.47, 9.05. The free base was converted into the corresponding oxalate salt. HRMS ($C_{20}H_{25}NO$ + H^+): calcd, 296.20089; found, 296.20150 (error 0.4 ppm). CHN ($C_{20}H_{25}NO$ + $H_2C_2O_4$) Calcd: C, 68.55; H, 7.06; N, 3.63. Found: C, 68.51; H, 7.15; N, 3.62. mp: 161−165 °C.

*tert-Butyl (5-(4-(2,3-Dichlorophenyl)piperazin-1-yl)-5-oxopentyl)carbamate (**20**).* A solution of 5-((*tert*-butoxycarbonyl)amino)pentanoic acid (470 mg, 2.16 mmol), 1-(2,3-dichlorophenyl)piperazine (500 mg, 2.16 mmol), and HCTU (895 mg, 2.16 mmol) in DCM (25 mL) was stirred at RT for 3 h. The solvent was removed under vacuum, and the residue was purified by flash chromatography eluting with hex/EtOAc (40/60). The desired product was obtained as yellow oil (550 mg, 59% yield). ^{1}H NMR (400 MHz, $CDCl_3$): δ 7.23−7.11 (m, 2H), 6.92 (dd, J = 7.7, 1.8 Hz, 1H), 4.63 (br s, 1H),

https://doi.org/10.1021/acs.jmedchem.1c00611
J. Med. Chem. 2021, 64, 7778−7808

3.79 (t, J = 4.9 Hz, 2H), 3.68−3.60 (m, 2H), 3.15 (q, J = 6.6 Hz, 2H), 3.00 (dq, J = 10.7, 5.2 Hz, 4H), 2.39 (t, J = 7.4 Hz, 2H), 1.76−1.62 (m, 2H), 1.60−1.51 (m, 2H), 1.43 (s, 9H).

*4-((5-(4-(2,3-Dichlorophenyl)piperazin-1-yl)-5-oxopentyl)-amino)-2,2-diphenylbutanenitrile (**21**).* TFA (1 mL, 12.8 mmol) was added to a solution of **20** (550 mg, 1.28 mmol) in DCM (10 mL). The mixture was stirred at RT for 24 h, basified with 2 N NaOH, and extracted with DCM. The organic layers were combined, dried over Na_2SO_4, filtered, and dried under vacuum to afford the crude primary amine intermediate, which was dissolved in ACN (20 mL), followed by the addition of 4-bromo-2,2-diphenylbutanenitrile (384 mg, 1.28 mmol) and K_2CO_3 (10 equiv). The reaction mixture was stirred at reflux overnight and filtered, and the solvent was removed under vacuum. The residue was purified by flash chromatography eluting with 15% DMA, and the desired product was obtained as yellow oil (20 mg, 3% yield). ^{1}H NMR (400 MHz, $CDCl_3$): δ 7.37−7.10 (m, 12H), 6.90 (dd, J = 7.8, 1.8 Hz, 1H), 3.78 (d, J = 5.8 Hz, 2H), 3.63 (t, J = 4.9 Hz, 2H), 3.59−3.51 (m, 2H), 3.28 (t, J = 6.2 Hz, 2H), 2.97 (dt, J = 9.3, 5.0 Hz, 4H), 2.72 (t, J = 6.2 Hz, 2H), 2.50−2.41 (m, 2H), 1.71 (m, 4H); ^{13}C NMR (101 MHz, $CDCl_3$): δ 171.48, 171.42, 150.64, 142.20, 134.16, 128.51, 128.47, 128.43, 127.74, 127.50, 127.25, 125.13, 118.75, 61.72, 51.69, 51.20, 46.41, 45.80, 44.41, 41.73, 37.36, 32.69, 26.68, 22.47. HRMS ($C_{31}H_{34}ON_4Cl_2$ + H^+): calcd, 549.21824; found, 549.21825 (error 0.0 ppm). HPLC analysis method: Chiralpak AD-H analytical column (4.5 mm × 250 mm—5 μm particle size); mobile phase: isocratic 30% 2-PrOH in hexanes; flow rate: 1 mL/min; injection volume: 20 μL; sample concentration: ∼1 mg/mL; multiple DAD λ absorbance signals measured in the range of 210−280 nm, Rt 27.693 min, purity >95% (absorbance at 254 nm).

*4-(Dimethylamino)-N,N-dimethyl-2,2-diphenylbutanamide (**22**).* Dimethylamine hydrochloride (1.18 g, 14.5 mmol) was added to a suspension of *N*-(3,3-diphenyldihydrofuran-2(3*H*)-ylidene)-*N*-methylmethanaminium bromide (500 mg, 1.45 mmol) and K_2CO_3 (2.0 g, 14.5 mmol) in TBME/ACN (25 mL/10 mL). The reaction mixture was heated in a sealed vessel for 24 h, the solvent was removed under vacuum, and the residue was purified by flash chromatography eluting with EtOAc/MeOH (95/5). The desired product was obtained as colorless oil (70 mg, 16% yield). ^{1}H NMR (400 MHz, $CDCl_3$): δ 7.43−7.24 (m, 10H), 2.97 (br s, 3H), 2.57−2.46 (m, 2H), 2.30 (m + br s, 2H + 9H). GC/MS (EI), Rt 11.256 min; 310.1 (M^+), purity >95%. The free base was converted into the corresponding oxalate salt. HRMS ($C_{20}H_{26}ON_2$ + H^+): found, 311.21098 (error −2.4 ppm). CHN ($C_{20}H_{26}ON_2$ + $1.5H_2C_2O_4$ + $0.75H_2O$) Calcd: C, 60.19; H, 6.70; N, 6.10. Found: C, 60.09; H, 6.36; N, 6.13. mp: 174−178 °C.

*4-(4-(2,3-Dichlorophenyl)piperazin-1-yl)-N,N-dimethyl-2,2-diphenylbutanamide (**23**).* 1-(2,3-Dichlorophenyl)piperazine hydrochloride (400 mg, 1 mmol) was added to a suspension of *N*-(3,3-diphenyldihydrofuran-2(3*H*)-ylidene)-*N*-methylmethanaminium bromide (500 mg, 1 mmol), K_2CO_3 (967 mg, 7 mmol), and DIPEA (1 mL, 7 mmol) in ACN (20 mL). The reaction mixture was stirred at reflux overnight, the solvent was removed under vacuum, and the residue was purified by flash chromatography eluting with 5% DMA. The desired product was obtained as colorless oil (640 mg, 91% yield). ^{1}H NMR (400 MHz, $CDCl_3$): δ 7.46−7.34 (m, 10H), 7.34−7.20 (m, 2H), 7.15−7.03 (m, 1H), 2.97 (br s, 6H), 2.56−2.43 (m, 8H), 2.19−2.10 (m, 2H), 1.69 (s, 2H); ^{13}C NMR (101 MHz, $CDCl_3$): δ 173.41, 151.42, 140.76, 133.89, 128.35, 128.10, 127.44, 127.30, 126.70, 124.29, 118.54, 59.70, 55.71, 53.16, 51.33, 42.24. The free base was converted into the corresponding oxalate salt. HRMS ($C_{28}H_{31}ON_3Cl_2$ + H^+): calcd, 496.19169; found, 496.19052 (error −2.3 ppm). CHN ($C_{28}H_{31}ON_3Cl_2$ + $1.5H_2C_2O_4$) Calcd: C, 58.96; H, 5.43; N, 6.65. Found: C, 58.69; H, 5.33; N, 6.65. mp: 199−205 °C.

*4-(7-Cyano-3,4-dihydroisoquinolin-2(1H)-yl)-N,N-dimethyl-2,2-diphenylbutanamide (**24**).* The reaction was performed following the same procedure described for **23**, starting from 1,2,3,4-tetrahydroisoquinoline-7-carbonitrile (100 mg, 0.63 mmol). The crude material was purified by flash chromatography eluting with 5% DMA, and the desired product was obtained as colorless oil (130 mg, 40% yield). ^{1}H NMR (400 MHz, $CDCl_3$): δ 7.46−7.18 (m, 12H), 7.10 (d, J = 7.9 Hz, 1H), 3.49 (br s, 2H), 2.98 (br s, 3H), 2.82 (t, J = 5.9 Hz, 2H), 2.63 (t, J = 5.9 Hz, 2H), 2.55−2.46 (m, 2H), 2.40−2.26 (br s, 3H), 2.26−2.17 (m, 2H); ^{13}C NMR (101 MHz, $CDCl_3$): δ 173.44, 140.62, 140.46, 136.71, 130.29, 129.39, 129.33, 128.42, 128.39, 128.07, 126.80, 119.18, 109.08, 59.74, 55.45, 55.42, 50.18, 42.84, 29.55. The free base was converted into the corresponding oxalate salt. HRMS ($C_{28}H_{29}ON_3$ + H^+): calcd, 424.23834; found, 424.23765 (error −1.6 ppm). CHN ($C_{28}H_{29}ON_3$ + $1.5H_2C_2O_4$ + $0.5H_2O$) Calcd: C, 65.60; H, 5.86; N, 7.40. Found: C, 65.76; H, 5.87; N, 7.29. mp: 178−181 °C.

*4-Hydroxy-N,N-dimethyl-2,2-diphenylbutanamide (**25**).* *N*-(3,3-Diphenyldihydrofuran-2(3*H*)-ylidene)-*N*-methylmethanaminium bromide (700 mg, 2 mmol) was suspended in 2 N NaOH (15 mL of aq solution) and then stirred at RT for 5 min. The mixture was extracted with DCM, and the organic layers were combined, dried over Na_2SO_4, filtered, and evaporated under vacuum to afford the pure desired product in quantitative yield, as colorless oil. ^{1}H NMR (400 MHz, $CDCl_3$): δ 7.48−7.25 (m, 10H), 3.17 (q, J = 5.0 Hz, 2H), 3.04−2.95 (m, 3H), 2.57−2.49 (m, 2H), 2.35−2.27 (m, 3H). GC/MS (EI), Rt 11.847 min; 283.1 (M^+).

*N,N-Dimethyl-4-oxo-2,2-diphenylbutanamide (**26**).* DMP was added portionwise to a solution of **25** (200 mg, 0.71 mmol) in DCM (10 mL) at 0 °C. The reaction mixture was slowly warmed to RT and stirred for 1 h. The suspension was washed with 10% $NaHCO_3$ (aq solution), and the organic layer was dried over Na_2SO_4, filtered, and evaporated under vacuum. The residue was purified by flash chromatography eluting with hex/EtOAc (50/50) to afford the desired product as a white solid (120 mg, 60% yield). ^{1}H NMR (400 MHz, $CDCl_3$): δ 9.17 (t, J = 2.2 Hz, 1H), 7.46−7.25 (m, 10H), 3.11−2.99 (m, 6H), 2.33 (s, 2H). GC/MS (EI), Rt 11.744 min; 281.1 (M^+).

*N,N-Dimethyl-4-(phenethylamino)-2,2-diphenylbutanamide (**27**).* A solution of **26** (90 mg, 0.32 mmol), 2-phenylethan-1-amine (77 mg, 0.64 mmol), and cat. AcOH in DCE (5 mL) was stirred at RT for 30 min. STAB (97 mg, 0.48 mmol) was added portionwise, and the mixture was stirred for additional 2 h. The solvent was removed under vacuum, and the residue was purified by flash chromatography eluting with 5% DMA. The desired product was obtained as colorless oil (quantitative yield). ^{1}H NMR (400 MHz, $CDCl_3$): δ 7.39−7.10 (m, 15H), 2.96 (m, 3H), 2.75 (br s, 7H), 2.48−2.28 (m + br s, 4H + 1H); ^{13}C NMR (101 MHz, $CDCl_3$): δ 176.89, 173.88, 140.40, 139.18, 128.82, 128.73, 128.54, 128.45, 128.04, 126.94, 126.22, 126.17, 60.51, 50.11, 46.28, 44.40, 43.46, 40.00, 35.13, 23.25. The free base was converted into the corresponding oxalate salt. HRMS ($C_{26}H_{30}ON_2$ + H^+): calcd, 387.24309; found, 387.24226 (error −2.1 ppm). CHN ($C_{26}H_{30}ON_2$ + $1.5H_2C_2O_4$ + $0.1NH_4OH$) Calcd: C, 66.33; H, 6.43; N, 5.60. Found: C, 66.10; H, 6.61; N, 5.91. mp: 112−117 °C.

*4-((4-(4-(2,3-Dichlorophenyl)piperazin-1-yl)butyl)amino)-N,N-dimethyl-2,2-diphenylbutanamide (**28**).* The reaction was performed following the same procedure described for **27**, starting from 4-(4-(2,3-dichlorophenyl)piperazin-1-yl)butan-1-amine (272 mg, 0.9 mmol). The desired product was purified by flash chromatography eluting with 25% DMA and obtained as colorless oil (300 mg, 65% yield). ^{1}H NMR (400 MHz, $CDCl_3$): δ 7.41−7.33 (m, 7H), 7.28−7.26 (m, 3H), 7.15−7.13 (m, 2H), 7.00−6.90 (m, 1H), 3.05 (s, 4H), 2.98 (s, 3H), 2.62 (br s, J = 6.0 Hz, 3H), 2.51 (t, J = 6.8 Hz, 6H), 2.45−2.37 (m, 4H), 2.29 (br s, 3H), 1.62−1.49 (m, 4H); ^{13}C NMR (101 MHz, $CDCl_3$): δ 178.09, 173.97, 151.17, 139.95, 133.94, 128.69, 128.65, 127.97, 127.48, 127.38, 127.15, 124.55, 118.73, 60.48, 57.93, 53.14, 51.06, 50.67, 47.97, 45.70, 43.25, 25.94, 24.19, 23.98. The free base was converted into the corresponding oxalate salt. HRMS ($C_{32}H_{40}ON_4Cl_2$ + H^+): calcd, 567.26519; found, 567.26458 (error −1.1 ppm). CHN ($C_{32}H_{40}ON_4Cl_2$ + $2.5H_2C_2O_4$ + H_2O) Calcd: C, 54.82; H, 5.84; N, 6.91. Found: C, 54.89; H, 5.68; N, 6.83. mp: initial decomposition ∼119 °C, complete melting 150−160 °C.

*4-((4-(4-(2,3-Dichlorophenyl)piperazin-1-yl)-3-hydroxybutyl)-amino)-N,N-dimethyl-2,2-diphenylbutanamide (**29**).* The reaction was performed following the same procedure described for **27**, starting from 4-amino-1-(4-(2,3-dichlorophenyl)piperazin-1-yl)butan-2-ol (130 mg, 0.41 mmol). The desired product was purified by flash

https://doi.org/10.1021/acs.jmedchem.1c00611
J. Med. Chem. 2021, 64, 7778−7808

chromatography eluting with 25% DMA and obtained as colorless oil (80 mg, 34% yield). ^{1}H NMR (400 MHz, $CDCl_3$): δ 7.37 (m, 8H), 7.31−7.22 (m, 2H), 7.16−7.07 (m, 2H), 6.93 (dd, J = 6.5, 3.1 Hz, 1H), 3.82 (m, 1H), 3.04 (br s, 6H), 2.97 (br s, 1H), 2.83−2.67 (m, 4H), 2.59 (dt, J = 11.8, 6.1 Hz, 4H), 2.50−2.30 (m, 4H), 2.30−2.17 (m, 4H), 1.56−1.32 (m, 2H); ^{13}C NMR (101 MHz, $CDCl_3$): δ 173.53, 151.32, 140.75, 140.71, 133.98, 128.38, 128.33, 128.12, 128.09, 128.04, 127.48, 127.36, 126.71, 126.68, 124.45, 118.56, 71.43, 68.18, 64.64, 62.95, 59.92, 53.04, 52.17, 51.35, 47.60, 47.30, 45.64, 43.84, 34.82, 34.04. HPLC analysis method A: Chiralpak AD-H analytical column (4.5 mm × 250 mm—5 μm particle size); mobile phase: isocratic 20% 2-PrOH in hexanes; flow rate: 1 mL/min; injection volume: 20 μL; sample concentration: ∼1 mg/mL; multiple DAD λ absorbance signals measured in the range of 210−280 nm, Rt 11.906 and 12.953 min, purity >99%, er 38:62 (absorbance at 254 nm). HPLC analysis method B: Chiralcel OD-H analytical column (4.5 mm × 250 mm—5 μm particle size); mobile phase: isocratic 20% 2-PrOH in hexanes; flow rate: 1 mL/min; injection volume: 20 μL; sample concentration: ∼1 mg/mL; multiple DAD λ absorbance signals measured in the range of 210−280 nm, Rt 12.011 min, purity >99% (absorbance at 254 nm). HPLC analysis method C: Chiralcel OZ-H analytical column (4.5 mm × 250 mm—5 μm particle size); mobile phase: isocratic 20% 2-PrOH in hexanes; flow rate: 1 mL/min; injection volume: 20 μL; sample concentration: ∼1 mg/mL; multiple DAD λ absorbance signals measured in the range of 210−280 nm, Rt 12.172 min, purity >95% (absorbance at 254 nm). The free base was converted into the corresponding oxalate salt. HRMS ($C_{32}H_{40}O_2N_4Cl_2$ + H^+): calcd, 583.26011; found, 583.26204 (error 2.3 ppm). CHN ($C_{32}H_{40}O_2N_4Cl_2$ + $2H_2C_2O_4$ + $1.5H_2O$) Calcd: C, 54.69; H, 5.99; N, 7.09. Found: C, 54.75; H, 5.71; N, 7.16. mp: salt decomposes above 116 °C.

*4-(4-(2-Chloro-3-ethylphenyl)piperazin-1-yl)-N,N-dimethyl-2,2-diphenylbutanamide (**30**).* The reaction was performed following the same procedure described for **27**, starting from 1-(2-chloro-3-ethylphenyl)piperazine[14] (120 mg, 0.53 mmol). The desired product was purified by flash chromatography eluting with 15% DMA and obtained as colorless oil (130 mg, 50% yield). ^{1}H NMR (400 MHz, $CDCl_3$): δ 7.44−7.34 (m, 8H), 7.29 (m, 2H), 7.13 (t, J = 7.8 Hz, 1H), 6.91 (ddd, J = 19.7, 7.8, 1.5 Hz, 2H), 3.07 (br s, 6H), 2.99 (br s, 2H), 2.74 (br s + q, 4H + 2H), 2.61−2.52 (m, 2H), 2.38 (m, 4H), 1.20 (t, J = 7.5 Hz, 3H); ^{13}C NMR (101 MHz, $CDCl_3$): δ 175.46, 173.36, 148.98, 143.16, 140.12, 128.63, 128.54, 128.49, 128.06, 126.98, 126.87, 124.19, 118.14, 59.68, 55.36, 52.67, 50.17, 40.52, 27.39, 22.19, 14.03. The free base was converted into the corresponding oxalate salt. HRMS ($C_{30}H_{36}ON_3Cl$ + H^+): found, 490.26239 (error 0.9 ppm). CHN ($C_{30}H_{36}ON_3Cl$ + $1.5H_2C_2O_4$) Calcd: C, 63.40; H, 6.29; N, 6.72. Found: C, 63.35; H, 6.46; N, 6.67. mp: 183−186 °C.

*4-((4-(4-(2-Chloro-3-ethylphenyl)piperazin-1-yl)butyl)amino)-N,N-dimethyl-2,2-diphenylbutanamide (**31**).* The reaction was performed following the same procedure described for **27**, starting from 4-(4-(2-chloro-3-ethylphenyl)piperazin-1-yl)butan-1-amine (390 mg, 1.33 mmol). The desired product was purified by flash chromatography eluting with 15% DMA and obtained as colorless oil (90 mg, 12% yield). ^{1}H NMR (400 MHz, $CDCl_3$): δ 7.43−7.30 (m, 8H), 7.30−7.21 (m, 2H), 7.13 (t, J = 7.8 Hz, 1H), 6.92 (ddd, J = 8.1, 6.6, 1.6 Hz, 2H), 3.03 (br s, 6H), 2.97 (br s, 2H), 2.76 (q, J = 7.5 Hz, 2H), 2.48−2.38 (m, 4H), 2.38−2.30 (m, 6H), 2.30−2.22 (m, 4H), 1.51−1.40 (m, 2H), 1.40−1.31 (m, 2H), 1.21 (t, J = 7.5 Hz, 3H); ^{13}C NMR (101 MHz, $CDCl_3$): δ 173.52, 149.69, 143.14, 140.85, 128.66, 128.32, 128.07, 126.83, 126.64, 123.85, 117.99, 59.90, 58.56, 53.42, 51.55, 49.76, 47.50, 45.75, 28.20, 27.46, 24.72, 23.03, 14.09. The free base was converted into the corresponding oxalate salt. HRMS ($C_{34}H_{45}ON_4Cl$ + H^+): calcd, 561.33547; found, 561.33350 (error −4.4 ppm). CHN ($C_{34}H_{45}ON_4Cl$ + $2H_2C_2O_4$ + $1.75H_2O$) Calcd: C, 59.06; H, 6.85; N, 7.25. Found: C, 59.09; H, 6.65; N, 7.17.

*4-((4-(4-(2-Chloro-3-ethylphenyl)piperazin-1-yl)-3-hydroxybutyl)amino)-N,N-dimethyl-2,2-diphenylbutanamide (**32**).* The reaction was performed following the same procedure described for **27**, starting from 4-amino-1-(4-(2-chloro-3-ethylphenyl)piperazin-1-yl)butan-2-ol (166 mg, 0.53 mmol). The desired product was purified by flash chromatography eluting with 25% DMA and obtained as colorless oil (110 mg, 36% yield). ^{1}H NMR (400 MHz, $CDCl_3$): δ 7.43−7.32 (m, 7H), 7.32−7.22 (m, 3H), 7.13 (t, J = 7.8 Hz, 1H), 6.92 (ddd, J = 11.9, 7.8, 1.6 Hz, 2H), 3.82 (m, 1H), 3.03 (s, 6H), 2.98 (s, 2H), 2.82−2.69 (m, 5H), 2.61 (ddd, J = 11.7, 8.1, 5.3 Hz, 3H), 2.47−2.19 (m, 8H), 1.58−1.34 (m, 2H), 1.22 (t, J = 7.5 Hz, 3H); ^{13}C NMR (101 MHz, $CDCl_3$): δ 173.55, 149.65, 143.17, 140.71, 128.67, 128.39, 128.05, 126.82, 126.72, 123.88, 117.98, 67.91, 64.64, 59.97, 53.73, 51.60, 47.48, 47.22, 45.49, 34.03, 27.45, 14.07. HPLC analysis method A: Chiralpak AD-H analytical column (4.5 mm × 250 mm—5 μm particle size); mobile phase: isocratic 20% 2-PrOH in hexanes; flow rate: 1 mL/min; injection volume: 20 μL; sample concentration: ∼1 mg/mL; multiple DAD λ absorbance signals measured in the range of 210−280 nm, Rt 8.242 and 9.055 min, purity >99%, er 37:63 (absorbance at 254 nm). HPLC analysis method B: Chiralcel OD-H analytical column (4.5 mm × 250 mm—5 μm particle size); mobile phase: isocratic 20% 2-PrOH in hexanes; flow rate: 1 mL/min; injection volume: 20 μL; sample concentration: ∼1 mg/mL; multiple DAD λ absorbance signals measured in the range of 210−280 nm, Rt 8.516 and 9.788 min, purity >99%, er 57:43 (absorbance at 254 nm). HPLC analysis method C: Chiralcel OZ-H analytical column (4.5 mm × 250 mm—5 μm particle size); mobile phase: isocratic 20% 2-PrOH in hexanes; flow rate: 1 mL/min; injection volume: 20 μL; sample concentration: ∼1 mg/mL; multiple DAD λ absorbance signals measured in the range of 210−280 nm, Rt 8.886 and 9.524 min, purity >99%. er 50:50 (absorbance at 254 nm). The free base was converted into the corresponding oxalate salt. HRMS ($C_{34}H_{45}O_2N_4Cl$ + H^+): found, 577.33059 (error 0.4 ppm). CHN ($C_{34}H_{45}O_2N_4Cl$ + $2H_2C_2O_4$ + H_2O) Calcd: C, 58.87; H, 6.63; N, 7.23. Found: C, 59.06; H, 6.46; N, 7.14. mp: 126−130 °C.

*2-(4-Aminobutyl)-1,2,3,4-tetrahydroisoquinoline-7-carbonitrile (**33**).* A suspension of 1,2,3,4-tetrahydroisoquinoline-7-carbonitrile (300 mg, 1.9 mmol), *N*-(4-bromobutyl)phthalimide (535 mg, 1.9 mmol), cat. KI (3.15 mg, 19 μmol), and K_2CO_3 (2.6 g, 19 mmol) in ACN (20 mL) was stirred under reflux overnight. The reaction mixture was cooled down to RT and filtered, the solvent was removed under vacuum, and the residue was dissolved in EtOH (10 mL), followed by the addition of hydrazine (0.175 mL). The solution was stirred under reflux for 3 h, EtOH was evaporated, and the residue was diluted with 20% K_2CO_3 aq solution and extracted with DCM. The organic layers were combined, dried over Na_2SO_4, filtered, and evaporated under vacuum. The crude material was used in the next step without further purification (300 mg, 94% yield).

*4-((4-(7-Cyano-3,4-dihydroisoquinolin-2(1H)-yl)butyl)amino)-N,N-dimethyl-2,2-diphenylbutanamide (**34**).* The reaction was performed following the same procedure described for **27**, starting from **33** (300 mg, 1.31 mmol) and **26** (368 mg, 1.31 mmol). The desired product was purified by flash chromatography eluting with 10% DMA and obtained as colorless oil (300 mg, 46% yield). ^{1}H NMR (400 MHz, $CDCl_3$): δ 7.42−7.21 (m, 12H), 7.16 (d, J = 7.9 Hz, 1H), 3.57 (s, 2H), 3.47 (d, J = 0.7 Hz, 6H), 2.99−2.87 (m, 4H), 2.68 (t, J = 5.9 Hz, 2H), 2.49−2.35 (m, 7H), 1.50 (q, J = 7.7 Hz, 2H), 1.41 (q, J = 7.3 Hz, 2H); ^{13}C NMR (101 MHz, $CDCl_3$): δ 173.55, 140.74, 140.36, 136.37, 130.37, 129.50, 129.46, 128.35, 128.04, 126.69, 119.13, 109.29, 59.89, 58.00, 55.45, 50.77, 50.10, 49.57, 47.45, 45.64, 29.41, 27.93, 24.82. The free base was converted into the corresponding oxalate salt. HRMS ($C_{32}H_{38}ON_4$ + H^+): found, 495.31212 (error 0.5 ppm). CHN ($C_{34}H_{45}O_2N_4Cl$ + $2H_2C_2O_4$ + $1.5H_2O$) Calcd: C, 61.61; H, 6.46; N, 7.98. Found: C, 61.59; H, 6.36; N, 7.98. mp: salt decomposes above 134 °C.

*(S)-3-Chloro-N-((1-(3-cyano-3,3-diphenylpropyl)pyrrolidin-2-yl)methyl)-5-ethyl-6-hydroxy-2-methoxybenzamide (**35**).* The reaction was performed following the same procedure described for **12**, starting from (*S*)-nor-eticlopride (250 mg, 0.8 mmol) and 4-bromo-2,2-diphenylbutanenitrile (240 mg, 0.8 mmol). The desired product was purified by flash chromatography eluting with hex/EtOAc (60/40) and obtained as colorless oil (98 mg, 23% yield). ^{1}H NMR (400 MHz, $CDCl_3$): δ 13.78 (s, 1H), 8.74 (s, 1H), 7.44−7.19 (m, 11H), 3.86 (s, 3H), 3.62 (ddd, J = 14.0, 6.9, 2.6 Hz, 1H), 3.29−3.12 (m,

https://doi.org/10.1021/acs.jmedchem.1c00611
J. Med. Chem. 2021, 64, 7778−7808

2H), 2.89−2.78 (m, 1H), 2.72−2.55 (m, 5H), 2.49−2.37 (m, 1H), 2.28 (q, J = 8.8 Hz, 1H), 1.90 (dq, J = 12.3, 8.1 Hz, 1H), 1.75 (t, J = 7.8 Hz, 2H), 1.67−1.51 (m, 1H), 1.32−1.15 (m, 3H); ^{13}C NMR (101 MHz, $CDCl_3$): δ 169.44, 160.15, 152.40, 140.02, 139.45, 132.90, 130.91, 128.95, 128.01, 127.97, 126.64, 122.00, 116.06, 108.18, 62.15, 61.44, 54.04, 50.33, 50.08, 40.43, 38.52, 29.68, 28.12, 22.71, 22.55, 13.43. CHN ($C_{31}H_{34}N_3O_3Cl$ + 0.4 hexanes) Calcd: C, 70.81; H, 7.05; N, 7.42. Found: C, 70.49; H, 7.15; N, 7.08. HPLC analysis method A: Chiralpak AD-H analytical column (4.5 mm × 250 mm—5 μm particle size); mobile phase: gradient from 10 to 40% 2-PrOH in hexanes; flow rate: 1 mL/min; injection volume: 20 μL; sample concentration: ∼1 mg/mL; multiple DAD λ absorbance signals measured in the range of 210−280 nm, Rt 7.799 min, purity >99%, ee >99% (absorbance at 254 nm). HPLC analysis method B: Chiralpak AD-H analytical column (4.5 mm × 250 mm—5 μm particle size); mobile phase: isocratic 10% 2-PrOH in hexanes; flow rate: 1 mL/min; injection volume: 20 μL; sample concentration: ∼1 mg/mL; multiple DAD λ absorbance signals measured in the range of 210−280 nm, Rt 9.043 min, purity >99%, ee >99% (absorbance at 254 nm). HRMS ($C_{31}H_{34}N_3O_3Cl$ + H^+): calcd, 532.23615; found, 532.23691 (error 0.4 ppm).

*(S)-N-((1-(4-Aminobutyl)pyrrolidin-2-yl)methyl)-3-chloro-5-ethyl-6-hydroxy-2-methoxybenzamide (**36**).* The reaction was performed following the same procedure described for **33**, starting from (*S*)-3-chloro-5-ethyl-6-hydroxy-2-methoxy-*N*-(pyrrolidin-2-ylmethyl)benzamide [(*S*)-nor-eticlopride 250 mg, 0.8 mmol]. The crude material was used in the next step without further purification (110 mg, 36% yield).

*(S)-3-Chloro-N-((1-(4-((3-cyano-3,3-diphenylpropyl)amino)-butyl)pyrrolidin-2-yl)methyl)-5-ethyl-6-hydroxy-2-methoxybenzamide (**37**).* The reaction was performed following the same procedure described for **12**, starting from **36** (110 mg, 0.29 mmol) and 4-bromo-2,2-diphenylbutanenitrile (78 mg, 0.26 mmol). The desired product was purified by flash chromatography eluting with 10% DMA and obtained as colorless oil (15 mg, 10% yield). ^{1}H NMR (400 MHz, $CDCl_3$ + CD_3OD): δ 7.39−7.23 (m, 6H), 7.18−7.06 (m, 5H), 3.83 (s, 3H), 3.82−3.50 (m, 6H), 3.36−3.26 (m, 6H), 2.82 (p, J = 6.9 Hz, 2H), 2.53 (q, J = 7.5 Hz, 2H), 1.74 (m, 5H), 1.11 (ddd, J = 8.2, 7.1, 0.8 Hz, 3H); ^{13}C NMR (101 MHz, $CDCl_3$): δ 174.69, 163.12, 156.56, 143.10, 142.99, 137.03, 134.45, 132.70, 132.67, 132.08, 132.06, 131.89, 131.85, 120.19, 112.47, 67.26, 66.39, 64.97, 57.87, 54.60, 49.82, 43.72, 42.16, 31.41, 27.77, 27.47, 26.07, 25.77, 16.57. HPLC analysis method A: Chiralpak AD-H analytical column (4.5 mm × 250 mm—5 μm particle size); mobile phase: gradient from 10 to 40% 2-PrOH in hexanes; flow rate: 1 mL/min; injection volume: 20 μL; sample concentration: ∼1 mg/mL; multiple DAD λ absorbance signals measured in the range of 210−280 nm, Rt 22.362 min, purity >95%, ee >99% (absorbance at 254 nm). HPLC analysis method B: Chiralpak AD-H analytical column (4.5 mm × 250 mm—5 μm particle size); mobile phase: isocratic 30% 2-PrOH in hexanes; flow rate: 1 mL/min; injection volume: 20 μL; sample concentration: ∼1 mg/mL; multiple DAD λ absorbance signals measured in the range of 210−280 nm, Rt 14.389 min, purity >99%, ee >99% (absorbance at 254 nm). HRMS ($C_{35}H_{43}N_4O_3Cl$ + 2H)$^{2+}$: found, 302.15901; ($C_{35}H_{43}N_4O_3Cl$ + H^+): calcd, 603.30965; found, 603.31020 (error 0.4 ppm).

*tert-Butyl ((1-(4-(1,3-Dioxoisoindolin-2-yl)butyl)pyrrolidin-2-yl)-methyl)carbamate (**38**).* A suspension of *tert*-butyl (pyrrolidin-2-ylmethyl)carbamate (500 mg, 2.5 mmol), *N*-(4-bromobutyl)-phthalimide (775 mg, 2.75 mmol), cat. KI (4.15 mg, 25 μmol), and K_2CO_3 (3.45 g, 25 mmol) in ACN (20 mL) was stirred under reflux overnight. The reaction mixture was cooled down to RT and filtered, the solvent was removed under vacuum, and the desired product, presenting both *N*-Boc and *N*-phthalimide protecting groups, was purified by flash chromatography eluting with 10% DMA and obtained as yellow oil (940 mg, 85% yield). ^{1}H NMR (400 MHz, $CDCl_3$): δ 7.84 (dd, J = 5.5, 3.0 Hz, 2H), 7.71 (dd, J = 5.5, 3.1 Hz, 2H), 5.00−4.95 (m, 1H), 3.77−3.64 (m, 2H), 3.27 (d, J = 10.9 Hz, 1H), 3.15−2.99 (m, 2H), 2.73 (dt, J = 11.9, 8.1 Hz, 1H), 2.47 (br s, 1H), 2.23−2.02 (m, 2H), 1.89−1.43 (m, 8H), 1.43 (s, 9H).

*3-Chloro-N-((1-(4-(1,3-dioxoisoindolin-2-yl)butyl)pyrrolidin-2-yl)methyl)-5-ethyl-6-hydroxy-2-methoxybenzamide (**39**).* A solution of **38** (940 mg, 2.34 mmol) and TFA (2.5 mL) in DCM (15 mL) was stirred at RT for 3 h. The reaction was quenched with $NaHCO_3$ (sat. aq solution) and extracted with DCM/2-PrOH (3:1). The organic layers were combined, dried over Na_2SO_4, filtered, and evaporated under vacuum. The crude material was dissolved in DCM (15 mL), followed by dropwise addition of a solution of 3-chloro-5-ethyl-6-hydroxy-2-methoxybenzoic acid[54] (647 mg, 2.81 mmol) and HCTU (1.16 g, 2.81 mmol) in DCM (15 mL). The reaction mixture was stirred at RT for 48 h, the solvent was removed under vacuum, and the crude material was purified by flash chromatography eluting with 5% DMA. The desired product was obtained as brown oil (310 mg, 26% yield). ^{1}H NMR (400 MHz, $CDCl_3$): δ 13.12 (s, 1H), 9.11 (s, 1H), 7.80 (dd, J = 5.4, 3.0 Hz, 2H), 7.69 (dd, J = 5.5, 3.0 Hz, 2H), 7.26−7.15 (m, 1H), 3.96−3.78 (m, 5H), 3.72 (m, J = 14.0 Hz, 4H), 3.57 (br s, 1H), 3.48 (br s, 1H), 3.26 (br s, 2H), 2.66−2.51 (m, 3H), 2.22 (dt, J = 15.0, 7.6 Hz, 1H), 1.99 (tt, J = 13.4, 6.9 Hz, 2H), 1.80−1.60 (m, 3H), 1.18 (dt, J = 10.7, 7.5 Hz, 3H).

*3-Chloro-N-((1-(4-((4-(dimethylamino)-4-oxo-3,3-diphenylbutyl)amino)butyl)pyrrolidin-2-yl)methyl)-5-ethyl-6-hydroxy-2-methoxybenzamide (**40**).* Hydrazine (0.2 mL, 50−60% wt in H_2O) was added to a solution of **39** (310 mg, 0.6 mmol) in EtOH (20 mL), and the solution was stirred at reflux for 3 h. The solvent was removed under vacuum, and the residue was diluted with 20% K_2CO_3 aq solution and extracted with DCM. The organic layers were combined, dried over Na_2SO_4, filtered, and evaporated under vacuum. The obtained crude material was dissolved in DCE (10 mL) and added to a solution of **26** (169 mg, 0.6 mmol) and catalytic AcOH in DCE (10 mL). The mixture was stirred for 10 min at RT, and STAB (190 mg, 0.9 mmol) was added portionwise. The reaction mixture was stirred for additional 12 h, the solvent was removed under vacuum, and the residue was purified by flash chromatography eluting with 10% DMA. The desired product was obtained as colorless oil (80.5 mg, 21% yield). ^{1}H NMR (400 MHz, $CDCl_3$): δ 8.79 (br s, 1H), 7.40−7.22 (m, 11H), 3.82 (s, 3H), 3.72 (dt, J = 12.1, 4.0 Hz, 2H), 3.28−3.19 (m, 1H), 3.14 (dt, J = 9.5, 4.5 Hz, 1H), 2.95 (br s, 3H), 2.74−2.52 (m, 3H), 2.47−2.35 (m, 4H), 2.25 (d, J = 14.1 Hz, 4H), 2.12 (q, J = 8.6 Hz, 3H), 1.93−1.80 (m, 1H), 1.72 (d, J = 7.8 Hz, 2H), 1.69−1.52 (m, 1H), 1.40 (dt, J = 16.4, 8.3 Hz, 4H), 1.20 (dt, J = 27.3, 7.3 Hz, 3H); ^{13}C NMR (101 MHz, $CDCl_3$): δ 173.62, 169.49, 160.11, 152.51, 140.71, 140.65, 132.82, 130.67, 128.37, 128.17, 128.16, 128.03, 126.72, 116.01, 108.17, 62.27, 61.41, 60.04, 54.01, 53.80, 49.38, 47.15, 45.23, 40.32, 28.10, 27.73, 26.57, 22.58, 22.51, 13.41. HPLC analysis method A: Chiralpak AD-H analytical column (4.5 mm × 250 mm—5 μm particle size); mobile phase: isocratic 30% 2-PrOH in hexanes; flow rate: 1 mL/min; injection volume: 20 μL; sample concentration: ∼1 mg/mL; multiple DAD λ absorbance signals measured in the range of 210−280 nm, Rt 9.538 and 10.664 min, purity >99%, er 46:54 (absorbance at 254 nm). HPLC analysis method B: Chiralpak AD-H analytical column (4.5 mm × 250 mm—5 μm particle size); mobile phase: isocratic 15% 2-PrOH in hexanes; flow rate: 1 mL/min; injection volume: 20 μL; sample concentration: ∼1 mg/mL; multiple DAD λ absorbance signals measured in the range of 210−280 nm, Rt 22.250 and 25.814 min, purity >99%, er 50:50 (absorbance at 254 nm). HRMS ($C_{37}H_{49}N_4O_4Cl$ + 2H)$^{2+}$: found, 325.18021; ($C_{37}H_{49}N_4O_4Cl$ + H^+): calcd, 649.35151; found, 649.35221 (error 1.0 ppm).

*3,3-Diphenylpyrrolidine (**41**).* A suspension of LAH (0.56 g, 14.8 mmol) in THF (50 mL) was cooled to 0 °C, and a solution of 4-bromo-2,2-diphenylbutanenitrile (1.5 g, 5 mmol) in THF (20 mL) was added dropwise. The mixture was stirred at RT for 15 h, quenched with MeOH (5 mL) and sat. aq $NaHCO_3$ solution (5 mL), filtered over Celite, and concentrated under vacuum. The residue was suspended in DCM and washed with sat. Na_2CO_3 solution. The organic layer was dried over Na_2SO_4, filtered, and evaporated under vacuum. The crude material was purified by flash chromatography eluting with 10% DMA. The desired product was obtained as yellow oil (0.450 g, 40% yield). ^{1}H NMR (400 MHz, $CDCl_3$): δ 7.34−7.22 (m, 8H), 7.22−7.13 (m, 2H), 3.52 (s, 2H), 3.13 (t, J = 7.2 Hz, 2H),

https://doi.org/10.1021/acs.jmedchem.1c00611
J. Med. Chem. 2021, 64, 7778−7808

2.80−2.70 (br s, 1H), 2.52 (t, J = 7.2 Hz, 2H). GC/MS (EI), Rt 9.987 min; 223.2 (M^+).

*1-Methyl-3,3-diphenylpyrrolidine (**42**).* Methyl chloroformate (85 mg, 69 μL, 0.9 mmol) was added dropwise to a solution of **41** (100 mg, 0.45 mmol) in THF (10 mL), followed by excess of DIPEA (5 equiv). The mixture was stirred at RT for 1 h, the solvent was evaporated under vacuum, and the residue was dissolved in THF (10 mL). This solution was added dropwise to a suspension of LAH (17 mg, 0.45 mmol) in THF (10 mL), at 0 °C. The mixture was warmed to RT, quenched with MeOH/2 N aq NaOH (1:1 ratio, 2 mL), and filtered over Celite, and the solvents were evaporated under vacuum. The crude material was purified by flash chromatography eluting with 10% DMA to afford the desired product as colorless oil (60 mg, 56% yield). ^{1}H NMR (400 MHz, $CDCl_3$): δ 7.26 (d, J = 4.6 Hz, 8H), 7.20−7.11 (m, 2H), 3.22 (s, 2H), 2.82 (td, J = 7.0, 0.6 Hz, 2H), 2.60 (dd, J = 7.7, 6.7 Hz, 2H), 2.42 (s, 3H). GC/MS (EI), Rt 9.650 min; 237.2 (M^+), purity >99%.

*1-(3,3-Diphenylpyrrolidin-1-yl)propan-1-one (**43**).* A solution of **41** (70 mg, 0.31 mmol), propionyl chloride (58 mg, 0.63 mmol), and DIPEA (5 equiv) in DCM (10 mL) was stirred under reflux overnight. The solvent was removed under vacuum, and the residue was purified by flash chromatography eluting with hex/EtOAc (70/30). The desired product was obtained as colorless oil (25 mg, 29% yield). ^{1}H NMR (400 MHz, $CDCl_3$) rotamer conformations observed (60:40; rotamer A/rotamer B): δ 7.34−7.14 (m, 10H), 4.16 (s, 2H, rotamer A), 4.04 (s, 2H, rotamer B), 3.53 (t, J = 6.9 Hz, 2H, rotamer B), 3.42 (t, J = 6.7 Hz, 2H, rotamer A), 2.63 (t, J = 6.7 Hz, 2H, rotamer A), 2.52 (t, J = 6.9 Hz, 2H, rotamer B), 2.41 (q, J = 7.5 Hz, 2H, rotamer B), 2.26 (q, J = 7.5 Hz, 2H, rotamer A), 1.21 (t, J = 7.5 Hz, 3H, rotamer B), 1.16 (t, J = 7.5 Hz, 3H, rotamer A). GC/MS (EI), Rt 12.154 min; 279.1 (M^+), purity >99%.

*2-Chloro-1-(3,3-diphenylpyrrolidin-1-yl)ethan-1-one (**44**).* 2-Chloroacetyl chloride (126 mg, 1.12 mmol) was added dropwise to a solution of **41** (250 mg, 1.12 mmol) in THF (10 mL) at 0 °C, followed by dropwise addition of DIPEA (0.3 mL, 1.68 mmol). The mixture was allowed to warm to RT and stirred for 1 h. The solvent was removed under vacuum, and the residue was used in the following step without further purification. GC/MS (EI), Rt 12.740 min; 299.1 (M^+).

*tert-Butyl ((1-(2-(3,3-Diphenylpyrrolidin-1-yl)-2-oxoethyl)-pyrrolidin-2-yl)methyl)carbamate (**45**).* A mixture of **44** (290 mg, 0.97 mmol), *tert*-butyl (pyrrolidin-2-ylmethyl)carbamate (194 mg, 0.97 mmol), KI (161 mg, 0.97 mmol), and K_2CO_3 (1.34 g, 9.67 mmol) in ACN (25 mL) was stirred under reflux for 3 h. The mixture was filtered, the solvent was evaporated under vacuum, and the residue was purified by flash chromatography eluting with 10% DMA. The desired product was obtained as yellow oil (330 mg, 74% yield). ^{1}H NMR (400 MHz, $CDCl_3$) rotamer conformations observed: δ 7.34−7.15 (m, 10H), 5.30 (m, 1H), 3.69−3.38 (m, 4H), 3.29−2.93 (m, 3H), 2.71−2.17 (m, 4H), 1.90 (tt, J = 19.2, 8.6 Hz, 2H), 1.73 (m, J = 17.3, 8.5 Hz, 4H), 1.50−1.38 (m, 9H).

*3-Chloro-N-((1-(2-(3,3-diphenylpyrrolidin-1-yl)-2-oxoethyl)-pyrrolidin-2-yl)methyl)-5-ethyl-6-hydroxy-2-methoxybenzamide (**46**).* TFA (0.3 mL) was added to a solution of **45** (330 mg, 0.71 mmol) in DCM (10 mL). The mixture was stirred at RT for 2 h, basified with NH_4OH (28% aq solution), and extracted with DCM. The organic layers were combined, dried over Na_2SO_4, filtered, and evaporated under vacuum to afford the crude material, which was filtered over a silica pad, eluting and washing with 25% DMA to isolate the desired primary amine intermediate. The amine was dissolved in DCM (10 mL) and added dropwise to a solution of 3-chloro-5-ethyl-6-hydroxy-2-methoxybenzoic acid (70 mg, 0.3 mmol), HCTU (0.2 g, 0.33 mmol), and DIPEA (1.5 equiv) in DCM (10 mL). The mixture was stirred at RT for 3 h, the solvent was removed under vacuum, and the residue was purified by flash chromatography eluting with 5% DMA. The desired product was obtained as colorless oil (26 mg, 15% yield). ^{1}H NMR (400 MHz, $CDCl_3$) rotamer conformations observed: δ 13.68 (s, 1H), 8.82 (s, 1H), 7.31−7.12 (m, 11H), 4.23 (t, J = 11.0 Hz, 1H), 4.02 (dd, J = 26.1, 11.5 Hz, 1H), 3.85 (ds, J = 17.4 Hz, 3H), 3.79−3.68 (m, 1H), 3.62−3.21 (m, 6H), 2.96 (br s, 1H), 2.68−2.52 (m, 4H), 2.14−1.97 (m, 1H), 1.92−1.66 (m, 4H), 1.28−1.14 (m, 3H); ^{13}C NMR (101 MHz, $CDCl_3$) rotamer conformations observed: δ 169.75, 160.07, 160.04, 152.47, 152.46, 144.94, 144.88, 144.79, 133.07, 130.79, 130.77, 128.57, 128.53, 128.51, 126.67, 126.62, 126.59, 126.58, 126.52, 116.16, 116.11, 107.98, 61.57, 61.49, 56.60, 56.14, 56.12, 55.10, 54.87, 54.68, 54.45, 53.40, 52.22, 44.57, 44.39, 40.88, 40.46, 37.52, 35.57, 29.68, 28.38, 28.26, 23.05, 22.86, 22.51, 13.39. HPLC analysis method A: Chiralpak AD-H analytical column (4.5 mm × 250 mm—5 μm particle size); mobile phase: isocratic 10% 2-PrOH in hexanes; flow rate: 1 mL/min; injection volume: 20 μL; sample concentration: ∼1 mg/mL; multiple DAD λ absorbance signals measured in the range of 210−280 nm, Rt 20.539 and 23.859 min, purity >99%, er 51:49 (absorbance at 254 nm). HRMS ($C_{33}H_{38}N_3O_4Cl$ + H^+): calcd, 576.26236; found, 576.26297 (error 1.0 ppm).

*3-Chloro-N-(((2S,4R)-4-(4-((4-(dimethylamino)-4-oxo-3,3-diphenylbutyl)amino)butoxy)pyrrolidin-2-yl)methyl)-5-ethyl-6-hydroxy-2-methoxybenzamide (**48**).* A solution of **47** (400 mg, 0.8 mmol), **26** (225 mg, 0.8 mmol), and cat. AcOH (0.05 equiv) in DCE (20 mL) was stirred at RT for 1 h, followed by portionwise addition of STAB (339 mg, 1.6 mmol). The mixture was stirred at RT for 3 h and basified with 10% NH_4OH in MeOH, the solvent was evaporated under vacuum, and the residue was purified by flash chromatography eluting with 10% DMA. The obtained intermediate was dissolved in DCM (20 mL) and TFA (10 mL), and the solution was stirred at RT overnight. The excess of TFA was removed under vacuum, and the residue resuspended in aq NH_4OH (pH 9) and extracted with DCM/2-PrOH (3:1). The organic layers were combined, dried over Na_2SO_4, filtered, and evaporated to afford the crude material, which was purified by flash chromatography eluting with 25% DMA. The desired product was obtained as colorless oil (45 mg, 8.5% yield). ^{1}H NMR (400 MHz, $CDCl_3$): δ 8.92 (s, 1H), 7.43−7.21 (m, 11H), 3.97 (t, J = 4.9 Hz, 1H), 3.89 (s, 3H), 3.57 (dq, J = 9.6, 4.7 Hz, 3H), 3.36 (dt, J = 5.8, 2.8 Hz, 3H), 3.22 (tt, J = 8.9, 4.5 Hz, 2H), 3.02−2.90 (m, 5H), 2.69−2.55 (m, 4H), 2.45 (dd, J = 21.5, 5.7 Hz, 4H), 2.30 (br s, 2H), 2.00 (dd, J = 13.7, 6.9 Hz, 1H), 1.70−1.50 (m, 5H), 1.31−1.14 (m, 3H); ^{13}C NMR (101 MHz, $CDCl_3$): δ 174.57, 169.21, 160.06, 152.48, 139.97, 132.89, 130.72, 128.78, 127.96, 127.93, 127.26, 116.16, 108.17, 80.67, 68.17, 61.57, 56.10, 51.78, 43.34, 36.07, 27.16, 22.50, 21.93, 13.41. HPLC analysis method: Chiralpak AD-H analytical column (4.5 mm × 250 mm—5 μm particle size); mobile phase: isocratic 20% 2-PrOH in hexanes; flow rate: 1 mL/min; injection volume: 20 μL; sample concentration: ∼1 mg/mL; multiple DAD λ absorbance signals measured in the range of 210−280 nm, Rt 18.518 min, purity >95%, ee >95% (absorbance at 210 nm). The free base was converted into the corresponding oxalate salt. HRMS ($C_{37}H_{49}N_4O_5Cl$ + $2H)^{2+}$: calcd, 333.17685; found, 333.17656 (error 0.9 ppm); ($C_{37}H_{49}N_4O_5Cl$ + $H)^+$: calcd, 665.34642; found, 665.34552 (error 1.4 ppm). CHN ($C_{37}H_{49}N_4O_5Cl$ + $2H_2C_2O_4$ + $1.5H_2O$) Calcd: C, 56.45; H, 6.47; N, 6.42. Found: C, 56.25; H, 6.24; N, 6.40. mp: salt decomposes above 90 °C.

*3,3-Bis(3-methoxyphenyl)acrylaldehyde (**49**).* A solution of bis(3-methoxyphenyl)methanone (1.0 g, 4.13 mmol) and $TiCl_4$ (1.0 M solution in DCM, 16.5 mL, 16.5 mmol) in DCM was cooled to 0 °C. TEA (2.3 mL, 16.5 mmol) was added dropwise, and the mixture was warmed to RT and stirred overnight.[55] The reaction was quenched with sat. NH_4Cl aq solution and stirred for 30 min. The mixture was extracted with DCM, and the organic layers were combined, dried over Na_2SO_4, filtered, and concentrated under vacuum. The crude material was purified by flash chromatography eluting with hex/EtOAc (95/5). The desired product was obtained as colorless oil (645 mg, 58% yield). ^{1}H NMR (400 MHz, $CDCl_3$): δ 9.60−9.53 (m, 1H), 7.42−7.25 (m, 2H), 7.07−6.77 (m, 6H), 6.64−6.56 (m, 1H), 3.89−3.74 (m, 6H). GC/MS (EI), Rt 11.647 min; 268.1 (M^+).

*N-(3,3-Bis(3-methoxyphenyl)allyl)-4-(4-(2,3-dichlorophenyl)-piperazin-1-yl)butan-1-amine (**50**).* A solution of **49** (302 mg, 1.12 mmol), 4-(4-(2,3-dichlorophenyl)piperazin-1-yl)butan-1-amine (340 mg, 1.12 mmol), and cat. AcOH (0.1 equiv) in DCE (20 mL) was stirred for 1 h at RT, followed by portionwise addition of STAB (715 mg, 3.37 mmol). The reaction mixture was stirred for 3 h, the solvent

https://doi.org/10.1021/acs.jmedchem.1c00611
J. Med. Chem. 2021, 64, 7778−7808

was evaporated under vacuum, and the residue was purified by flash chromatography eluting with 5% DMA. The desired product was obtained as colorless oil (550 mg, 88% yield). ^{1}H NMR (400 MHz, $CDCl_3$): δ 7.26 (m, 1H), 7.16 (q, J = 7.6 Hz, 2H), 6.90−6.79 (m, 3H), 6.79−6.67 (m, 4H), 6.67−6.60 (m, 1H), 6.20−6.11 (m, 1H), 3.74 (d, J = 5.4 Hz, 6H), 3.38−3.33 (m, 4H), 3.08 (br s, 4H), 2.74 (m, 2H), 2.58 (br s, 2H), 2.42 (m, 2H), 1.47 (m, 2H), 1.28 (m, 2H); ^{13}C NMR (101 MHz, $CDCl_3$): δ 175.73, 159.49, 159.43, 150.75, 142.64, 140.20, 134.01, 129.39, 129.11, 127.48, 127.47, 124.83, 122.01, 119.88, 118.71, 115.22, 113.32, 112.98, 112.85, 57.48, 55.20, 55.16, 53.39, 52.57, 52.48, 51.42, 50.27, 30.90, 23.33, 23.10, 21.27. HPLC analysis method: Chiralpak AD-H analytical column (4.5 mm × 250 mm—5 μm particle size); mobile phase: isocratic 20% 2-PrOH in hexanes; flow rate: 1 mL/min; injection volume: 20 μL; sample concentration: ∼1 mg/mL; multiple DAD λ absorbance signals measured in the range of 210−280 nm, Rt 6.538 min, purity >95% (absorbance at 254 nm). HRMS ($C_{31}H_{37}N_3O_2Cl_2$ + H)$^+$: calcd, 554.23356; found, 554.23390.

*3,3′-(3-((4-(4-Phenylpiperazin-1-yl)butyl)amino)propane-1,1-diyl)diphenol (**51**).* A suspension of **50** (250 mg, 0.45 mmol) and Pd/C (20% wt wet, 0.05 equiv) in EtOH (10 mL) was shaken in a Parr apparatus under 50 psi pressure of hydrogen gas for 12 h. The mixture was filtered through a pad of Celite, the solvent was evaporated under vacuum, and the residue was purified trough a pad of silica eluting with 5% DMA. This intermediate was dissolved in 33% HBr (solution in AcOH, 2 mL) and stirred under reflux for 48 h. The solvent was removed under vacuum, and the residue was basified with 10% v/v NH_4OH solution in methanol. The crude material was purified by flash chromatography eluting with 25% DMA. The desired product was obtained as yellow oil (6.8 mg, 29% yield). ^{1}H NMR (400 MHz, $CDCl_3$): δ 7.28−7.19 (m, 1H), 7.09 (t, J = 7.8 Hz, 2H), 6.90−6.80 (m, 2H), 6.71−6.60 (m, 4H), 6.55 (s, 2H), 5.44 (br s, 2H), 3.81 (t, J = 7.9 Hz, 1H), 3.09 (t, J = 5.0 Hz, 4H), 2.61 (s, 2H), 2.49 (dt, J = 11.8, 5.4 Hz, 6H), 2.25 (p, J = 7.5 Hz, 4H), 1.30−1.16 (m, 4H); ^{13}C NMR (101 MHz, $CDCl_3$): δ 172.49, 157.37, 150.94, 145.43, 129.75, 129.07, 119.90, 119.43, 116.11, 114.54, 114.47, 65.83, 58.11, 52.97, 34.26, 26.57, 25.34, 24.12, 22.59, 15.25. HPLC analysis method: Chiralpak AD-H analytical column (4.5 mm × 250 mm—5 μm particle size); mobile phase: isocratic 20% 2-PrOH in hexanes + 0.1% DEA; flow rate: 1 mL/min; injection volume: 20 μL; sample concentration: ∼1 mg/mL; multiple DAD λ absorbance signals measured in the range of 210−280 nm, Rt 38.741 min, purity >95% (absorbance at 254 nm). HRMS ($C_{29}H_{37}N_3O_2$ + H)$^+$: found, 460.29628.

*1-(3,3-Bis(3-methoxyphenyl)allyl)-4-(2-chloro-3-ethylphenyl)-piperazine (**52**).* The reaction was performed following the same procure described for **50**, starting from 1-(2-chloro-3-ethylphenyl)-piperazine[14] (180 mg, 0.78 mmol). The desired product was obtained as colorless oil (330 mg, 88% yield). ^{1}H NMR (400 MHz, $CDCl_3$): δ 7.24−7.11 (m, 3H), 7.00−6.66 (m, 8H), 6.31 (t, J = 7.0 Hz, 1H), 3.79 (d, J = 14.0 Hz, 6H), 3.34 (d, J = 6.9 Hz, 2H), 3.14 (br s, 4H), 3.00−2.76 (br s, 4H), 2.76 (q, J = 7.5 Hz, 2H), 1.21 (t, J = 7.5 Hz, 3H).

*1-(3,3-Bis(3-methoxyphenyl)propyl)-4-(2-chloro-3-ethylphenyl)-piperazine (**53**).* A suspension of **52** (330 mg, 0.69 mmol) and Pd/C (20% wt wet, 0.05 equiv) in EtOAc/EtOH (10:5 mL) was shaken in a Parr apparatus under 30 psi pressure of H_2 for 3 h. The mixture was filtered through a pad of Celite, the solvent was evaporated under vacuum, and the desired product was obtained as colorless oil (250 mg, 75% yield). ^{1}H NMR (400 MHz, $CDCl_3$): δ 7.18 (dt, J = 20.9, 7.8 Hz, 3H), 6.94 (ddd, J = 11.1, 7.8, 1.5 Hz, 2H), 6.90−6.67 (m, 6H), 3.96−3.86 (m, 1H), 3.82−3.67 (br s, 6H), 3.10 (br s, 4H), 2.76 (br s + q, J = 7.5 Hz, 6H), 2.50 (dd, J = 9.9, 5.8 Hz, 2H), 2.06 (m, 2H), 1.29−1.15 (t, J = 7.5 Hz, 3H). HRMS ($C_{29}H_{35}ClN_2O_2$ + H)$^+$: calcd, 479.24598; found, 479.24505 (error 1.9 ppm). The free base (50 mg) was converted into the corresponding oxalate salt. mp: salt decomposes above 100 °C.

*3-(3-(4-(2-Chloro-3-ethylphenyl)piperazin-1-yl)-1-(3-methoxyphenyl)propyl)phenol (**54**) and 3,3′-(3-(4-(2-Chloro-3-ethylphenyl)piperazin-1-yl)propane-1,1-diyl)diphenol (**55**).* A solution of **53** (200 mg, 0.42 mmol) in 33% HBr (solution in AcOH, 5 mL) and DCM (10 mL) was stirred under reflux for 24 h. The solvent was removed under vacuum, and the residue was basified with 28−30% v/v aq NH_4OH and extracted with DCM/2-PrOH (3:1). The crude material was purified by flash chromatography eluting with 10% DMA. **54** eluted first as yellow oil (60 mg, 31% yield): ^{1}H NMR (400 MHz, $CDCl_3$): δ 7.20−7.07 (m, 3H), 6.94 (dd, J = 7.6, 1.5 Hz, 1H), 6.91−6.66 (m, 4H), 6.64 (d, J = 1.0 Hz, 1H), 6.64−6.47 (m, 2H), 3.83 (t, J = 7.6 Hz, 1H), 3.73 (s, 3H), 3.01 (br s, 4H), 2.76 (br s + q, J = 7.5 Hz, 6H), 2.49−2.36 (m, 2H), 2.35−2.15 (m, 2H), 1.36−1.17 (t, J = 7.5 Hz, 3H). HRMS ($C_{28}H_{33}ClN_2O_2$ + H)$^+$: calcd, 465.23033; found, 465.22945 (error 1.9 ppm). **55** eluted second as a yellow oil (25 mg, 13% yield): ^{1}H NMR (400 MHz, $CDCl_3$): δ 7.09 (td, J = 7.8, 2.4 Hz, 3H), 6.93 (dd, J = 7.6, 1.5 Hz, 1H), 6.85−6.69 (m, 3H), 6.63 (ddd, J = 8.1, 2.5, 0.9 Hz, 2H), 6.55 (t, J = 1.9 Hz, 2H), 3.75 (q, J = 7.9 Hz, 1H), 2.97 (br s, 4H), 2.75−2.60 (br s + q, J = 7.6 Hz, 6H), 2.43 (br s, 2H), 2.26−2.15 (m, 2H), 1.30−1.16 (t, J = 7.5 Hz, 3H). HRMS ($C_{27}H_{31}ClN_2O_2$ + H)$^+$: calcd, 451.21468; found, 451.21429 (error 0.9 ppm).

*trans-Ethyl (Z)-2-((1S,5S)-2-(4-(1H-Indole-2-carboxamido)butyl)-5-(3-hydroxyphenyl)-2-azabicyclo[3.3.1]nonan-9-ylidene)acetate (**57**).* A solution of **56** (20 mg, 66 μmol), *N*-(4-oxobutyl)-1*H*-indole-2-carboxamide[57] (18 mg, 80 μmol), and catalytic AcOH (0.01 equiv) in DCE (10 mL) was stirred at RT for 1 h, followed by portionwise addition of STAB (30 mg, 66 μmol). The reaction mixture was stirred for additional 30 min and basified with 10% NH_4OH solution in MeOH (10 mL), the solvent was evaporated under vacuum, and the residue was purified by flash chromatography eluting with 20% DMA. The desired product was obtained as colorless oil (30 mg, 88% yield). ^{1}H NMR (400 MHz, $CDCl_3$): δ 9.30 (s, 1H), 7.61 (dd, J = 8.0, 1.0 Hz, 1H), 7.46−7.38 (m, 1H), 7.32−7.08 (m, 3H), 6.97−6.78 (m, 4H), 6.78−6.70 (m, 1H), 5.30 (s, 1H), 5.16 (d, J = 17.9 Hz, 2H), 4.13−3.92 (m, 2H), 3.63−3.44 (m, 2H), 3.20 (ddd, J = 13.2, 8.9, 4.8 Hz, 1H), 2.73 (ddt, J = 17.8, 12.3, 5.8 Hz, 3H), 2.46 (ddd, J = 14.4, 8.7, 6.0 Hz, 1H), 2.27−2.00 (m, 5H), 1.90−1.50 (m, 6H), 1.14 (t, J = 7.1 Hz, 3H); ^{13}C NMR (101 MHz, $CDCl_3$): δ 167.91, 166.96, 161.79, 155.61, 148.65, 136.14, 131.04, 129.25, 127.68, 124.33, 121.83, 120.55, 119.46, 115.00, 114.38, 113.60, 111.89, 102.22, 59.92, 55.45, 53.31, 48.76, 45.69, 40.19, 39.34, 38.73, 30.66, 27.22, 24.50, 20.48, 14.13. HPLC analysis method A: Chiralpak AD-H analytical column (4.5 mm × 250 mm—5 μm particle size); mobile phase: isocratic 20% 2-PrOH in hexanes; flow rate: 1 mL/min; injection volume: 20 μL; sample concentration: ∼1 mg/mL; multiple DAD λ absorbance signals measured in the range of 210−280 nm, Rt 30.677 min, purity >99%, ee >99% (absorbance at 254 nm). HPLC analysis method B: Chiralpak AD-H analytical column (4.5 mm × 250 mm—5 μm particle size); mobile phase: isocratic 30% 2-PrOH in hexanes; flow rate: 1 mL/min; injection volume: 20 μL; sample concentration: ∼1 mg/mL; multiple DAD λ absorbance signals measured in the range of 210−280 nm, Rt 13.495 min, purity >99%, ee >99% (absorbance at 254 nm). HRMS ($C_{31}H_{37}O_4N_3$ + H$^+$): calcd, 516.28568; found, 516.28475 (error −1.8 ppm).

*trans-Ethyl (Z)-2-((2S,6R)-6-(((2-(2-(1H-Indole-2-carboxamido)-ethyl)cyclopropyl)methyl)(ethyl)amino)-2-(3-hydroxyphenyl)-2-methylcyclohexylidene)acetate (**58**).* The reaction was performed following the same procure described for **57**, starting from **56** (20 mg, 66 μmol) and *N*-(2-(2-formylcyclopropyl)ethyl)-1*H*-indole-2-carboxamide[45] (17 mg, 66 μmol). The desired product was obtained as colorless oil (23 mg, 65% yield). ^{1}H NMR (400 MHz, $CDCl_3$) mixture of diastereomers observed: δ 9.33 (s, 1H, dr 60:40), 7.62 (dd, J = 8.1, 3.8 Hz, 1H), 7.47−7.39 (m, 1H), 7.34−7.25 (m, 1H), 7.23−7.08 (m, 2H), 6.93 (d, J = 10.1 Hz, 1H), 6.89−6.69 (m, 3H), 6.60 (s, 1H), 5.25−5.10 (m, 2H), 4.13−3.95 (m, 2H), 3.72−3.49 (m, 2H), 3.16 (d, J = 12.3 Hz, 1H), 2.96−2.74 (m, 2H), 2.46 (dd, J = 14.2, 6.9 Hz, 1H), 2.37−2.27 (m, 1H), 2.25−1.98 (m, 7H), 1.64−1.49 (m, 4H), 1.38−1.24 (m, 1H), 1.15 (dt, J = 8.2, 7.1 Hz, 3H), 0.89 (d, J = 62.8 Hz, 1H, dr **60**:40), 0.69 (d, J = 52.6 Hz, 1H, dr 60:**40**), 0.32 (dt, J = 17.8, 5.9 Hz, 1H); ^{13}C NMR (101 MHz, $CDCl_3$): δ 166.85, 166.83, 161.95, 161.69, 156.18, 155.88, 136.29, 136.20, 130.95, 130.50, 129.23, 129.13, 127.69, 127.56, 124.62, 124.40, 121.90,

https://doi.org/10.1021/acs.jmedchem.1c00611
J. Med. Chem. 2021, 64, 7778−7808

121.85, 120.74, 120.58, 115.31, 115.13, 113.95, 113.82, 112.01, 111.90, 102.62, 60.90, 60.56, 59.87, 59.81, 55.32, 54.77, 50.85, 48.21, 48.08, 45.64, 45.60, 40.24, 40.17, 40.09, 39.74, 33.47, 33.42, 30.86, 20.19, 18.92, 17.04, 16.55, 15.72, 14.17, 14.15, 10.91, 9.23. HPLC analysis method: Chiralpak AD-H analytical column (4.5 mm × 250 mm—5 μm particle size); mobile phase: isocratic 20% 2-PrOH in hexanes; flow rate: 1 mL/min; injection volume: 20 μL; sample concentration: ∼1 mg/mL; multiple DAD λ absorbance signals measured in the range of 210−280 nm, Rt 22.572 and 27.023 min, purity >99%, dr 45:55 (absorbance at 254 nm). HRMS ($C_{33}H_{39}O_4N_3$ + H^+): calcd, 542.30133; found, 542.29988 (error −3.6 ppm). The two diastereoisomers **58a** and **58b** were resolved and separated by preparative chiral HPLC (Chiralpak AD-H 21 mm × 250 mm × 5 μm): mobile phase: gradient from 10 to 40% 2-PrOH in hexanes; temperature: 25 °C; flow rate: 15−18 mL/min; injection volume: 3 mL (∼15−20 mg/mL sample concentration); detection at λ 230 and 254 nm with the support of ELS detector. **58a** eluted first; HPLC analysis method: Chiralpak AD-H analytical column (4.5 mm × 250 mm—5 μm particle size); mobile phase: isocratic 20% 2-PrOH in hexanes; flow rate: 1 mL/min; injection volume: 20 μL; sample concentration: ∼1 mg/mL; multiple DAD λ absorbance signals measured in the range of 210−280 nm, Rt 28.905 min, purity >99%, de >99% (absorbance at 254 nm). **58b** eluted second; HPLC analysis method: Chiralpak AD-H analytical column (4.5 mm × 250 mm—5 μm particle size); mobile phase: isocratic 20% 2-PrOH in hexanes; flow rate: 1 mL/min; injection volume: 20 μL; sample concentration: ∼1 mg/mL; multiple DAD λ absorbance signals measured in the range of 210−280 nm, Rt 34.205 min, purity >99%, de >99% (absorbance at 254 nm).

*N-(4-((1S,5S,9R)-9-Hydroxy-5-(3-hydroxyphenyl)-2-azabicyclo-[3.3.1]nonan-2-yl)butyl)-1H-indole-2-carboxamide (**61**).* The reaction was performed following the same procure described for **57**, starting from (1*S*,5*S*,9*R*)-5-(3-hydroxyphenyl)-2-azabicyclo[3.3.1]-nonan-9-ol (**59**; 40 mg, 0.17 mmol). The desired product was purified by flash chromatography eluting with 20% DMA and obtained as a white solid (20 mg, 26% yield). ^{1}H NMR (400 MHz, CD_3OD): δ 7.57 (ddt, *J* = 9.0, 8.0, 1.0 Hz, 2H), 7.41 (dt, *J* = 8.2, 0.8 Hz, 2H), 7.24−6.94 (m, 4H), 6.89−6.73 (m, 2H), 6.66−6.58 (m, 1H), 4.25 (m, 1H), 4.07 (s, 1H), 3.74 (d, *J* = 0.5 Hz, 2H), 3.46 (d, *J* = 6.1 Hz, 1H), 3.44−3.25 (m, 3H), 2.96 (d, *J* = 9.8 Hz, 1H), 2.70 (br s, 3H), 2.48 (td, *J* = 13.5, 7.8 Hz, 2H), 2.31 (d, *J* = 12.8 Hz, 1H), 2.23−2.08 (m, 1H), 1.93−1.61 (m, *J* = 4.2, 3.2 Hz, 6H), 1.28 (br s, 1H). HPLC analysis method: Chiralpak AD-H analytical column (4.5 mm × 250 mm—5 μm particle size); mobile phase: isocratic 50% 2-PrOH in hexanes + 0.1% DEA; flow rate: 1 mL/min; injection volume: 20 μL; sample concentration: ∼1 mg/mL; multiple DAD λ absorbance signals measured in the range of 210−280 nm, Rt 29.790, purity >99%, ee >99% (absorbance at 254 nm). HRMS ($C_{27}H_{34}O_3N_3$ + H^+): calcd, 448.25947; found, 448.25979.

*N-(4-((1S,5S,9S)-9-Hydroxy-5-(3-hydroxyphenyl)-2-azabicyclo-[3.3.1]nonan-2-yl)butyl)-1H-indole-2-carboxamide (**62**).* The reaction was performed following the same procedure described for **57**, starting from (1*S*,5*S*,9*S*)-5-(3-hydroxyphenyl)-2-azabicyclo[3.3.1]-nonan-9-ol (**60**; 40 mg, 0.17 mmol). The desired product was purified by flash chromatography eluting with 20% DMA and obtained as a white solid (20 mg, 26% yield). ^{1}H NMR (400 MHz, CD_3OD): δ 7.62−7.53 (m, 2H), 7.42 (t, *J* = 8.3 Hz, 2H), 7.25−7.12 (m, 2H), 7.12−6.80 (m, 4H), 6.40 (m, 1H), 4.30 (m, 1H), 4.07 (s, 1H), 3.75 (s, 2H), 3.49−3.37 (m, 4H), 2.98 (br s, 1H), 2.20−1.93 (m, 7H), 1.73−1.66 (m, 5H), 1.28 (br s, 2H). HPLC analysis method: Chiralpak AD-H analytical column (4.5 mm × 250 mm—5 μm particle size); mobile phase: isocratic 50% 2-PrOH in hexanes + 0.1% DEA; flow rate: 1 mL/min; injection volume: 20 μL; sample concentration: ∼1 mg/mL; multiple DAD λ absorbance signals measured in the range of 210−280 nm, Rt 32.837, purity >99%, ee >99% (absorbance at 254 nm). HRMS ($C_{27}H_{34}O_3N_3$ + H^+): calcd, 448.25947; found, 448.25982.

*2-(4-(2,3-Dichlorophenyl)piperazin-1-yl)ethan-1-ol (**63**).* A solution of 1-(2,3-dichlorophenyl)piperazine hydrochloride (500 mg, 1.87 mmol) and K_2CO_3 (1.29 g, 9.34 mmol) in ACN (30 mL) was stirred for 25 min under gentle heating, followed by dropwise addition of 2-bromoethan-1-ol (257 mg, 2.06 mmol) and cat. KI. The suspension was stirred under reflux overnight and filtered, and the solvent was evaporated under vacuum to afford the crude material. The desired product was purified by flash chromatography eluting with 100% EtOAc and obtained as yellow oil (310 mg, 60% yield). ^{1}H NMR (400 MHz, $CDCl_3$): δ 7.21−7.10 (m, 2H), 6.96 (dd, *J* = 6.7, 2.8 Hz, 1H), 3.72−3.62 (m, 2H), 3.08 (br s, 4H), 2.71 (br s, 4H), 2.67−2.60 (m, 2H).

*2-(4-(2,3-Dichlorophenyl)piperazin-1-yl)ethyl 4-Methylbenzene-sulfonate (**64**).* *p*-Toluenesulfonyl chloride (*p*-TsCl, 200 mg, 1.05 mmol) was added portionwise to a solution of **63** (240 mg, 0.87 mmol) and DIPEA (0.310 mL, 225 mg, 1.74 mmol) in DCM (15 mL). The mixture was stirred at RT overnight, the solvent was evaporated under vacuum, and the crude residue was purified by flash chromatography eluting with hex/EtOAc (1/1). The desired product was obtained as a white solid (135 mg, 36% yield). ^{1}H NMR (400 MHz, $CDCl_3$): δ 7.81 (d, *J* = 7.9 Hz, 2H), 7.34 (d, *J* = 7.9 Hz, 2H), 7.18−7.08 (m, 2H), 6.91 (dd, *J* = 6.8, 2.9 Hz, 1H), 4.16 (t, *J* = 5.7 Hz, 2H), 3.06−2.99 (br s, 4H), 2.72 (t, *J* = 5.8 Hz, 2H), 2.61 (br s, 4H), 2.44 (s, 3H).

*Ethyl (Z)-2-((1S,5S)-2-(2-(4-(2,3-Dichlorophenyl)piperazin-1-yl)-ethyl)-5-(3-hydroxyphenyl)-2-azabicyclo[3.3.1]nonan-9-ylidene)-acetate (**65**).* A suspension of **56** (50 mg, 0.175 mmol), **64** (71.5 mg, 0.166 mmol), and $NaHCO_3$ (100 mg, 1.2 mmol) in ACN (7 mL) was heated and stirred in a sealed vessel for 6 h. The reaction mixture was filtered, the solvent was evaporated under vacuum, and the residue was purified by flash chromatography eluting with 10% DMA. The desired product was obtained as yellow oil (40 mg, 43% yield). ^{1}H NMR (400 MHz, CD_3OD): δ 7.33−7.14 (m, 3H), 7.14−7.05 (m, 1H), 6.92 (m, 2H), 6.65 (m, 1H), 5.48 (s, 1H), 4.08 (dq, *J* = 21.4, 7.1 Hz, 2H), 3.34−3.21 (m, 2H), 3.08 (br s, 4H), 2.97−2.70 (m, 10H), 2.56−2.42 (m, 1H), 2.22−1.98 (m, 4H), 1.74 (m, 1H), 1.65 (s, 1H), 1.19 (t, *J* = 7.2 Hz, 3H); ^{13}C NMR (101 MHz, CD_3OD): δ 168.38, 167.92, 158.33, 152.58, 149.48, 134.91, 130.18, 129.03, 128.40, 125.82, 120.17, 119.71, 116.02, 115.67, 114.48, 111.42, 59.50, 57.16, 56.04, 54.80, 54.16, 52.08, 46.63, 41.34, 39.27, 31.73, 21.35, 14.54. The free base was converted into the corresponding oxalate salt. HRMS ($C_{30}H_{37}N_3O_3Cl_2$ + H^+): calcd, 558.22847; found, 558.22925 (error 1.4 ppm). CHN ($C_{30}H_{37}N_3O_3Cl_2$ + $2.5H_2C_2O_4$ + $2H_2O$) Calcd: C, 51.29; H, 5.66; N, 5.13. Found: C, 51.07; H, 5.28; N, 5.21. mp: salt decomposes above 110 °C.

Radioligand Binding Studies. *hD_2R, hD_3R, and hD_4R.* Radioligand binding assays were conducted similar to those previously described.[45,67] HEK293 cells stably expressing human D_2LR or D_3R or $D_{4.4}$ were grown in a 50:50 mix of Dulbecco's modified Eagle medium (DMEM) and Ham's F12 culture media, supplemented with 20 mM *N*-(2-hydroxyethyl)piperazine-*N*′-ethanesulfonic acid, 2 mM L-glutamine, 0.1 mM nonessential amino acids, 1× antibiotic/antimycotic, 10% heat-inactivated fetal bovine serum (FBS), and 200 μg/mL hygromycin (Life Technologies, Grand Island, NY) and kept in an incubator at 37 °C and 5% CO_2. Upon reaching 80−90% confluence, cells were harvested using premixed Earle's balanced salt solution with 5 mM ethylenediaminetetraacetic acid (EDTA) (Life Technologies) and centrifuged at 3000 rpm for 10 min at 21 °C. The supernatant was removed, and the pellet was resuspended in 10 mL of hypotonic lysis buffer (5 mM $MgCl_2$, 5 mM Tris, pH 7.4 at 4 °C) and centrifuged at 14,500 rpm (∼25,000*g*) for 30 min at 4 °C. The pellet was then resuspended in binding buffer. Bradford protein assay (Bio-Rad, Hercules, CA) was used to determine the protein concentration. For [^{3}H]-*N*-methylspiperone binding studies, membranes were diluted to 500 μg/mL, in fresh EBSS binding buffer made from 8.7 g/L Earle's balanced salts without phenol red (US Biological, Salem, MA), 2.2 g/L sodium bicarbonate, pH to 7.4, and stored in a −80 °C freezer for later use. For [^{3}H]-(*R*)-(+)-7-OH-DPAT binding studies, membranes were harvested fresh; the binding buffer was made from 50 mM Tris, 10 mM $MgCl_2$, and 1 mM EDTA, pH 7.4. On the test day, each test compound was diluted into half-log serial dilutions using the 30% dimethyl sulfoxide (DMSO) vehicle. When it was necessary to assist solubilization of the drugs at the highest tested

https://doi.org/10.1021/acs.jmedchem.1c00611
J. Med. Chem. 2021, 64, 7778−7808

concentration, 0.1% AcOH (final concentration v/v) was added alongside the vehicle. Membranes were diluted in fresh binding buffer. Radioligand competition experiments were conducted in 96-well plates containing 300 μL of fresh binding buffer, 50 μL of the diluted test compound, 100 μL of membranes (for [^{3}H]-*N*-methylspiperone assays: 10−20, 10−20, and 20−30 μg/well total protein for $hD_{2L}R$, hD_3R, and $hD_{4.4}R$, respectively; for [^{3}H]-(*R*)-(+)-7-OH-DPAT assays: 40−80 and 20−40 μg/well total protein for $hD_{2L}R$ and hD_3R, respectively), and 50 μL of radioligand diluted in binding buffer ([^{3}H]-*N*-methylspiperone: 0.4 nM final concentration for all the hD_2-like receptor subtypes; [^{3}H]-(*R*)-(+)-7-OH-DPAT: 1.5 nM final concentration for hD_2L, and 0.5 nM final concentration for hD_3; PerkinElmer). Aliquots of radioligand solution were also quantified accurately in each experiment replicate to determine how much radioactivity was added, taking into account the experimentally determined counter efficiency. Nonspecific binding was determined using 10 μM (+)-butaclamol (Sigma-Aldrich, St. Louis, MO), and total binding was determined with the 30% DMSO vehicle. All compound dilutions were tested in triplicate, and the reaction was incubated for 60 min ([^{3}H]-*N*-methylspiperone assays) or 90 min ([^{3}H]-(*R*)-(+)-7-OH-DPAT assays) at RT. The reaction was terminated by filtration through PerkinElmer UniFilter-96 GF/B, presoaked for the incubation time in 0.5% polyethylenimine, using a Brandel 96-well plates harvester manifold (Brandel Instruments, Gaithersburg, MD). The filters were washed thrice with 3 mL (3 Å—1 mL/well) of ice-cold binding buffer. PerkinElmer MicroScint 20 scintillation cocktail (65 μL) was added to each well, and filters were counted using a PerkinElmer MicroBeta microplate counter. IC_{50} values for each compound were determined from dose−response curves, and K_i values were calculated using the Cheng−Prusoff equation.[63] K_d values were determined *via* separate homologous competitive binding experiments. When a complete inhibition could not be achieved at the highest tested concentrations, K_i values have been extrapolated by constraining the bottom of the dose−response curves (=0% residual specific binding) in the nonlinear regression analysis. These analyses were performed using GraphPad Prism version 8 for Macintosh (GraphPad Software, San Diego, CA). All results were rounded to the third significant figure. K_i values were determined from at least three independent experiments and are reported as the mean ± SEM.

hMOR. Radioligand binding experiments were conducted, and the results were analyzed, as described above and similar to those previously reported.[62] HEK293 cells stably expressing the hMOR were grown in a DMEM, supplemented with 10% FBS, 2 mM L-glutamine, 1% penicillin−streptomycin (or antibiotic/antimycotic), and hygromycin B (50 μg/mL). Upon reaching confluence, the cells were harvested and the membranes were prepared as detailed before. The binding buffer was made of 50 mM Tris and 5 mM $MgCl_2$ at pH 7.4. The experiments were performed in the presence of [^{3}H]-DAMGO (final concentration 3 nM; PerkinElmer) and 30 μg/well of membranes (final concentration). The reactions were incubated for 60 min at RT and terminated by rapid filtration through PerkinElmer UniFilter-96 GF/B, presoaked for 60 min in 0.5% polyethylenimine. The nonspecific binding was determined using 10 μM C-TOP or cold DAMGO. The radioligand K_d was measured *via* radioligand saturation experiments.

BRET Studies. All reagents were purchased from Sigma-Aldrich-Merck unless otherwise stated. BRET experiments were performed in transiently transfected human embryonic kidney 293 T (HEK 293T) cells, as described previously.[31,68] Briefly, cells were grown and maintained at 37 °C in 5% CO_2 in DMEM supplemented with 10% (v/v) FBS. Cells were seeded in 10 cm Petri dishes (2.5×10^6 cells per dish) and allowed to grow overnight in media at 37 °C, 5% CO_2. The following day, cells were transiently transfected in media supplemented with antibiotics (100 U/mL penicillin and 100 μg/mL streptomycin, Gibco) using a 1:6 total DNA to PEI (PolySciences Inc.) ratio. BRET constructs were as follows: 4 μg of Nb33-Venus and 1 μg of mMOR-Rluc8 for Nb33 recruitment, 2 μg of WT-Gα (i2 or oA), 1 μg of Gβ1-Venus(156−239), 1 μg of Gγ2-Venus(1−155), 1 μg of masGRK3ct-Rluc8, and 1 μg of receptor (SNAP-mMOR or hD3R) for GPA,[69] and 4 μg of arrestin-3-Venus, 2 μg of WT-GRK2, and 1 μg of mMOR-Rluc8 for arrestin-3 recruitment. Cells were then allowed to grow overnight at 37 °C, 5% CO_2. The next day, cells were plated in Greiner poly-D-lysine-coated 96-well plates (SLS) in media and allowed to grow overnight. On the day of the assay (48 h post-transfection), cells were washed once with D-PBS (Lonza, SLS) and incubated in D-PBS for 30 min at 37 °C. For the antagonist-mode assays that require preincubation, the cells were washed once with D-PBS and incubated with ligands in D-PBS (supplemented with 10 mM glucose) at 37 °C, 5% CO_2 for 3 h prior to starting the assay. The Rluc substrate coelenterazine h (NanoLight) was added to each well (final concentration of 5 μM), and cells were incubated for 5 min at 37 °C. After 5 min, ligands (final concentration from 10 μM to 1 nM in D-PBS) were added to the plate and cells were incubated for a further 10 min at 37 °C before reading the plate in a PHERAstar FSX microplate reader (Venus and Rluc emission signals at 535 and 475 nm, respectively, BMG Labtech). The ratio of Venus/Rluc counts was used to quantify the BRET signal in each well. Data were normalized to the wells containing 10 μM DAMGO/quinpirole or no drug for maximal or minimal response, respectively, and as indicated in the figure legends. All experiments were performed in duplicate and at least three times independently. All data points represent the mean, and error bars represent the SEM and were fitted using the built-in log(agonist) versus response (three parameters) model in Prism 8.0 (GraphPad Software Inc., San Diego, CA).For agonist-mode assays, data were fitted to a three-parameter concentration−response model where EC_{50} is the concentration of the agonist needed to elicit half the maximal response of the particular agonist, defined as E_{max}. For the antagonist-mode assays, data points were fitted using a three-parameter concentration−response model where IC_{50} is the concentration required to inhibit half the maximum response of the agonist used at a particular concentration. Values of pEC_{50} or pIC_{50} ± error are given as the error has a Gaussian distribution, whereas the error associated with the antilog value does not. For some ligands for which the lower asymptote of the curve was not well defined within the concentration range (represented by a dotted line), the bottom was constrained to be equal to 0%.

Molecular Docking and CADD. The receptor structures corresponding to PDB accession code 6CM4, 3PBL, and 5C1M were extracted from RCSB for the inactive-state D_2R, inactive-state D_3R, and active-state MOR, respectively. All the objects except the receptor protein subunit, the crystallized ligand, and in the case of active-state MOR, three crystallographic waters were deleted, and this was followed by the addition of hydrogens and optimization of the side-chain residues. Ligands were sketched, assigned formal charges, and energy-optimized prior to docking. The ligand docking box for potential grid docking was defined as the whole extracellular half of the protein, and all-atom docking was performed using the energy minimized structures for all ligands with a thoroughness value of 10. The best-scored docking solutions were further optimized by several rounds of minimization and Monte Carlo sampling of the ligand conformation, including the surrounding side-chain residues (within 5 Å of the ligand) and the three crystallographic waters in the MOR orthosteric sites. All the abovementioned molecular modeling operations were performed in ICM-Pro v3.8-5 molecular modeling package.

■ ASSOCIATED CONTENT

Supporting Information

The Supporting Information is available free of charge at https://pubs.acs.org/doi/10.1021/acs.jmedchem.1c00611.

Molecular formula strings (CSV)

PDB files of all the ligand/target complexes studied (ZIP)

Analytical data summary of the products (combustion elemental analyses, HRMS−MS/MS, GC/MS, and HPLC), supporting table reporting biased agonism

https://doi.org/10.1021/acs.jmedchem.1c00611
J. Med. Chem. 2021, 64, 7778−7808

analysis at MOR signaling pathways, and supplemental figures of all the ligand/target complexes studied (PDF)

AUTHOR INFORMATION

Corresponding Authors

Alessandro Bonifazi − *Medicinal Chemistry Section, Molecular Targets and Medications Discovery Branch, National Institute on Drug Abuse—Intramural Research Program, National Institutes of Health, Baltimore, Maryland 21224, United States;* orcid.org/0000-0002-7306-0114; Phone: (443)-740-2897; Email: alessandro.bonifazi2@nih.gov; Fax: (443)-740-2111

Amy Hauck Newman − *Medicinal Chemistry Section, Molecular Targets and Medications Discovery Branch, National Institute on Drug Abuse—Intramural Research Program, National Institutes of Health, Baltimore, Maryland 21224, United States;* orcid.org/0000-0001-9065-4072; Phone: (443)-740-2887; Email: anewman@intra.nida.nih.gov; Fax: (443)-740-2111

Authors

Francisco O. Battiti − *Medicinal Chemistry Section, Molecular Targets and Medications Discovery Branch, National Institute on Drug Abuse—Intramural Research Program, National Institutes of Health, Baltimore, Maryland 21224, United States*

Julie Sanchez − *Division of Physiology, Pharmacology and Neuroscience, School of Life Sciences, Queen's Medical Centre, University of Nottingham, Nottingham NG7 2UH, U.K.; Centre of Membrane Protein and Receptors, Universities of Birmingham and Nottingham, Midlands NG2 7AG, U.K.*

Saheem A. Zaidi − *Bridge Institute, Michelson Center for Convergent Bioscience, Department of Chemistry, Department of Biological Sciences, University of Southern California, Los Angeles, California 90089, United States*

Eric Bow − *Drug Design and Synthesis Section, Molecular Targets and Medications Discovery Branch, National Institute on Drug Abuse—Intramural Research Program, National Institutes of Health, Bethesda, Maryland 20892, United States*

Mariia Makarova − *Drug Design and Synthesis Section, Molecular Targets and Medications Discovery Branch, National Institute on Drug Abuse—Intramural Research Program, National Institutes of Health, Bethesda, Maryland 20892, United States*

Jianjing Cao − *Medicinal Chemistry Section, Molecular Targets and Medications Discovery Branch, National Institute on Drug Abuse—Intramural Research Program, National Institutes of Health, Baltimore, Maryland 21224, United States*

Anver Basha Shaik − *Medicinal Chemistry Section, Molecular Targets and Medications Discovery Branch, National Institute on Drug Abuse—Intramural Research Program, National Institutes of Health, Baltimore, Maryland 21224, United States;* orcid.org/0000-0001-9894-5544

Agnieszka Sulima − *Drug Design and Synthesis Section, Molecular Targets and Medications Discovery Branch, National Institute on Drug Abuse—Intramural Research Program, National Institutes of Health, Bethesda, Maryland 20892, United States*

Kenner C. Rice − *Drug Design and Synthesis Section, Molecular Targets and Medications Discovery Branch, National Institute on Drug Abuse—Intramural Research Program, National Institutes of Health, Bethesda, Maryland 20892, United States*

Vsevolod Katritch − *Bridge Institute, Michelson Center for Convergent Bioscience, Department of Chemistry, Department of Biological Sciences, University of Southern California, Los Angeles, California 90089, United States;* orcid.org/0000-0003-3883-4505

Meritxell Canals − *Division of Physiology, Pharmacology and Neuroscience, School of Life Sciences, Queen's Medical Centre, University of Nottingham, Nottingham NG7 2UH, U.K.; Centre of Membrane Protein and Receptors, Universities of Birmingham and Nottingham, Midlands NG2 7AG, U.K.;* orcid.org/0000-0002-7942-5006

J. Robert Lane − *Division of Physiology, Pharmacology and Neuroscience, School of Life Sciences, Queen's Medical Centre, University of Nottingham, Nottingham NG7 2UH, U.K.; Centre of Membrane Protein and Receptors, Universities of Birmingham and Nottingham, Midlands NG2 7AG, U.K.;* orcid.org/0000-0002-7361-7875

Complete contact information is available at: https://pubs.acs.org/10.1021/acs.jmedchem.1c00611

Author Contributions

A.B. and A.H.N. designed the project; A.B., F.O.B., and A.H.N. wrote the manuscript with input of all the authors; A.B., F.O.B., J.S., S.A.Z., A.S., K.C.R., V.K., M.C., J.R.L., and A.H.N. designed and supervised the experiments and data analysis; A.B., F.O.B., J.S., S.A.Z., E.B., M.M., J.C., A.B.S., and A.S. performed experiments.

Notes

The authors declare no competing financial interest.

ACKNOWLEDGMENTS

This project was supported by the National Institute on Drug Abuse—Intramural Research Program (ZIADA000609; ZIADA000424), as well as grant funding R33DA038858 for V.K. The authors thank Drs. Ludovic Muller and Shelley Jackson from the Structural Biology Core at NIDA-IRP for high-resolution MS/MS analyses, Dr. Ning Sheng Cai from the Integrative Neurobiology Section at NIDA-IRP for assistance with cell lines and tissue culture protocols, and Dr. Arthur Jacobson from the Drug Design and Synthesis Section at NIDA-IRP for insightful suggestions to the manuscript.

ABBREVIATIONS

DA, dopamine; $D_{2\text{-like}}R$, dopamine $D_{2\text{-like}}$ receptors; OUD, opioid use disorders; CADD, computer-aided drug design; BRET, bioluminescence resonance energy transfer; HEK 293 cells, human embryonic kidney 293 cells; HPLC, high-performance liquid chromatography; HRMS, high-resolution mass spectrometry; DMA, dichloromethane, methanol, and ammonium hydroxide; EDC, 1-ethyl-3-(3-dimethylaminopropyl)carbodiimide; HOBt, hydroxybenzotriazole; HCTU, *O*-(1*H*-6-chlorobenzotriazole-1-yl)-1,1,3,3-tetramethyluronium hexafluorophosphate; DIPEA, *N*,*N*-diisopropylethylamine; STAB, sodium triacetoxyborohydride; DMP, Dess−Martin periodinane; ACN, acetonitrile; LAH, lithium aluminum hydride; GPA, G-protein activation

REFERENCES

(1) CDC/NCHS National Vital Statistics System, Mortality. CDC WONDER; US Department of Health and Human Services, CDC:

Atlanta, GA. https://www.cdc.gov/nchs/nvss/deaths.htm (accessed Feb 10, 2021).
(2) Roy, L. https://www.forbes.com/sites/lipiroy/2020/05/23/collision-of-crises-how-covid-19-will-propel-drug-overdose-from-bad-to-worse/#5cbc00837d3a (accessed Feb 10, 2021).
(3) Silva, M. J.; Kelly, Z. The escalation of the opioid epidemic due to COVID-19 and sesulting lessons about treatment alternatives. *Am. J. Manag. Care* **2020**, *26*, e202−e204.
(4) NIH/NIDA. https://www.drugabuse.gov/drugs-abuse/opioids/opioid-overdose-crisis (accessed Feb 10, 2021).
(5) Vowles, K. E.; McEntee, M. L.; Julnes, P. S.; Frohe, T.; Ney, J. P.; van der Goes, D. N. Rates of opioid misuse, abuse, and addiction in chronic pain: a systematic review and data synthesis. *Pain* **2015**, *156*, 569−576.
(6) Muhuri, P. K.; Gfroerer, J. C.; Davies, M. C. *CBHSQ Data Review: Associations of Nonmedical Pain Reliever Use and Initiation of Heroin Use in the United States*, August 2013.
(7) Cicero, T. J.; Ellis, M. S.; Surratt, H. L.; Kurtz, S. P. The changing face of heroin use in the United States: a retrospective analysis of the past 50 years. *JAMA Psychiatry* **2014**, *71*, 821−826.
(8) Carlson, R. G.; Nahhas, R. W.; Martins, S. S.; Daniulaityte, R. Predictors of transition to heroin use among initially non-opioid dependent illicit pharmaceutical opioid users: A natural history study. *Drug Alcohol Depend.* **2016**, *160*, 127−134.
(9) Rasmussen, K.; White, D. A.; Acri, J. B. NIDA's medication development priorities in response to the opioid crisis: ten most wanted. *Neuropsychopharmacology* **2019**, *44*, 657−659.
(10) Keck, T. M.; John, W. S.; Czoty, P. W.; Nader, M. A.; Newman, A. H. Identifying medication targets for psychostimulant addiction: unraveling the dopamine D3 receptor hypothesis. *J. Med. Chem.* **2015**, *58*, 5361−5380.
(11) Appel, N. M.; Li, S.-H.; Holmes, T. H.; Acri, J. B. Dopamine D3 receptor antagonist (GSK598809) potentiates the hypertensive effects of cocaine in conscious, freely-moving dogs. *J. Pharmacol. Exp. Ther.* **2015**, *354*, 484−492.
(12) Jordan, C. J.; Humburg, B.; Rice, M.; Bi, G.-H.; You, Z.-B.; Shaik, A. B.; Cao, J.; Bonifazi, A.; Gadiano, A.; Rais, R.; Slusher, B.; Newman, A. H.; Xi, Z.-X. The highly selective dopamine D3R antagonist, R-VK4-40 attenuates oxycodone reward and augments analgesia in rodents. *Neuropharmacology* **2019**, *158*, 107597.
(13) You, Z.-B.; Bi, G.-H.; Galaj, E.; Kumar, V.; Cao, J.; Gadiano, A.; Rais, R.; Slusher, B. S.; Gardner, E. L.; Xi, Z.-X.; Newman, A. H. Dopamine D3R antagonist VK4-116 attenuates oxycodone self-administration and reinstatement without compromising its anti-nociceptive effects. *Neuropsychopharmacology* **2019**, *44*, 1415−1424.
(14) Kumar, V.; Bonifazi, A.; Ellenberger, M. P.; Keck, T. M.; Pommier, E.; Rais, R.; Slusher, B. S.; Gardner, E.; You, Z.-B.; Xi, Z.-X.; Newman, A. H. Highly selective dopamine D3 receptor (D3R) antagonists and partial agonists based on eticlopride and the D3R crystal structure: new leads for opioid dependence treatment. *J. Med. Chem.* **2016**, *59*, 7634−7650.
(15) Jordan, C. J.; Humburg, B. A.; Thorndike, E. B.; Shaik, A. B.; Xi, Z.-X.; Baumann, M. H.; Newman, A. H.; Schindler, C. W. Newly developed dopamine D3 receptor antagonists, R-VK4-40 and R-VK4-116, do not potentiate cardiovascular effects of cocaine or oxycodone in rats. *J. Pharmacol. Exp. Ther.* **2019**, *371*, 602−614.
(16) Rosenblum, A.; Marsch, L. A.; Joseph, H.; Portenoy, R. K. Opioids and the treatment of chronic pain: controversies, current status, and future directions. *Exp. Clin. Psychopharmacol.* **2008**, *16*, 405−416.
(17) Kaye, A. D.; Jones, M. R.; Kaye, A. M.; Ripoll, J. G.; Galan, V.; Beakley, B. D.; Calixto, F.; Bolden, J. L.; Urman, R. D.; Manchikanti, L. Prescription opioid abuse in chronic pain: an updated review of opioid abuse predictors and strategies to curb opioid abuse: part 1. *Pain Physician* **2017**, *2*, S93−S109.
(18) Morrone, L.; Scuteri, D.; Rombola, L.; Mizoguchi, H.; Bagetta, G. Opioids resistance in chronic pain management. *Curr. Neuropharmacol.* **2017**, *15*, 444−456.
(19) Schmid, C. L.; Kennedy, N. M.; Ross, N. C.; Lovell, K. M.; Yue, Z.; Morgenweck, J.; Cameron, M. D.; Bannister, T. D.; Bohn, L. M. Bias factor and therapeutic window correlate to predict safer opioid analgesics. *Cell* **2017**, *171*, 1165−1175.e13.
(20) Grim, T. W.; Acevedo-Canabal, A.; Bohn, L. M. Toward directing opioid receptor signaling to refine opioid therapeutics. *Biol. Psychiatry* **2020**, *87*, 15−21.
(21) Bossert, J. M.; Hoots, J. K.; Fredriksson, I.; Adhikary, S.; Zhang, M.; Venniro, M.; Shaham, Y. Role of mu, but not delta or kappa, opioid receptors in context-induced reinstatement of oxycodone seeking. *Eur. J. Neurosci.* **2019**, *50*, 2075−2085.
(22) Grim, T. W.; Schmid, C. L.; Stahl, E. L.; Pantouli, F.; Ho, J.-H.; Acevedo-Canabal, A.; Kennedy, N. M.; Cameron, M. D.; Bannister, T. D.; Bohn, L. M. A G protein signaling-biased agonist at the mu-opioid receptor reverses morphine tolerance while preventing morphine withdrawal. *Neuropsychopharmacology* **2020**, *45*, 416−425.
(23) Kennedy, N. M.; Schmid, C. L.; Ross, N. C.; Lovell, K. M.; Yue, Z.; Chen, Y. T.; Cameron, M. D.; Bohn, L. M.; Bannister, T. D. Optimization of a series of mu opioid receptor (MOR) agonists with high G protein signaling bias. *J. Med. Chem.* **2018**, *61*, 8895−8907.
(24) Imam, M. Z.; Kuo, A.; Ghassabian, S.; Cai, Y.; Qin, Y.; Li, T.; Smith, M. T. Intracerebroventricular administration of CYX-6, a potent mu-opioid receptor agonist, a delta- and kappa-opioid receptor antagonist and a biased ligand at mu, delta & kappa-opioid receptors, evokes antinociception with minimal constipation and respiratory depression in rats in contrast to morphine. *Eur. J. Pharmacol.* **2020**, *871*, 172918.
(25) Kliewer, A.; Schmiedel, F.; Sianati, S.; Bailey, A.; Bateman, J. T.; Levitt, E. S.; Williams, J. T.; Christie, M. J.; Schulz, S. Phosphorylation-deficient G-protein-biased mu-opioid receptors improve analgesia and diminish tolerance but worsen opioid side effects. *Nat. Commun.* **2019**, *10*, 367.
(26) Montandon, G.; Ren, J.; Victoria, N. C.; Liu, H.; Wickman, K.; Greer, J. J.; Horner, R. L. G-protein-gated inwardly rectifying potassium channels modulate respiratory depression by opioids. *Anesthesiology* **2016**, *124*, 641−650.
(27) Levitt, E. S.; Abdala, A. P.; Paton, J. F. R.; Bissonnette, J. M.; Williams, J. T. mu opioid receptor activation hyperpolarizes respiratory-controlling Kolliker-Fuse neurons and suppresses post-inspiratory drive. *J. Physiol.* **2015**, *593*, 4453−4469.
(28) Galligan, J. J.; Akbarali, H. I. Molecular physiology of enteric opioid receptors. *Am. J. Gastroenterol. Suppl.* **2014**, *2*, 17−21.
(29) Kliewer, A.; Gillis, A.; Hill, R.; Schmiedel, F.; Bailey, C.; Kelly, E.; Henderson, G.; Christie, M. J.; Schulz, S. Morphine-induced respiratory depression is independent of beta-arrestin2 signalling. *Br. J. Pharmacol.* **2020**, *177*, 2923−2931.
(30) Imam, M. Z.; Kuo, A.; Ghassabian, S.; Smith, M. T. Progress in understanding mechanisms of opioid-induced gastrointestinal adverse effects and respiratory depression. *Neuropharmacology* **2018**, *131*, 238−255.
(31) Gillis, A.; Gondin, A. B.; Kliewer, A.; Sanchez, J.; Lim, H. D.; Alamein, C.; Manandhar, P.; Santiago, M.; Fritzwanker, S.; Schmiedel, F.; Katte, T. A.; Reekie, T.; Grimsey, N. L.; Kassiou, M.; Kellam, B.; Krasel, C.; Halls, M. L.; Connor, M.; Lane, J. R.; Schulz, S.; Christie, M. J.; Canals, M. Low intrinsic efficacy for G protein activation can explain the improved side effect profiles of new opioid agonists. *Sci. Signaling* **2020**, *13*, No. eaaz3140.
(32) Negus, S. S.; Freeman, K. B. Abuse potential of biased mu opioid receptor agonists. *Trends Pharmacol. Sci.* **2018**, *39*, 916−919.
(33) Altarifi, A. A.; David, B.; Muchhala, K. H.; Blough, B. E.; Akbarali, H.; Negus, S. S. Effects of acute and repeated treatment with the biased mu opioid receptor agonist TRV130 (oliceridine) on measures of antinociception, gastrointestinal function, and abuse liability in rodents. *J. Psychopharmacol.* **2017**, *31*, 730−739.
(34) Austin Zamarripa, C.; Edwards, S. R.; Qureshi, H. N.; Yi, J. N.; Blough, B. E.; Freeman, K. B. The G-protein biased mu-opioid agonist, TRV130, produces reinforcing and antinociceptive effects that are comparable to oxycodone in rats. *Drug Alcohol Depend.* **2018**, *192*, 158−162.

https://doi.org/10.1021/acs.jmedchem.1c00611
J. Med. Chem. 2021, 64, 7778−7808

(35) Jullié, D.; Gondin, A. B.; Von Zastrow, M. E.; Canals, M. Opioid pharmacology under the microscope. *Mol. Pharmacol.* **2020**, *98*, 425−432.
(36) Stanley, T. H.; Egan, T. D.; Van Aken, H. A tribute to Dr. Paul A. J. Janssen: entrepreneur extraordinaire, innovative scientist, and significant contributor to anesthesiology. *Anesth. Analg.* **2008**, *106*, 451−462.
(37) Komoto, T.; Okada, T.; Sato, S.; Niino, Y.; Oka, T.; Sakamoto, T. New mu-opioid receptor agonists with piperazine moiety. *Chem. Pharm. Bull.* **2001**, *49*, 1314−1320.
(38) Jevtić, I.; Penjišević, J.; Ivanović, M.; Kostić-Rajačić, S. Synthetic route towards potential bivalent ligands possessing opioid and D2/D3 pharmacophores. *J. Serb. Chem. Soc.* **2019**, *84*, 639−647.
(39) Jevtić, I.; Penjišević, J.; Savić-Vujović, K.; Srebro, D.; Vučković, S.; Ivanović, M.; Kostić-Rajačić, S. mi-Opioid/D2 dopamine receptor pharmacophore containing ligands: Synthesis and pharmacological evaluation. *J. Serb. Chem. Soc.* **2020**, *85*, 711−720.
(40) Bao, X.; Liu, D.; Jin, Y.; Yang, Y. A facile synthesis for novel loperamide analogs as potential μ opioid receptor agonists. *Molecules* **2012**, *17*, 14288−14297.
(41) Feinberg, A. P.; Creese, I.; Snyder, S. H. The opiate receptor: a model explaining structure-activity relationships of opiate agonists and antagonists. *Proc. Natl. Acad. Sci. U.S.A.* **1976**, *73*, 4215−4219.
(42) Qian, M.; Vasudevan, L.; Huysentruyt, J.; Risseeuw, M. D. P.; Stove, C.; Vanderheyden, P. M. L.; Van Craenenbroeck, K.; Van Calenbergh, S. Design, synthesis, and biological evaluation of bivalent ligands targeting dopamine D2-like receptors and the mu-opioid receptor. *ChemMedChem* **2018**, *13*, 944−956.
(43) Newman, A. H.; Battiti, F. O.; Bonifazi, A. 2016 Philip S. Portoghese medicinal chemistry lectureship: designing bivalent or bitopic molecules for G-protein coupled receptors. The whole is greater than the sum of its parts. *J. Med. Chem.* **2020**, *63*, 1779−1797.
(44) Chien, E. Y. T.; Liu, W.; Zhao, Q.; Katritch, V.; Won Han, G.; Hanson, M. A.; Shi, L.; Newman, A. H.; Javitch, J. A.; Cherezov, V.; Stevens, R. C. Structure of the human dopamine D3 receptor in complex with a D2/D3 selective antagonist. *Science* **2010**, *330*, 1091−1095.
(45) Battiti, F. O.; Cemaj, S. L.; Guerrero, A. M.; Shaik, A. B.; Lam, J.; Rais, R.; Slusher, B. S.; Deschamps, J. R.; Imler, G. H.; Newman, A. H.; Bonifazi, A. The significance of chirality in drug design and synthesis of bitopic ligands as D3 receptor (D3R) selective agonists. *J. Med. Chem.* **2019**, *62*, 6287−6314.
(46) Battiti, F. O.; Newman, A. H.; Bonifazi, A. Exception that proves the rule: investigation of privileged stereochemistry in designing dopamine D3R bitopic agonists. *ACS Med. Chem. Lett.* **2020**, *11*, 1956−1964.
(47) Michino, M.; Boateng, C. A.; Donthamsetti, P.; Yano, H.; Bakare, O. M.; Bonifazi, A.; Ellenberger, M. P.; Keck, T. M.; Kumar, V.; Zhu, C.; Verma, R.; Deschamps, J. R.; Javitch, J. A.; Newman, A. H.; Shi, L. Toward understanding the structural basis of partial agonism at the dopamine D3 receptor. *J. Med. Chem.* **2017**, *60*, 580−593.
(48) Goldberg, J. S. Stereochemical basis for a unified structure activity theory of aromatic and heterocyclic rings in selected opioids and opioid peptides. *Perspect. Med. Chem.* **2010**, *4*, 1−10.
(49) Kumar, V.; Moritz, A. E.; Keck, T. M.; Bonifazi, A.; Ellenberger, M. P.; Sibley, C. D.; Free, R. B.; Shi, L.; Lane, J. R.; Sibley, D. R.; Newman, A. H. Synthesis and pharmacological characterization of novel trans-cyclopropylmethyl-linked bivalent ligands that exhibit selectivity and allosteric pharmacology at the dopamine D3 receptor (D3R). *J. Med. Chem.* **2017**, *60*, 1478−1494.
(50) Kopinathan, A.; Draper-Joyce, C.; Szabo, M.; Christopoulos, A.; Scammells, P. J.; Lane, J. R.; Capuano, B. Subtle modifications to the indole-2-carboxamide motif of the negative allosteric modulator N-((trans)-4-(2-(7-Cyano-3,4-dihydroisoquinolin-2(1 H)-yl)ethyl)-cyclohexyl)-1 H-indole-2-carboxamide (SB269652) yield dramatic changes in pharmacological activity at the dopamine D2 receptor. *J. Med. Chem.* **2019**, *62*, 371−377.
(51) Draper-Joyce, C. J.; Verma, R. K.; Michino, M.; Shonberg, J.; Kopinathan, A.; Klein Herenbrink, C.; Scammells, P. J.; Capuano, B.; Abramyan, A. M.; Thal, D. M.; Javitch, J. A.; Christopoulos, A.; Shi, L.; Lane, J. R. The action of a negative allosteric modulator at the dopamine D2 receptor is dependent upon sodium ions. *Sci. Rep.* **2018**, *8*, 1208.
(52) Verma, R. K.; Abramyan, A. M.; Michino, M.; Free, R. B.; Sibley, D. R.; Javitch, J. A.; Lane, J. R.; Shi, L. The E2.65A mutation disrupts dynamic binding poses of SB269652 at the dopamine D2 and D3 receptors. *PLoS Comput. Biol.* **2018**, *14*, No. e1005948.
(53) Newman, A. H.; Grundt, P.; Cyriac, G.; Deschamps, J. R.; Taylor, M.; Kumar, R.; Ho, D.; Luedtke, R. R. N-(4-(4-(2,3-dichloro- or 2-methoxyphenyl)piperazin-1-yl)butyl)heterobiarylcarboxamides with functionalized linking chains as high affinity and enantioselective D3 receptor antagonists. *J. Med. Chem.* **2009**, *52*, 2559−2570.
(54) De Paulis, T.; Hall, H.; Ogren, S. O.; Wagner, A.; Stensadn, B.; Csoregh, I. Synthesis, crystal structure and anti-dopaminergic properties of eticlopride (FLB 131). *Eur. J. Med. Chem.* **1985**, *20*, 273−276.
(55) Bharathi, P.; Periasamy, M. Metalation of iminium ions formed in the reaction of tertiary amines with TiCl4. *Org. Lett.* **1999**, *1*, 857−859.
(56) Hiebel, A.-C.; Lee, Y. S.; Bilsky, E.; Giuvelis, D.; Deschamps, J. R.; Parrish, D. A.; Aceto, M. D.; May, E. L.; Harris, L. S.; Coop, A.; Dersch, C. M.; Partilla, J. S.; Rothman, R. B.; Cheng, K.; Jacobson, A. E.; Rice, K. C. Probes for narcotic receptor mediated phenomena. 34. Synthesis and structure-activity relationships of a potent mu-agonist delta-antagonist and an exceedingly potent antinociceptive in the enantiomeric C9-substituted 5-(3-hydroxyphenyl)-N-phenylethylmorphan series. *J. Med. Chem.* **2007**, *50*, 3765−3776.
(57) Bonifazi, A.; Yano, H.; Guerrero, A. M.; Kumar, V.; Hoffman, A. F.; Lupica, C. R.; Shi, L.; Newman, A. H. Novel and potent dopamine D2 receptor Go-protein biased agonists. *ACS Pharmacol. Transl. Sci.* **2019**, *2*, 52−65.
(58) Huang, W.; Manglik, A.; Venkatakrishnan, A. J.; Laeremans, T.; Feinberg, E. N.; Sanborn, A. L.; Kato, H. E.; Livingston, K. E.; Thorsen, T. S.; Kling, R. C.; Granier, S.; Gmeiner, P.; Husbands, S. M.; Traynor, J. R.; Weis, W. I.; Steyaert, J.; Dror, R. O.; Kobilka, B. K. Structural insights into micro-opioid receptor activation. *Nature* **2015**, *524*, 315−321.
(59) Totrov, M.; Abagyan, R. Flexible protein-ligand docking by global energy optimization in internal coordinates. *Proteins* **1997**, *29*, 215−220.
(60) Keck, T. M.; Free, R. B.; Day, M. M.; Brown, S. L.; Maddaluna, M. S.; Fountain, G.; Cooper, C.; Fallon, B.; Holmes, M.; Stang, C. T.; Burkhardt, R.; Bonifazi, A.; Ellenberger, M. P.; Newman, A. H.; Sibley, D. R.; Wu, C.; Boateng, C. A. Dopamine D4 receptor-selective compounds reveal structure-activity relationships that engender agonist efficacy. *J. Med. Chem.* **2019**, *62*, 3722−3740.
(61) Volpe, D. A.; Tobin, G. A. M.; Mellon, R. D.; Katki, A. G.; Parker, R. J.; Colatsky, T.; Kropp, T. J.; Verbois, S. L. Uniform assessment and ranking of opioid mu receptor binding constants for selected opioid drugs. *Regul. Toxicol. Pharmacol.* **2011**, *59*, 385−390.
(62) Cai, N.-S.; Quiroz, C.; Bonaventura, J.; Bonifazi, A.; Cole, T. O.; Purks, J.; Billing, A. S.; Massey, E.; Wagner, M.; Wish, E. D.; Guitart, X.; Rea, W.; Lam, S.; Moreno, E.; Casadó-Anguera, V.; Greenblatt, A. D.; Jacobson, A. E.; Rice, K. C.; Casadó, V.; Newman, A. H.; Winkelman, J. W.; Michaelides, M.; Weintraub, E.; Volkow, N. D.; Belcher, A. M.; Ferré, S. Opioid-galanin receptor heteromers mediate the dopaminergic effects of opioids. *J. Clin. Invest.* **2019**, *129*, 2730−2744.
(63) Cheng, Y.; Prusoff, W. H. Relationship between the inhibition constant (K1) and the concentration of inhibitor which causes 50 per cent inhibition (I50) of an enzymatic reaction. *Biochem. Pharmacol.* **1973**, *22*, 3099−3108.
(64) Sounier, R.; Mas, C.; Steyaert, J.; Laeremans, T.; Manglik, A.; Huang, W.; Kobilka, B. K.; Déméné, H.; Granier, S. Propagation of conformational changes during mu-opioid receptor activation. *Nature* **2015**, *524*, 375−378.

https://doi.org/10.1021/acs.jmedchem.1c00611
J. Med. Chem. 2021, 64, 7778−7808

(65) Wager, T. T.; Hou, X.; Verhoest, P. R.; Villalobos, A. Moving beyond rules: the development of a central nervous system multiparameter optimization (CNS MPO) approach to enable alignment of druglike properties. *ACS Chem. Neurosci.* **2010**, *1*, 435−449.
(66) Wager, T. T.; Hou, X.; Verhoest, P. R.; Villalobos, A. Central nervous system multiparameter optimization desirability: application in drug discovery. *ACS Chem. Neurosci.* **2016**, *7*, 767−775.
(67) Shaik, A. B.; Kumar, V.; Bonifazi, A.; Guerrero, A. M.; Cemaj, S. L.; Gadiano, A.; Lam, J.; Xi, Z.-X.; Rais, R.; Slusher, B. S.; Newman, A. H. Investigation of novel primary and secondary pharmacophores and 3-substitution in the linking chain of a series of highly selective and bitopic dopamine D3 receptor antagonists and partial agonists. *J. Med. Chem.* **2019**, *62*, 9061−9077.
(68) Klein Herenbrink, C.; Sykes, D. A.; Donthamsetti, P.; Canals, M.; Coudrat, T.; Shonberg, J.; Scammells, P. J.; Capuano, B.; Sexton, P. M.; Charlton, S. J.; Javitch, J. A.; Christopoulos, A.; Lane, J. R. The role of kinetic context in apparent biased agonism at GPCRs. *Nat. Commun.* **2016**, *7*, 10842.
(69) Hollins, B.; Kuravi, S.; Digby, G. J.; Lambert, N. A. The c-terminus of GRK3 indicates rapid dissociation of G protein heterotrimers. *Cell. Signalling* **2009**, *21*, 1015−1021.

https://doi.org/10.1021/acs.jmedchem.1c00611
J. Med. Chem. 2021, 64, 7778−7808